

**NASA CONTRACTOR
REPORT**



NASA CR-1857
2.1

0061042



**LOAN COPY: RETURN TO
AFWL (DOUL)
KIRTLAND AFB, N. M.**

NASA CR-1857

**A FEASIBILITY STUDY OF
HEAT-PIPE-COOLED LEADING EDGES
FOR HYPERSONIC CRUISE AIRCRAFT**

by Calvin C. Silverstein

Prepared by
CALVIN C. SILVERSTEIN
ENGINEERING CONSULTANT
Baltimore, Md. 21209
for Langley Research Center

NATIONAL AERONAUTICS AND SPACE ADMINISTRATION • WASHINGTON, D. C. • NOVEMBER 1971



0061042

1. Report No. NASA CR-1857		2. Government Accession No.		3. Recipient's Accession No. 0061042	
4. Title and Subtitle A FEASIBILITY STUDY OF HEAT-PIPE-COOLED LEADING EDGES FOR HYPERSONIC CRUISE AIRCRAFT				5. Report Date November 1971	
				6. Performing Organization Code	
7. Author(s) Calvin C. Silverstein				8. Performing Organization Report No. SIL-106	
9. Performing Organization Name and Address Engineering Consultant Baltimore, Md. 21209				10. Work Unit No.	
				11. Contract or Grant No. NAS1-9872	
12. Sponsoring Agency Name and Address National Aeronautics and Space Administration Washington, D.C. 20546				13. Type of Report and Period Covered Contractor Report	
				14. Sponsoring Agency Code	
15. Supplementary Notes					
16. Abstract A theoretical study of the use of heat pipe structures for cooling the leading edges of hypersonic cruise aircraft was carried out over a Mach number range of 6 to 12. Preliminary design studies showed that a heat pipe cooling structure with a 33-in. chordwise length could maintain the maximum temperature of a 65° sweepback wing with a 0.5-in. leading edge radius below 1600° F during cruise at Mach 8. A few relatively minor changes in the steady-state design of the structure were found necessary to insure satisfactory cooling during the climb to cruise speed and altitude. It was concluded that heat pipe cooling is an attractive, feasible technique for limiting leading edge temperatures of hypersonic cruise aircraft.					
17. Key Words (Suggested by Author(s)) Hypersonic Vehicle Leading Edge Heat Pipe Design Thermal Protection System			18. Distribution Statement Unclassified - Unlimited		
19. Security Classif. (of this report) Unclassified		20. Security Classif. (of this page) Unclassified		21. No. of Pages 149	22. Price* \$3.00



TABLE OF CONTENTS

	<u>Page</u>
SYMBOLS	vii
SUMMARY	1
INTRODUCTION	2
BASIC DESIGN CONCEPT	3
HEAT PIPE DESIGN FACTORS	6
Internal Fluid Pressures	6
Heat Pipe Fluid	9
Heat Pipe Materials	9
Wick Types	10
Heat Transport Limits	11
Sonic limit	12
Isothermal limit	12
Entrainment limit	12
Capillary pumping limit	13
Boiling limit	13
Environmental Effects	14
Vibration	14
Acceleration	14
Gaseous diffusion	15
Startup	15
PARAMETRIC STUDY OF HEAT LOAD AND HEAT PIPE LENGTH ...	15
Aerodynamic Heating	21
Radiation Equilibrium Temperatures	24
Heat Pipe Heat Load	27
Maximum Surface Temperature	35
Heat Pipe Length	35
PRELIMINARY DESIGN STUDIES	42
Selection of Heat Pipe Fluid	43
Selection of Heat Pipe Materials	48
Candidate alloys	48

	<u>Page</u>
Compatibility with sodium	49
Gaseous diffusion	51
Materials selection	53
Minimum Thickness of Heat Pipe Cooling Structure	54
Assumptions	54
Analytical approach	55
Results	56
Design for Mach 8, 65 Degree Sweepback Wing	58
Overall length	59
Cross-sectional dimensions	63
Stress and deflection	63
Wick design	68
Selection of cross-section	75
Selection of flow channel	76
Final design	78
Design Modifications	80
Designs for leading edge radii of 0.25 and 1 inch	80
Use of entire internal volume for vapor space	82
Separate extension of heat pipe cooling structure	84
Effect of angle of attack on design	88
Operation of Mach 8 design at Mach 10	91
 TRANSIENT BEHAVIOR OF HEAT PIPE COOLING STRUCTURE	 94
Input Data	95
Transient Analysis	96
Experimental observations	96
Description of transient model	98
Transient equations	101
Results of transient analysis	106
Heat Transport Limits During Transient	108
Entrainment limit	108
Boiling and capillary pumping limits	110
Vapor and liquid pressures	111
Expansion of Liquid Sodium During Startup	114
Conclusions	114
 DISCUSSION OF RESULTS	 115
Summary of Major Findings	115
Design Uncertainties	116
 CONCLUDING REMARKS	 118

	<u>Page</u>
APPENDIX A - HEAT TRANSFER COEFFICIENT FOR AERODYNAMIC HEATING OF FLAT WING SURFACES	119
Local Free Stream Flow Properties at Flat Surfaces	119
APPENDIX B - HEAT PIPE HEAT TRANSPORT LIMITS	123
Sonic Limit	123
Entrainment Limit	124
Isothermal Limit	125
Capillary Pumping Limit	127
Boiling Limit	130
APPENDIX C - LIQUID METAL PROPERTY DATA	134
APPENDIX D - EXPERIMENTAL PROGRAM	136
REFERENCES	139

SYMBOLS

a, b, c, d, e	fluid parameters defined in Appendix B
A	cross-sectional area
B	wing span, rib-to-rib spacing
c	specific heat
c_p	specific heat at constant pressure
C	maximum wing chord, sonic velocity, volumetric heat capacity per unit of heat pipe length
C_d	drag coefficient
C_f	skin friction coefficient
D	heat pipe diameter
D_a	pore diameter of liquid flow channel
D_b	diameter of curvature below which heat pipe liquid will boil
D_c	diameter of curvature at liquid-vapor interface
D_e	wick pore diameter above which liquid will be entrained
D_p	wick pore diameter of inner wick layer
D_v	vapor space diameter
E	modulus of elasticity
g	acceleration of gravity
h	heat transfer coefficient
H	rib height
H_v	vapor space thickness
I	moment of inertia of wall cross-section about centerline
k	thermal conductivity, ratio of constant pressure and constant volume specific heats
K	friction factor for flow through porous medium
l	straight-line distance between condenser end of heat pipe cooling structure and some other point along the structure
L	heat pipe length
L_a	straight-line distance between ends of heat pipe cooling structure
L_c	length of heat pipe cooling structure over flat upper wing surface needed to dissipate heat from leading edge
L_e	length of heat pipe cooling structure over upper wing surface needed to dissipate heat from lower wing surface
L_ℓ	length of heat pipe cooling structure which covers lower wing surface
L_n	chordwise length of isothermal nose section of heat pipe cooling structure
ΔL_n	added chordwise length of L_n needed to cool lower surface of isothermal nose section

L_t	overlapped length for heat pipe cooling structure with separate extension
L_u	length of upper leg of heat pipe cooling structure
L_l	length of inclined upper wing surface adjacent to leading edge
M	Mach number, bending moment, molecular weight
n	number of g's of acceleration
P	pressure
q	heat flux due to aerodynamic heating
Q	heat pipe heat load from leading edge
Q_c	heat transport rate from leading edge to upper leg of heat pipe cooling structure
Q_e	aerodynamic heating rate on flat wing surface, heat transport rate for entrainment
Q_{il}	net heating rate over lower leg of heat pipe cooling structure
Q_{in}	net heating rate over leading edge of heat pipe cooling structure
Q_l	heat pipe heat load from lower surface of isothermal nose section
Q_p	aerodynamic heating rate over leading edge
$Q_{ru}(x_l)$	net heat rejection rate over length x_l of upper leg of heat pipe cooling structure
Q_s	sonic heat transport limit
r	radius
R	radius of wing leading edge in plane normal to leading edge
R_o	universal gas constant
R_a	gas constant for air
Re	Reynolds number
R_n	radius of nucleation sites at which boiling is initiated
s	periphery of leading edge, stress
t	thickness, time
T	temperature behind continuum front
T_c	temperature at which initiation of continuum flow is assured
T_{aw}	adiabatic wall temperature at wing surface
T_e	equilibrium temperature
T_m	maximum (stagnation line) temperature of heat pipe cooling structure
T_o	reference wall temperature
T_v	temperature of saturated heat pipe vapor
T_w	surface temperature of wing
T_{wo}	temperature at interface between heat pipe wall and wick
V	flow velocity
w	specific weight or density
W	centerline distance between ribs
W_v	vapor space width
x	distance along leading edge
x_l	distance of continuum wave front in upper leg of heat pipe cooling structure from leading edge

x_2	distance of continuum wave front in lower leg of heat pipe cooling structure from leading edge
y	maximum deflection of heat pipe walls
α	angle of attack, linear expansion coefficient
β	airfoil wedge angle in plane normal to leading edge
γ	airfoil wedge angle in chordal plane
Λ	wing sweepback angle
δ	dimensionless geometric parameter defined in Appendix B
Δ	geometric boiling parameter defined by equation (67)
ϵ	ratio of liquid pressure drops in porous and open flow channels of same dimensions, emissivity
κ	heat of evaporation
λ	mean free path
μ	absolute viscosity
ν	Poisson's ratio, Prandtl-Meyer angle
η	dimensionless geometric parameter defined in Appendix B
ξ	axial heat flux = heat pipe heat load per unit vapor space cross-sectional area
Ω	angle between acceleration vector and line segment l
σ	surface tension
θ	co-ordinate angle at leading edge, in plane normal to leading edge

Subscripts

a	air, liquid flow channel
b	boiling, buckling
c	capillary wick
e	extension, entrainment
h	horizontal
i	liquid-vapor interface, condition at time t , internal
$i + 1$	condition at time $t + \Delta t$
j	j th component of acceleration
l	liquid, lower leg of heat pipe cooling structure
$l m$	liquid metal
$l s$	liquid static pressure drop
n	nose section
o	open liquid flow channel, external
p	porous liquid flow channel, inner wick layer
s	leading edge of wing, sonic
t	fluid property when fluid is stagnant
u	upper leg of heat pipe cooling structure
v	vapor, vertical
w	heat pipe wall

A FEASIBILITY STUDY OF
HEAT-PIPE-COOLED LEADING EDGES
FOR HYPERSONIC CRUISE AIRCRAFT

By Calvin C. Silverstein
Engineering Consultant

SUMMARY

A theoretical study of the use of heat pipe structures for cooling the leading edges of hypersonic cruise aircraft was carried out. In the basic cooling concept, a continuous isothermal heat pipe structure covers the leading edge, a portion of the lower wing surface, and a portion of the upper wing surface. Aerodynamic heat is absorbed at the leading edge and lower wing surface and transported through the heat pipe structure to the upper wing surface, where it is rejected by thermal radiation.

Parametric studies of length and heat load for the heat pipe cooling structure were performed for the following range of variables: Mach number, 6 to 12; wing sweepback angle, 0° to 75° ; leading edge radius, 0.25 to 24 in.; and heat pipe vapor temperature, 1340 to 1940°F .

Preliminary design studies were carried out for a Mach 8, 65° sweepback wing with a 0.5-in. leading edge radius. The heat pipe cooling structure for this case had a chordwise length of 33 in., a weight of 2.5 lb/ft^2 of surface area, and operated at a maximum (stagnation line) temperature of 1578°F . Additional design studies were carried out for leading edge radii of 0.25 and 1 in., and for Mach 10 flight.

The transient behavior of the Mach 8, 65° sweep angle, 0.5-in. leading edge radius design was studied during the climb to cruise altitude and speed. A maximum transient temperature of about 1700°F was experienced by the heat pipe cooling structure. Some conditions which could possibly interfere with

cooling during the transient climb period were identified. However, these conditions could be avoided by the adoption of relatively minor design changes.

It was concluded that heat pipe cooling is a feasible, attractive technique for limiting maximum leading edge temperatures of hypersonic cruise aircraft.

INTRODUCTION

The design of air-breathing aircraft for extended flight at hypersonic speeds will require the solution of unprecedented structural and materials problems (ref. 1). Of particular concern are the leading edges of the aircraft wing, tail, engine nacelles, and fuselage. Temperatures at these regions of maximum aerodynamic heating may easily exceed the maximum temperature limits of available structural materials if provision is not made for removal and dissipation of the absorbed heat.

This report explores the feasibility of a technique for cooling the leading edges of hypersonic aircraft which is based on the principles of the heat pipe. The heat pipe is a structure which, by virtue of its internal construction, has the capability for transporting heat at high rates over appreciable distances while remaining relatively isothermal and without the need for external pumping. By employing heat pipe design principles and radiative cooling, it may be possible to devise a completely passive cooling system with the capability of restricting peak leading edge temperatures to levels which are compatible with the temperature limits of nickel- and cobalt-base superalloys.

The basic design concept for a heat-pipe-cooled leading edge is described first. Then, design factors essential to an understanding of heat pipe operation are discussed. Next, heat pipe lengths and heat loads required for leading edge cooling are presented for a wide range of cruise Mach numbers, wing leading edge radii, wing sweepback angles, and operating temperatures. Preliminary design studies of heat-pipe-cooled leading edges for several specific design conditions are then described. An analysis of system transient response during the climb to cruising altitude and speed follows. In the final section of the report, the feasibility of heat-pipe-cooled leading edges is evaluated. Detailed calculational methods, relevant design data, and suggestions for an experimental program to resolve areas of design uncertainty are included in the Appendixes.

BASIC DESIGN CONCEPT

While the leading edge of a hypersonic aircraft wing must be cooled in order to avoid excessive temperatures, cooling is generally not required for portions of the wing surface aft of the leading edge. In the basic concept for heat pipe cooling, then, a continuous heat pipe structure covers the leading edge and a portion of the adjacent wing surface. (See figure 1.) Heat is transported along the heat pipe structure from the leading edge of the wing to the aft section, and then radiated to the environment from the surface of the structure. In order to dissipate the heat by radiation, the heat pipe temperature must exceed the radiation equilibrium temperature of the wing surface aft of the leading edge. The radiation equilibrium temperature is the temperature assumed by the wing surface when the heat rejection rate by radiation is equal to the heat input rate due to aerodynamic heating. Since radiation equilibrium temperatures on the upper wing surface are smaller than on the lower surface, the rejection of heat is more readily accomplished from the upper wing surface. Hence, the heat pipe structure preferably extends along the upper wing surface.

From the structural standpoint, it is desirable that the nose section be relatively isothermal. Thermal stresses arising from temperature differentials between the upper and lower wing surfaces are then minimized. With heat pipe cooling, the desired isothermal nose section is readily achieved by extending the heat pipe structure over a portion of the lower wing surface, as is shown in figure 1. Then, if the heat pipe temperature is greater than the radiation equilibrium temperature of the lower wing surface, additional heat dissipation capability will result. On the other hand, if the heat pipe temperature is less than the lower surface radiation equilibrium temperature, an additional heat pipe heat load will result.

The heat pipe cooling structure can be confined to a thin layer near the surface, as is shown in figure 1, or, for thin wing sections, the structure can extend through the entire wing interior. The internal composition is shown in section A-A of figure 1. An enclosure is formed by the aircraft skin, an internal skin, and supporting ribs. The interior surface is lined with a porous layer called a capillary wick. The capillary wick is saturated with a liquid whose vapor pressure at the desired operating temperature is neither excessively high nor low. The interior space is filled with the saturated vapor of the liquid, at a pressure equal to the vapor pressure. At the leading edge (and along the lower wing surface if the heat pipe temperature is less than the lower surface radiation equilibrium temperature), heat is conducted through the skin and the capillary wick to the liquid-vapor interface, causing liquid to evaporate. The vapor formed travels through the vapor space and condenses on the wick along

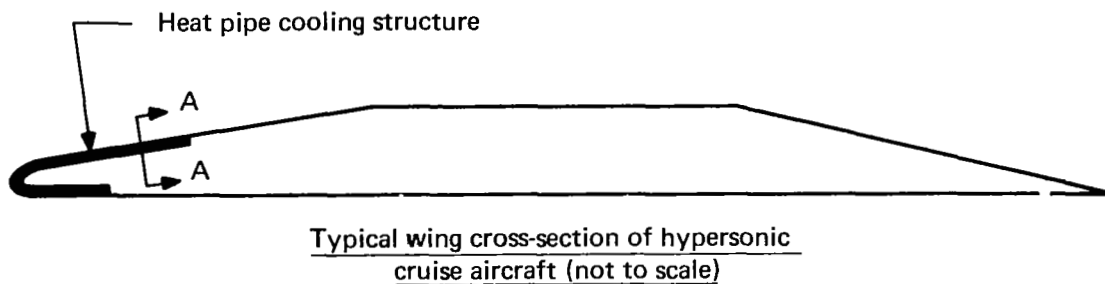
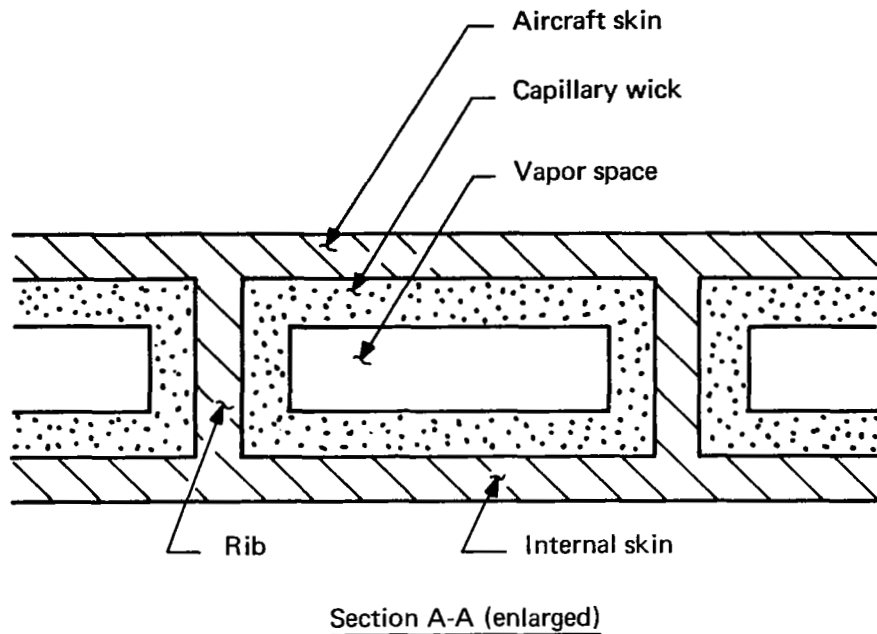


Figure 1. Basic design concept for heat-pipe-cooled leading edge.

the upper wing surface (and also along the lower wing surface if the heat pipe temperature exceeds the lower surface radiation equilibrium temperature). The condensate returns to the leading edge by flowing through the capillary wick.

In a properly designed heat pipe, the vapor temperature is virtually constant over the entire heat pipe length. However, finite temperature gradients are necessary to conduct heat across the thickness of the wing skin and the

capillary wick. Thus, the outer surface of the skin will be hotter than the vapor at heat input zones and colder than the vapor at zones of heat rejection. The maximum temperature occurs at the stagnation line along the leading edge, since the heat flux is greatest there.

The heat pipe cooling structure is divided by the supporting ribs into individual cells, each of which can function independently of the others. The rib spacing will be determined by allowable deformation and/or stress in the skin which results from internal (vapor) or external (atmospheric) pressure. The ribs may be oriented either normal to the leading edge or in the chordwise direction, as shown in figure 2. The chordwise orientation requires longer, but fewer ribs. The chordwise orientation also permits the heat pipe cooling structure to extend all the way to the fuselage. With the normal-to-leading-edge orientation, a portion of the leading edge adjacent to the fuselage will be unprotected.

The normal-to-leading-edge orientation is advantageous for swept wings when the aircraft is subjected to longitudinal acceleration, as will be the case during the climb phase of a flight. Then the liquid column in the capillary wick will be subjected to a smaller liquid static pressure head because of the smaller

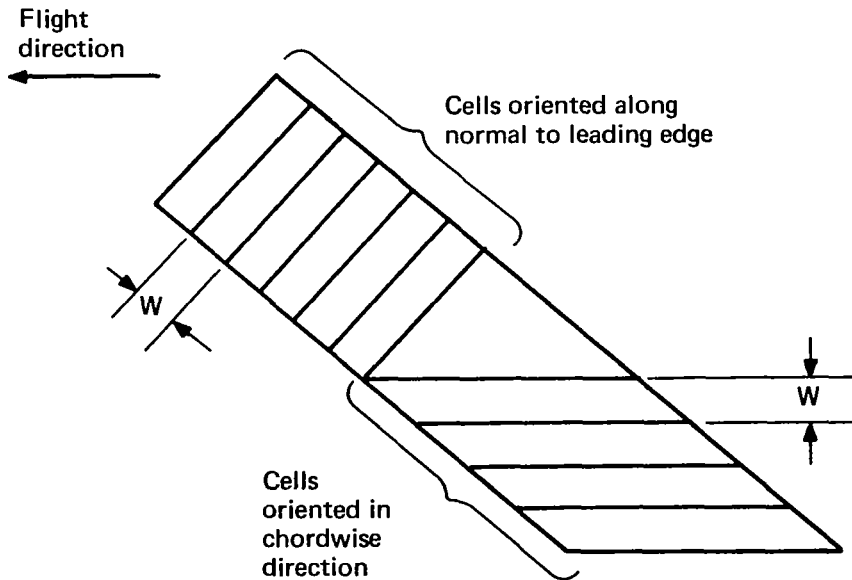


Figure 2. Orientation of cells in heat pipe cooling structure.

component of acceleration along the liquid column and the shorter column length. The smaller static head facilitates the internal design of the heat pipe cooling structure.

The length of each cell of the structure and its heat transport load can be determined solely from aerodynamic heating and thermal radiation considerations, without concern for internal thermal and fluid flow processes. The operating temperature of the heat pipe cooling structure will be established by a reasonable balance between material strength and oxidation characteristics, which degrade as the temperature increases, and heat pipe length, which decreases with an increase in temperature. However, in all cases the operating temperature must exceed the radiation equilibrium temperature on the upper surface of the wing.

The determination of cell dimensions normal to the wing surface, as well as details of internal construction, requires familiarity with heat pipe design techniques and operating characteristics. Those techniques and characteristics which are relevant to the use of heat pipes for leading edge cooling are discussed next.

HEAT PIPE DESIGN FACTORS

In this section the principal factors which are involved in the design of heat pipes are discussed, with emphasis on their relevance to heat-pipe-cooled leading edges. These factors include: internal fluid pressures, the heat pipe fluid, heat pipe materials, the heat pipe wick, heat transport limits, environmental effects, and startup behavior.

Internal Fluid Pressures

As shown in figure 3, the heat pipe is a closed hollow structure whose interior surface is lined with a layer of porous material called a capillary wick. An appropriate heat pipe liquid fills the pores of the wick, and vapor occupies the remaining internal volume. The flow of vapor and liquid during heat transport results in pressure drops in both phases. The vapor pressure drop has two components: that due to momentum generation and that due to friction. The liquid pressure drop is due to friction and, if the heat pipe is inclined or subject

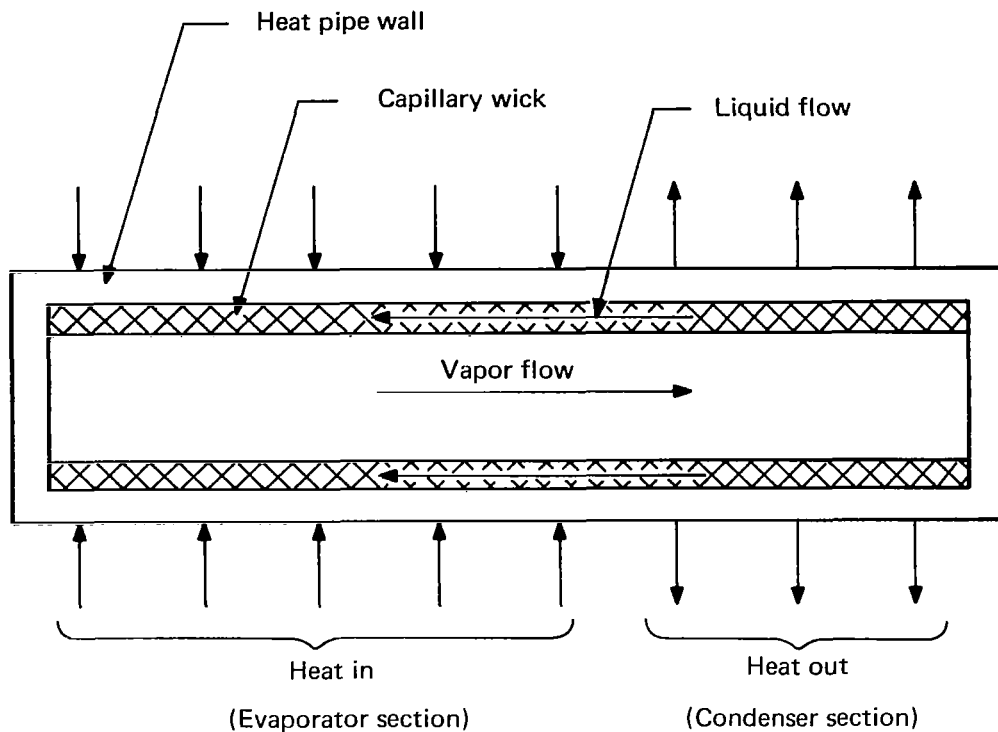


Figure 3. Cross-section of typical heat pipe.

to acceleration, a static liquid head. Depending on which end is inclined or the direction of acceleration, the static liquid head may increase or decrease the overall pressure drop in the liquid phase.

Figure 4 shows the pressure distribution for the case when the evaporator (heat input) section is above the condenser (heat rejection) section. It can be seen that at a given point along the heat pipe, the vapor pressure exceeds the liquid pressure. The pressure difference between the vapor and liquid is a maximum at the beginning of the evaporator section. The pressure difference is balanced by surface tension forces at the liquid-vapor interface in the wick pores. The interface must be curved such that the surface tension force will have a component toward the phase with the highest pressure.

It can be seen from figure 4 that the maximum pressure difference to be balanced by surface tension is equal to the sum of the vapor and liquid pressure drops. Usually, the fractional pressure drop in the saturated vapor is so small that the associated change in the vapor temperature is negligible. The heat

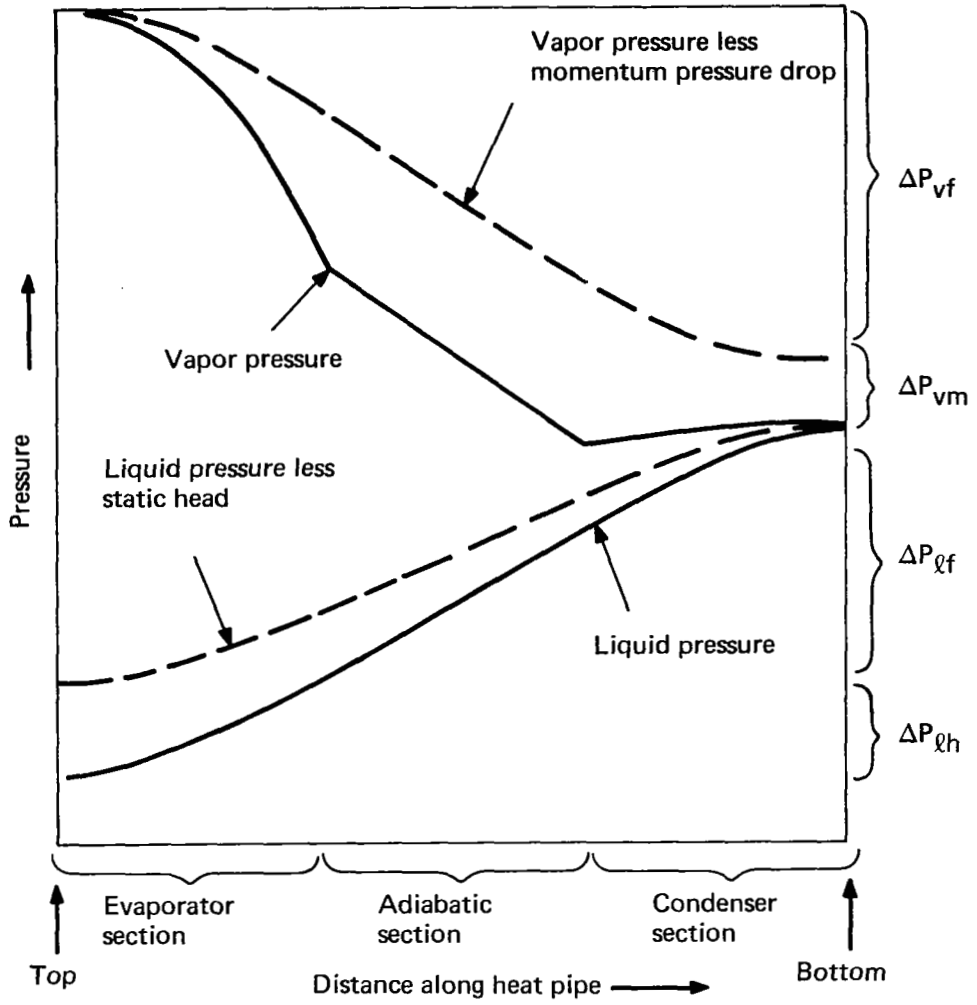


Figure 4. Fluid pressure distribution in heat pipe.

pipe may then be regarded as isothermal, although significant temperature differences may develop across the thickness of the heat pipe wick and wall if the input or output heat flux is large.

Heat Pipe Fluid

The initial consideration involved in selection of a heat pipe fluid is the expected operating temperature. For the leading-edge-cooling application, the heat pipe temperature is expected to lie within the range of 1340 to 1940° F. Once the operating temperature has been determined, attention should be focused on those fluids whose vapor pressures at the operating temperature lie in the range of roughly 1 to 100 psia. Below 1 psia, the heat transport capacity per unit cross-sectional area may be so small that heat pipe cross-sections become impractically large. Above 100 psia, the heat transport capacity will be increasingly limited in order to prevent the initiation of disruptive boiling at the heat input section of the wick, and relatively thick heat pipe walls may be needed to prevent excessive stresses.

In the temperature range of interest, the liquid metals sodium, potassium, and cesium are the prime candidate heat pipe fluids. Lithium may be a marginal choice near the upper temperature limit.

Heat Pipe Materials

The heat pipe wall and wick must be compatible with the heat pipe fluid, and should preferably be fabricated from the same material. In addition, the wall material must be compatible with the environment in which the heat pipe will operate. The wall material must also possess adequate strength and stiffness at the heat pipe operating temperature.

Sodium, potassium, and cesium are compatible with nickel- and cobalt-base superalloys, while lithium requires refractory metal containment. Special precautions must be taken to minimize the presence of oxygen, since the oxides of the liquid metals can be quite corrosive. Since the superalloys, including René 41 and Haynes 25, are characterized by good strength and oxidation resistance over at least part of the temperature range of interest, materials will probably not represent a major restriction on the use of heat pipes for cooling the leading edges of hypersonic aircraft.

Wick Types

Three basic wick types may be used in a heat pipe: the single-layer or homogeneous wick, the two-layer or two-component wick, and the artery. These wick types are illustrated in figure 5. The single-layer wick is a relatively homogeneous porous structure, with essentially the same mean pore size in both the axial and radial directions. Since a small pore size is desirable in order that large differences between the vapor pressure and liquid pressure can be balanced by surface tension at the liquid-vapor interface, while a large pore size is desirable to minimize the pressure drop in the liquid condensate, the use of a single-layer wick inevitably compromises heat pipe performance. Single-layer wicks are best suited for situations where the heat load is relatively light and/or heat pipe weight and volume are not overriding considerations.

With the two-layer wick, the dual wick functions of flow path for the returning condensate and surface tension barrier between the liquid and vapor are completely separated. A coarse-pored layer adjacent to the heat pipe wall

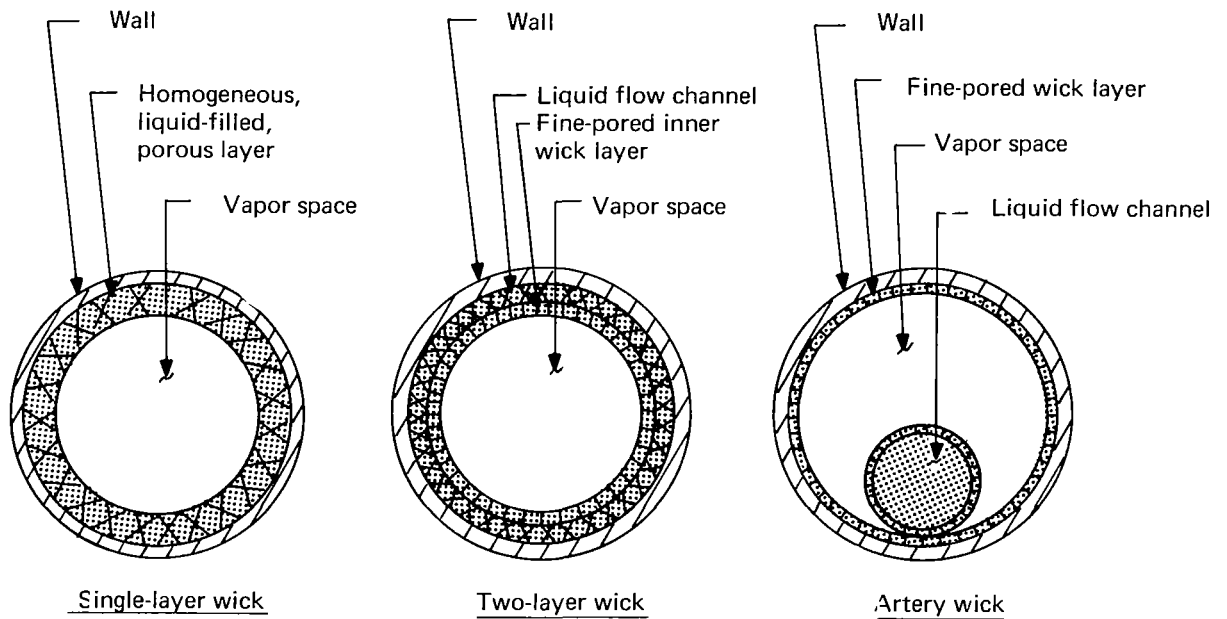


Figure 5. Basic wick types for heat pipe.

provides a low-resistance axial flow channel for returning condensate, while a fine-pored layer adjacent to the vapor space provides the necessary surface tension barrier between liquid and vapor. The pore size in each layer can be independently varied to maximize heat transport capacity for a given situation. For maximum performance, the outer wick layer is completely devoid of porous material, in which case a completely open channel is provided for the return flow of condensate. Two-layer wicks are generally characterized by small wick thickness and good heat transport capability. They are preferable in situations where low heat pipe weight and volume are important considerations.

The artery wick is really a variation of the two-layer wick with an open flow channel. Instead of using a layer next to the heat pipe wall as the flow channel, a porous-walled tube or artery which extends into the vapor space is used. Condensate formed at the heat removal zone flows circumferentially to the artery through the fine-pored layer adjacent to the heat pipe wall, then axially along the artery to the heat input section, where it flows circumferentially from the artery and is re-evaporated. Because of its more favorable geometry, the artery requires less volume than an open flow channel along the wall for the same liquid pressure drop. However, if the liquid column in the artery should be disrupted, refilling of the artery may be difficult because of the small capillary force which can be developed in a tube of significant diameter. Also, fabrication of the artery wick may be difficult for small heat pipe cross-sections.

The porous material for the single- or two-layer wicks may be fabricated from any material which is compatible with the heat pipe fluid. Depending on the requirements of a particular application, wicks may be fabricated from layers of wire screening, sintered metal fibers, or sintered metal powder. The wick may also be formed by cutting small axial grooves into the heat pipe wall.

Heat Transport Limits

For a given heat pipe operating at a given temperature, there is a maximum heat transport rate, called the heat transport capacity, beyond which normal heat pipe operation will be disrupted. At least five physical phenomena have been identified which can interfere with normal heat pipe operation. The heat transport rate at which a given phenomenon comes into play is called the heat transport limit for that phenomenon. At a given operating temperature, the heat transport capacity is equal to the lowest heat transport limit at that temperature. The five heat transport limits are: the sonic limit, the isothermal limit, the entrainment limit, the capillary pumping limit, and the boiling limit. The first four limits are increasing functions of temperature, while the boiling

limit is a decreasing function of temperature. The phenomena associated with each heat transport limit will now be described. More detailed information on heat transport limits in liquid metal heat pipes can be found in reference 2.

Sonic limit. - As the heat input rate increases, the vapor flow rate leaving the evaporator section of a heat pipe increases in proportion. When the velocity of the vapor leaving the evaporator becomes equal to the sonic velocity, the rate of vapor flow into the condenser section will no longer increase with an increase in the heat input rate. With any further increase in the heat input rate, the rate of evaporation from the wick will exceed the rate of liquid replenishment by returning condensate, the wick will dry out, and the evaporator temperature will rise rapidly. The heat transport rate at which vapor leaving the evaporator reaches sonic velocity is called the sonic limit.

The sonic limit is the highest heat transport rate which is physically achievable in a heat pipe, and can be quite large. For example, the sonic limit in sodium heat pipes at 1500° F is about 93 Btu/sec/in² of vapor space cross-sectional area (ref. 2). At 1700° F, the sonic limit rises to 265 Btu/sec/in² of vapor space cross-sectional area.

At the sonic limit, there is an appreciable axial temperature drop along the evaporator section of a heat pipe, of the order of 100° F to 200° F. Consequently, a heat pipe would not be designed to operate at the sonic limit where heat transport under relatively isothermal conditions is important. However, the sonic limit is frequently encountered during the startup phase of heat pipe operation.

Isothermal limit. - The isothermal limit is the highest heat transport rate for which the temperature drop along the heat pipe axis does not exceed some prescribed allowable maximum temperature drop. The isothermal limit is not a limit in the sense that heat pipe operation will be disrupted if it should be exceeded. Nonetheless, it is a useful concept for design situations where isothermal heat transport is important.

In many applications, an axial temperature drop of 10° F to 20° F would be tolerable. For these cases, the isothermal limit would be about 50 per cent of the sonic limit. However, the isothermal limit could be appreciably smaller if the vapor pressure drop due to friction were to significantly exceed the vapor pressure drop due to momentum generation in the evaporator section, as could occur in a heat pipe with a large length/diameter ratio.

Entrainment limit. - Since, in a heat pipe, the heat pipe vapor and liquid are in direct contact, the flowing vapor exerts a drag force on the adjacent liquid. The drag force is resisted by surface tension at the liquid-vapor interface. When the vapor velocity is sufficiently large, the drag force will exceed

the restraining force of surface tension, and liquid will be entrained in the vapor. The liquid which is entrained will reduce the rate at which the evaporator section of the wick can be replenished by returning condensate, leading to wick dryout and overheating of the evaporator section. The heat transport rate at which entrainment first occurs is called the entrainment limit. The entrainment limit is affected by the size of the wick pores at the liquid-vapor interface as well as by properties of the heat transport fluid. The smaller the wick pores, the larger is the entrainment limit.

Capillary pumping limit. - The capillary pumping limit is related to the fundamental operating principle of heat pipes, and historically was the first recognized limitation on heat pipe heat transport. During heat pipe operation, a difference develops between the vapor pressure and liquid pressure at a given point along the heat pipe axis. This pressure difference is balanced by the surface tension of the curved liquid-vapor interface in the wick pores. As the heat input rate increases, the pressure difference between vapor and liquid increases. The curvature of the liquid-vapor interface must decrease so that a larger component of the surface tension is available to offset the increased pressure differential.

If the heat pipe liquid is fully wetting, as is usually the case with the liquid metals, the minimum possible radius of curvature of the liquid-vapor interface is equal to the effective radius of the wick pores. The heat transfer rate at which the radius of curvature is equal to the pore radius is called the capillary pumping limit. If the heat transport rate is increased further, pressure equilibrium can no longer be maintained in the radial direction, the liquid-vapor interface will be destroyed, and the evaporator section will overheat. The capillary limit can be increased by reducing the resistance to liquid and/or vapor flow in the axial direction, and by reducing the wick pore size at the liquid-vapor interface.

Boiling limit. - During normal heat pipe operation, vapor is produced by evaporation at the liquid-vapor interface. Although the heat pipe liquid is superheated (its pressure is less than that of the adjacent saturated vapor), boiling will not occur until some critical value of superheat is reached. At this critical value, vapor bubbles at nucleation sites in the heat pipe wall are hemispherical, and the difference between the vapor pressure inside the bubbles and the pressure of the external liquid is the maximum which can be balanced by surface tension. The heat transport rate corresponding to this condition is called the boiling limit. Any further increase in the heat transport rate will increase the wall temperature and hence the vapor pressure inside the bubbles, while simultaneously decreasing the liquid pressure. The pressure difference between the inside of the bubble and the surrounding liquid can no longer be balanced by surface tension, and the bubbles will leave the nucleation sites, initiating boiling. While the initiation of boiling is not necessarily catastrophic,

it is best avoided in liquid metal heat pipes because of the large pressure fluctuations which usually characterize boiling in liquid metals.

Because of the large superheat needed to initiate boiling in liquid metals, boiling has rarely been encountered in liquid metal heat pipes. However, depending on the particulars of the heat pipe design, there will be some critical temperature above which the heat transport capacity will be determined by the boiling limit.

Environmental Effects

Heat pipe characteristics can be influenced by the nature of the operating environment. The effects of vibration, acceleration, and gaseous diffusion will now be considered.

Vibration. - Heat pipes have been operated successfully under a vibrational environment typical of that encountered during a missile launch (ref. 3). In one test with a water heat pipe, performance actually improved under vibration, the temperature drop along the heat pipe falling from 2° C to 1° C.

Acceleration. - Since the heat pipe structure for cooling the leading edge of hypersonic aircraft wings will be oriented so that the liquid flow channels are within a few degrees of the horizontal, the influence of gravity on heat pipe performance will be minimal. However, the aircraft may be expected to experience significant longitudinal acceleration and deceleration. Deceleration will tend to facilitate the return of condensate to the heat input region (leading edge) while acceleration will tend to retain condensate in the heat rejection region.

In the case of deceleration, the liquid will develop a static head which acts to reduce the overall liquid pressure drop, the net effect of which is to increase the capillary pumping limit. In the case of acceleration, the liquid develops a static head which acts to increase the overall liquid pressure drop, the net effect of which is to decrease the capillary pumping limit.

If the heat pipe is operating in a temperature range within which the heat transport capacity is determined by the capillary pumping limit, design modifications may be necessary to prevent a drop in heat transport capacity under longitudinal acceleration. These changes would include one or a combination of the following: a reduction in the wick pore size at the liquid-vapor interface, an increase in wick thickness, or substitution of a porous material in the liquid flow channel with less flow resistance.

Gaseous diffusion. - Since the heat pipe is a closed system, any significant internal accumulation of gas could adversely affect performance. The possibility of diffusion of atmospheric gases through the heat pipe walls into the interior over an extended operating period must be considered. While little diffusion data is available for heat pipes, tests have shown that nitrogen can diffuse at a significant rate through stainless steel pipe into a liquid potassium flow loop (ref. 4). There is also evidence that hydrogen, formed by the reduction of water vapor at the heat pipe surface, can diffuse into the interior of a sodium heat pipe quite rapidly.* The diffusion rate is governed by the nature of the diffusing gas, its partial pressure, the heat pipe temperature, the nature and thickness of the heat pipe wall, and the reactivity of the wall material with the diffusing gas.

Extended testing of heat pipes under expected design conditions is presently necessary to assess whether heat pipe performance will be degraded by the diffusion of gas through the walls.

Startup

When a liquid metal heat pipe is at room temperature, the liquid metal may be frozen, and its vapor pressure will be extremely low. The addition of heat at a substantial rate to the evaporator section generally produces in a fairly rapid initial temperature rise in this section, followed by a more gradual temperature rise accompanied by gradual extension of the hot zone into the cold condenser section. If, during the startup period, the heat input rate should exceed the heat transport capacity, the resultant disruption of normal heat pipe operation could result in overheating before the design operating condition was reached. Whether a given heat pipe design will start up normally during a specified heat input transient must ultimately be determined by experiment.

PARAMETRIC STUDY OF HEAT LOAD AND HEAT PIPE LENGTH

The initial step in the design of a heat-pipe-cooled leading edge is to determine the heat load to be transported and the required length of the heat

* Personal communication with J. Kemme, Los Alamos Scientific Laboratory, Los Alamos, N. Mex.

pipe structure. These parameters can be established from the aerodynamic heating rate and the thermal radiation rate along the portion of the wing surface which is covered by the heat pipe structure.

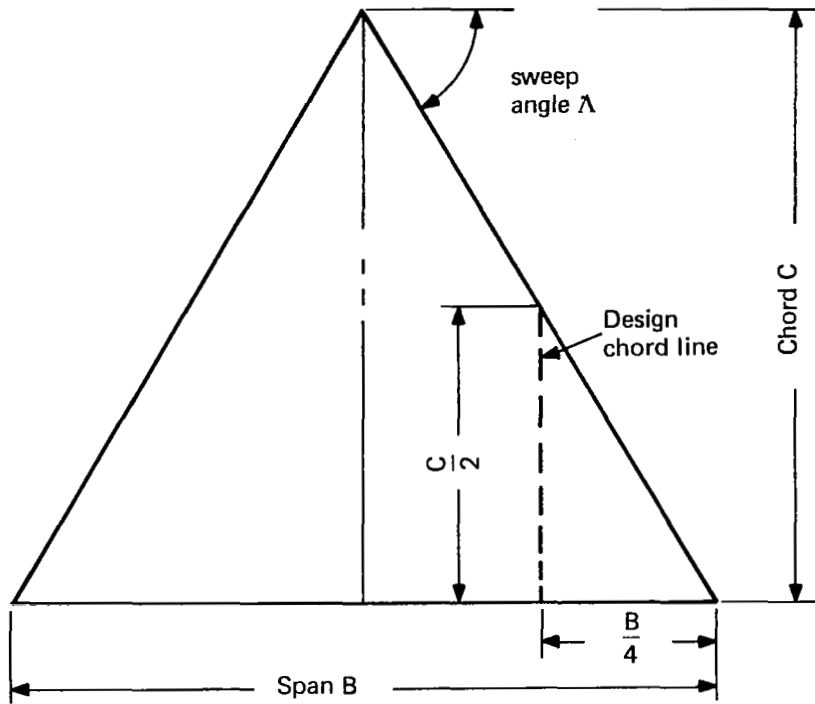
A parametric study was carried out to determine the heat pipe heat load and the heat transport length in the chordwise direction for the range of aircraft cruise conditions and wing geometries presented in table 1, figure 6 and figure 7.

TABLE 1. - INPUT DATA FOR PARAMETRIC STUDY

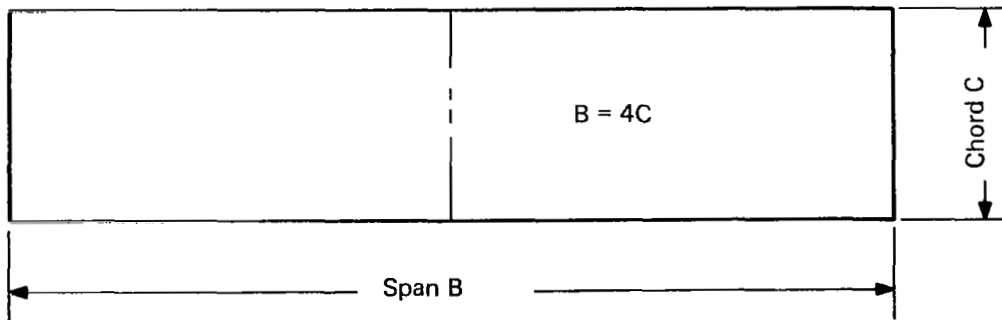
Cruise conditions	
Heat pipe temperature, ° F	1340, 1540, 1740, 1940
Mach number	6, 8, 10, 12
Angle of attack, deg	7
Vertical acceleration	+ 1g (just offsets gravity)
Surface emissivity	0.8
Dynamic pressure	800 psf
Wing geometry	
Sweepback angle, deg	0, 45, 55, 65, 75
Leading edge radius, in. ^a	1/4, 1/2, 1, 2, 6, 12, 24
Area, ft ²	10 000
Planform	See figure 6.
Cross-section	See figure 7.

^a In plane normal to leading edge.

As is shown in figure 6, the wing planform is triangular for sweep angles greater than 0° and rectangular with an aspect ratio (span/chord) of 4 for a sweep angle of 0°. The study was carried out for a wing section located at one-half the semispan. The airfoil shape is shown in figure 7. The maximum thickness is 0.03 times the chord. Longitudinally, the airfoil is divided into three sections, each of equal length. Two wedge-shaped sections flank the constant-thickness central section. The leading edge of the forward wedge is rounded off. As is shown in figure 8, the cross-section of the leading edge is



A. Sweep angle $\Lambda > 0^\circ$



B. Sweep angle $\Lambda = 0^\circ$

Figure 6. Wing planform.

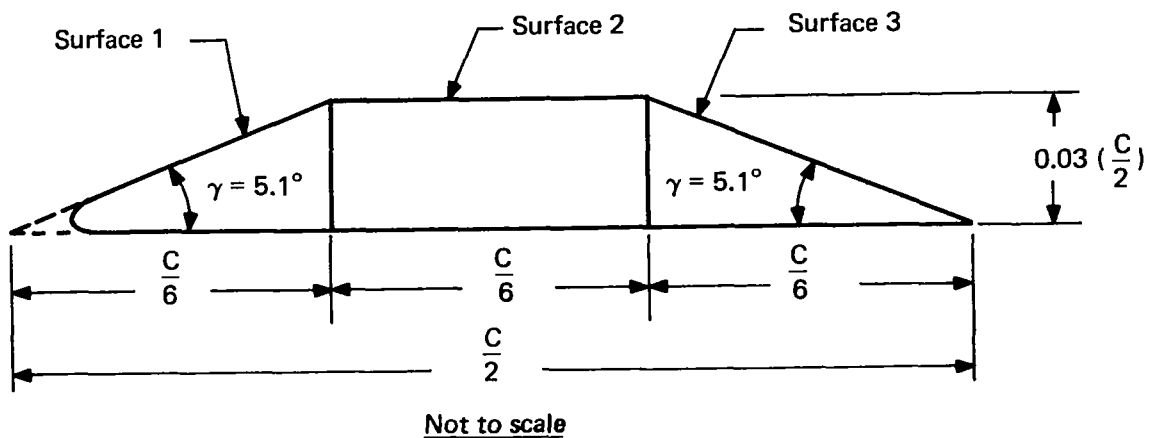
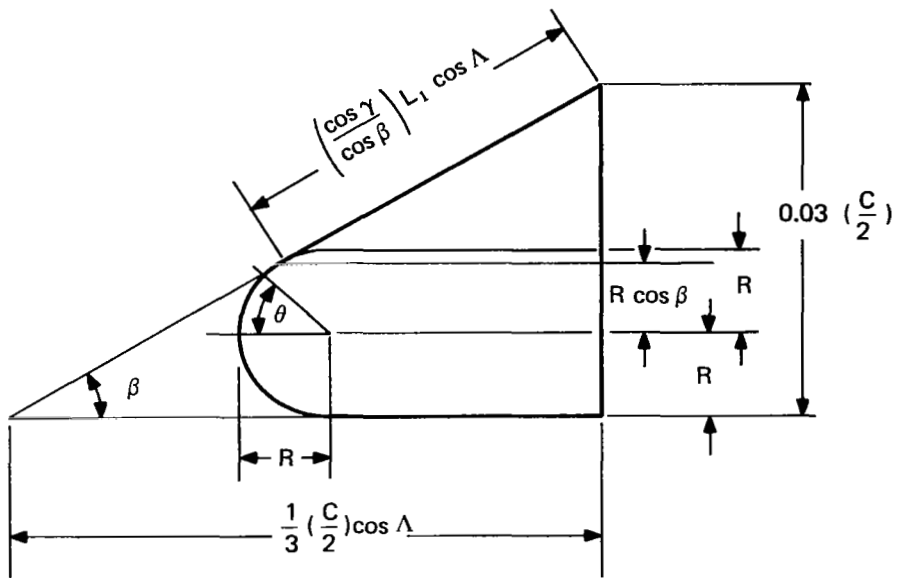


Figure 7. Airfoil shape at one-half wing semispan.

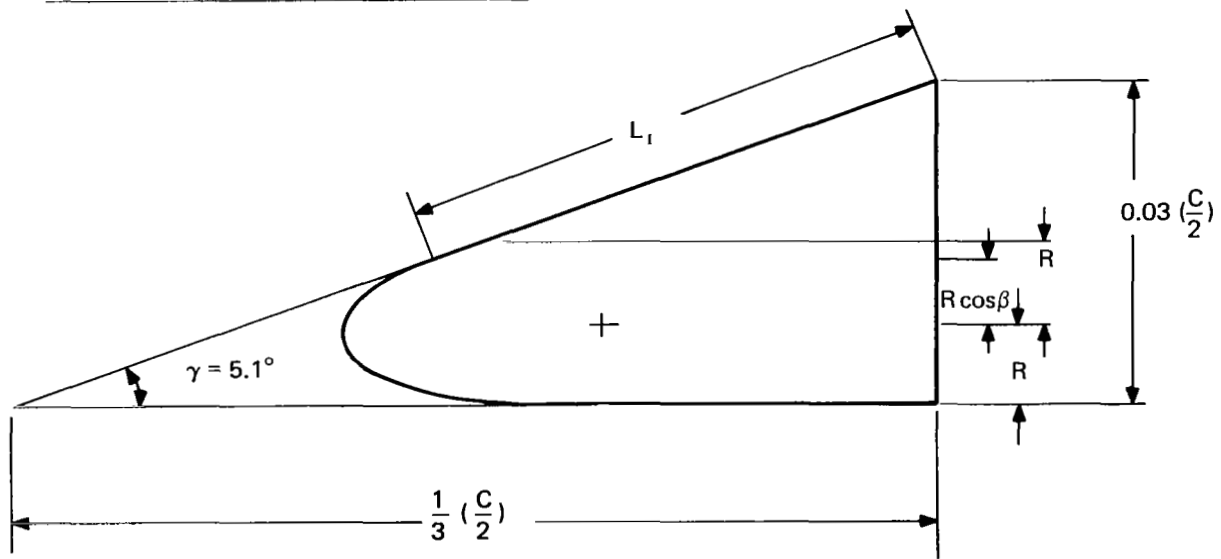
circular in the plane normal to the leading edge and elliptical in the chordal plane.

The airfoil wedge angle γ of 5.1° was established from the basic geometry of figure 7, and is independent of the sweepback angle Λ . The chord $C/2$ was found from the planform geometry and the specified planform area of $10\,000\text{ ft}^2$. It should be noted from figure 7 that the actual chord will be smaller than the calculated value because the leading edge has been rounded off.

Also, airfoils with different leading edge radii are not geometrically similar, the chord decreasing with increasing radius. The geometric differences become quite significant as the leading edge diameter approaches the wing thickness. When the leading edge diameter is equal to the wing thickness, as determined from figure 7, the length of the inclined plane section of the upper wing surface adjacent to the leading edge will have shrunk to zero. When the leading edge diameter exceeds the maximum wing thickness, the thickness was taken to be constant and equal to the leading edge diameter. The principal geometric parameters of the wing are shown in tables 2 and 3 as a function of sweep angle Λ and leading edge radius R .



Plane normal to leading edge (not to scale)



Chordal plane (not to scale)

Figure 8. Geometry of forward section of wing (see Figure 2).

TABLE 2. - GEOMETRIC PARAMETERS OF HYPERSONIC WING

Sweep angle, deg	Chord, ft	Span, ft	Chord at 1/2 semispan, ft	Thickness at 1/2 semispan, ft ^a	Wedge angle β , deg
0	50.0	200.0	50.0	1.50	5.1
45	100.0	200.0	50.0	1.50	7.3
55	119.5	167.4	59.8	1.79	9.0
65	146.4	136.6	73.2	2.20	12.0
75	193.2	103.5	96.6	2.90	19.2

^aWhen the leading edge diameter \geq the thickness shown in this column, the thickness is taken to be equal to the leading edge diameter.

TABLE 3. - LENGTH OF WING SURFACE IN CHORDAL PLANE

Sweep angle, deg	Leading edge radius (in plane normal to leading edge), in.							
	0.25	0.5	1	2	6	12	24	
	Length L_1 of inclined surface adjacent to leading edge, ft							
0	16.28	15.80	14.90	13.01	5.60	0	0	
45	16.28	15.80	14.90	13.01	5.60	0	0	
55	18.82	18.40	17.48	15.60	8.19	0	0	
65	24.0	23.6	22.8	21.2	14.52	4.75	0	
75	32.0	31.6	30.8	29.2	22.6	12.96	0	
Sweep angle, deg	Periphery of semi-ellipse at leading edge, in.							
	0	0.78	1.57	3.14	6.28	18.85	37.7	75.4
	45	0.95	1.90	3.81	7.62	22.8	45.0	91.5
	55	1.10	2.20	4.39	8.78	26.4	52.8	105.6
	65	1.37	2.75	5.50	11.00	33.0	66.0	132.0
	75	2.12	4.24	8.28	16.56	49.6	99.2	198.4

Aerodynamic Heating

Figure 9 shows the stagnation line heat flux due to aerodynamic heating as a function of dynamic pressure (refs. 5, 6). The data apply for a circular leading edge of 1-inch radius, a sweep angle of 0°, and a reference wall temperature T_o of 1540° F. The heat flux incident on the circular leading edge for other conditions was calculated from the expression

$$\frac{q(\Lambda, \theta, R, T_w)}{q(0, 0, 1, T_o)} = \left(\frac{T_{aw} - T_w}{T_{aw} - T_o} \right) \left(\frac{1}{R} \right)^{1/2} \cos \Lambda \cos^{3/2} \theta \quad (1)$$

In equation (1), $q(0, 0, 1, T_o)$ is the stagnation line heat flux given in figure 9, θ is the angle from the stagnation line at which the heat flux is to be determined, Λ is the sweep angle, R is the leading edge radius in inches, T_{aw} is the adiabatic wall temperature in ° F, T_w is the surface temperature in ° F, and $q(\Lambda, \theta, R, T_w)$ is the desired heat flux at sweep angle Λ , angle θ , radius R , and surface temperature T_w .

The adiabatic wall temperature is given in table 4 for a dynamic pressure of 800 psf and angles θ of 0° and 70°. The adiabatic wall temperature corresponding to $\theta = 0^\circ$ (i. e., at the stagnation line) was used for calculations with equation (1).

TABLE 4. - ADIABATIC WALL TEMPERATURE FOR
DYNAMIC PRESSURE OF 800 PSF

Mach number	Adiabatic wall temperature, ° F	
	θ = 0 deg	θ = 70 deg
6	2540	2423
8	4160	4010
10	5390	5255
12	6430	6292

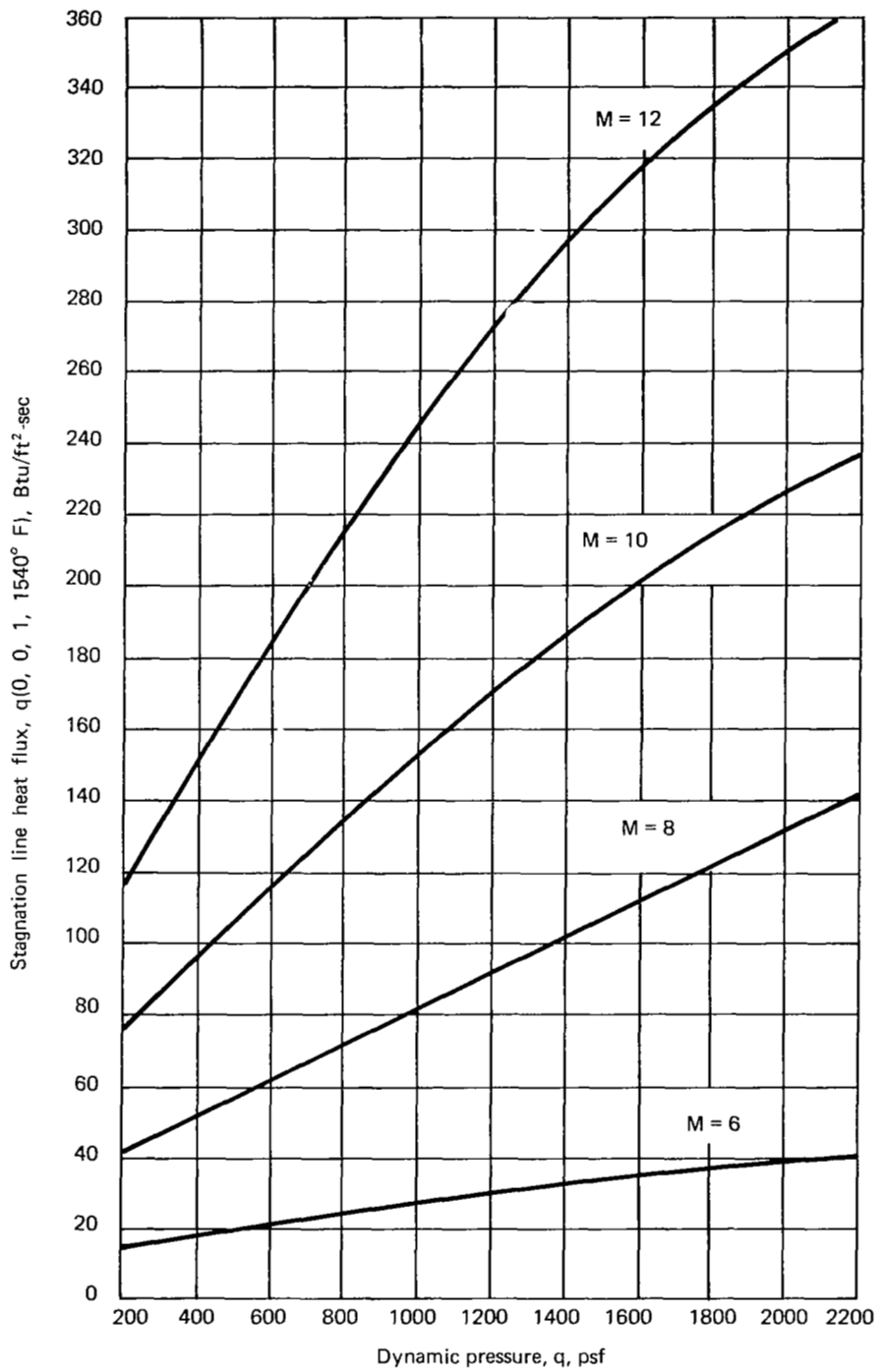


Figure 9. Stagnation line heat flux (refs. 5, 6).

The heat flux due to aerodynamic heating on the flat surfaces of the wing was calculated from the equation

$$q = h (T_{aw} - T_w) \quad (2)$$

In equation (2), q is the heat flux in Btu/ft²-sec and h is the heat transfer coefficient in Btu/ft²-sec°F. The adiabatic wall temperature T_{aw} was taken to be the value for the circular leading edge at the point where the flat surface is tangent to the leading edge. For an angle of attack of 7° and sweep angle in the range 0 to 75°, the point of tangency on the lower wing surface occurs when θ lies in the range 64 to 83°. On the upper wing surface, the point of tangency occurs when θ lies in the range 92 to 96°. Since T_{aw} varies slowly with θ in these ranges, T_{aw} corresponding to $\theta = 70^\circ$ was used for calculations with equation (2).

The heat transfer coefficient h was calculated by the method described in Appendix A. The heat transfer coefficient for a given flat surface was evaluated at a distance from the leading edge of the flat surface at which the Reynolds number was 10^6 . Also, a surface temperature of 1540° F was used in the calculation of h . (The heat transfer coefficient varies slowly with the distance from the leading edge and with the wall temperature.)

The resulting flat-plate heat transfer coefficients are given in table 5. The distance from the leading edge of a given flat surface at which the heat transfer coefficient was evaluated is also given. It can be seen from figure 7 that there is one flat surface on the lower edge of the wing and that there are three flat surfaces on the upper edge of the wing. Heat transfer coefficients for the upper edge are given for surfaces 1 and 2 only. The coefficient for surface 3 is somewhat smaller than that calculated for surface 2.

TABLE 5. - HEAT TRANSFER COEFFICIENTS FOR FLAT SURFACES OF WING

Mach number	Surface ^a	Distance from leading edge of flat surface, ft	Heat transfer coefficient, Btu/ft ² -sec-° F
6	Lower	0.72	45.5 x 10 ⁻⁴
	Upper -1	1.25	15.02 x 10 ⁻⁴
	Upper -2	1.77	7.70 x 10 ⁻⁴
8	Lower	0.74	37.5 x 10 ⁻⁴
	Upper -1	1.38	9.56 x 10 ⁻⁴
	Upper -2	3.18	3.60 x 10 ⁻⁴
10	Lower	0.97	32.2 x 10 ⁻⁴
	Upper -1	2.44	5.85 x 10 ⁻⁴
	Upper -2	4.98	1.62 x 10 ⁻⁴
12	Lower	1.05	28.6 x 10 ⁻⁴
	Upper -1	3.20	3.64 x 10 ⁻⁴
	Upper -2	8.23	0.63 x 10 ⁻⁴

^a See figure 7.

Radiation Equilibrium Temperatures

While not explicitly required for the determination of heat pipe heat loads and lengths, radiation equilibrium temperatures are nevertheless of interest. The radiation equilibrium temperature is the temperature which would exist at a perfectly insulated segment of wing surface when the rate of heat loss by radiation from that segment just equals the rate at which heat is added by aerodynamic heating. Actual equilibrium temperatures will be somewhat lower than those calculated according to the above definition because some of the incident heat will be dissipated by conduction and radiation to adjacent cooler portions of the wing structure.

The radiation equilibrium temperatures at the stagnation line and on the flat surfaces of the wing are of most interest. The stagnation line radiation equilibrium temperature is the maximum wing temperature which could develop

without cooling, and thus is indicative of the need for cooling. The heat pipe temperature must exceed the radiation equilibrium temperature on the flat surfaces if heat from the leading edge is to be rejected in addition to the heat which is directly incident on those surfaces.

Radiation equilibrium temperatures at the stagnation line are given in table 6. The equilibrium temperature is seen to increase with Mach number and to decrease as the leading edge radius and sweep angle increase.

TABLE 6. - RADIATION EQUILIBRIUM TEMPERATURES AT STAGNATION LINE (Dynamic pressure = 800 psf)

Mach number	Sweep angle, deg	Leading edge radius, in.						
		0.25	0.50	1	2	6	12	24
		Equilibrium temperature, ° F						
6	0	2170	2080	1980	1875	1702	1601	1470
	45	2078	1980	1875	1771	1601	1470	-
	55	2022	1918	1811	1697	1516	-	-
	65	1929	1827	1709	1597	-	-	-
	75	1773	1665	1552	1433	-	-	-
8	0	3080	2909	2727	2540	2275	2090	1940
	45	2909	2727	2540	2369	2090	1940	1773
	55	2800	2620	2440	2270	1997	1840	1684
	65	2640	2465	2290	2110	1854	1698	1540
	75	2400	2220	2050	1882	1651	1480	-
10	0	3720	3500	3280	3050	2711	2500	2300
	45	3500	3280	3050	2830	2500	2300	2110
	55	3360	3150	2920	2710	2380	2180	1998
	65	3160	2940	2720	2530	2210	2020	1848
	75	2850	2630	2440	2240	1940	1780	1620

TABLE 6. - Continued

Mach number	Sweep angle, deg	Leading edge radius, in.						
		0.25	0.50	1	2	6	12	24
		Equilibrium temperature, ° F						
12	0	4265	4010	3740	3500	3080	2840	2620
	45	4010	3740	3500	3230	2840	2620	2410
	55	3840	3590	3330	3090	2720	2490	2280
	65	3630	3361	3120	2880	2520	2320	2120
	75	3250	3015	2770	2570	2230	2023	1840

If a maximum permissible structural temperature of 1600° F is assumed, which would be feasible with superalloy construction, table 6 indicates that cooling will be required for all sweep angles and leading edge radii at Mach numbers greater than 10. At Mach 8, cooling will be required for leading edge radii up to 6 in., and for larger leading edge radii at sweep angles of 55° and less. At Mach 6, cooling will be required for leading edge radii of 0.5 in. and less, and may be required for leading edge radii up to 6 in., depending on the sweep angle.

For a maximum permissible structural temperature of 2200° F, cooling will be required at Mach 12 for leading edge radii up to 6 in., and at Mach 10 for leading edge radii up to 2 in. Cooling may be required at these Mach numbers for leading edge radii up to 24 inches, depending on the sweep angle. At Mach 8, cooling will be required for leading edge radii up to 0.5 in., and may be needed for leading edge radii up to 6 in., depending on the sweep angle. At Mach 6, cooling is not needed.

These relationships are shown more clearly in figure 10, where the leading edge radii for stagnation line equilibrium temperatures of 1600° F and 2200° F are plotted as a function of Mach number and sweep angle.

Estimated equilibrium temperatures for the flat wing surfaces are shown in figure 11 as a function of Mach number. For the upper surface, temperatures are given for surface 1 only. Equilibrium temperatures on surface 2 will be considerably lower than for surface 1 because of the lower heat transfer coefficients for surface 2. (See table 5.) Since, as has already been pointed out, the heat pipe temperature must exceed the equilibrium temperature, it is

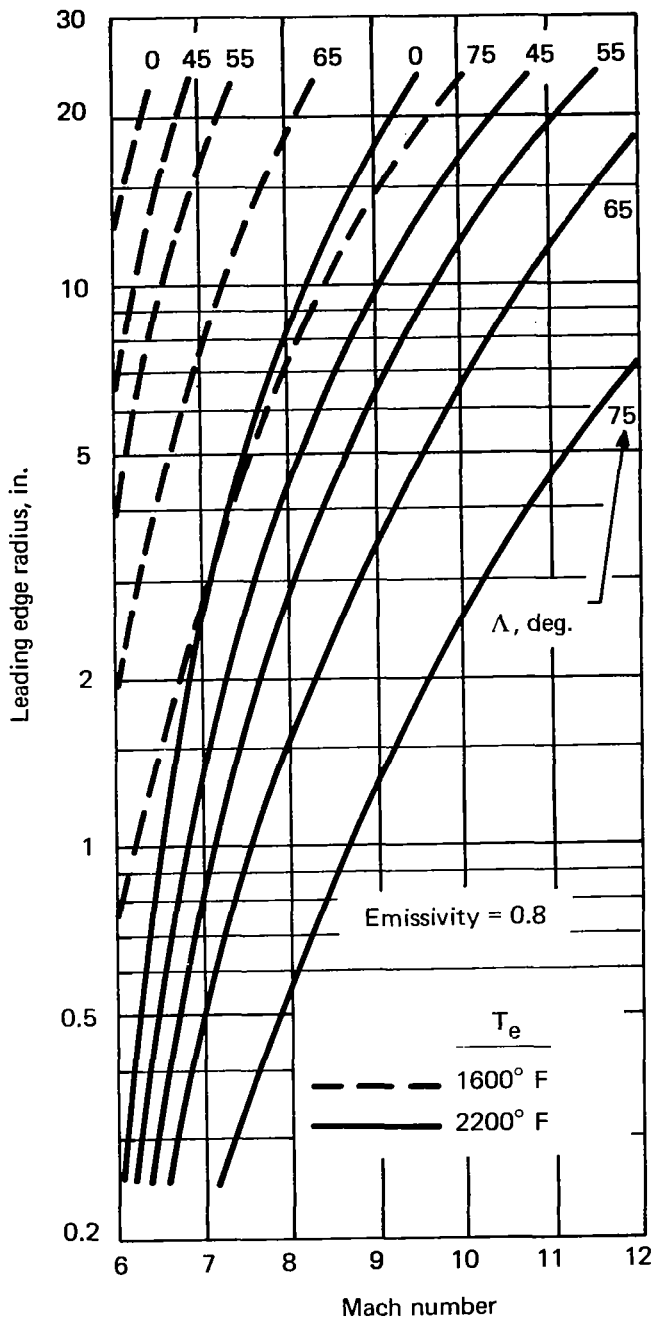


Figure 10. Leading edge radius for stagnation line radiation equilibrium temperatures of 1600° F and 2200° F.

evident from figure 11 that much higher heat pipe temperatures will be required to dissipate heat from the lower wing surface than from the upper surface. Therefore, the upper surface is preferred for the heat rejection portion of the heat pipe cooling structure. Further, the minimum possible heat pipe temperature will be approximately 1200° F. In the parametric study of heat pipe length and heat load, a minimum heat pipe temperature of 1340° F was selected.

Heat Pipe Heat Load

The heat pipe heat load is the rate at which heat is transported from the heat input zone to the heat rejection zone of the heat pipe cooling structure. Its determination requires knowledge of the heat flux distribution over the surface of the heat pipe cooling structure.

As is shown in figure 12, the heat pipe cooling structure is assumed to completely cover the rounded leading edge of the wing and a portion of the upper surface. Depending on the length which is needed to dissipate heat, the structure may extend over surfaces 1 and 2 as shown, or it may be confined to a portion of surface 1. For the larger leading edge radii, if surface 1 does not exist, the

heat pipe cooling structure will cover a portion of surface 2 in addition to the rounded leading edge.

The heat pipe cooling structure can also be extended over a portion of the flat lower surface. Then, if the heat pipe temperature is higher than the equilibrium temperature of the lower surface, additional heat dissipation surface will be available. If the heat pipe temperature is lower than the equilibrium temperature, the heat pipe heat load will be increased, requiring additional dissipative surface on the upper surface of the wing. In the parametric study, the heat pipe structure was assumed to cover only the rounded leading edge and a portion of the upper wing surface.

The assumed distribution of heat flux due to aerodynamic heating over the heat pipe surface is also shown in figure 12.* The distribution over the rounded leading edge is given by equation (1). However, the actual heat flux is not symmetrical around the leading edge. Instead, the stagnation line position, which is determined by the angle of attack, is displaced toward the lower surface. While the heat flux distribution is influenced by the angle of attack, the integral of the heat flux, which is required in order

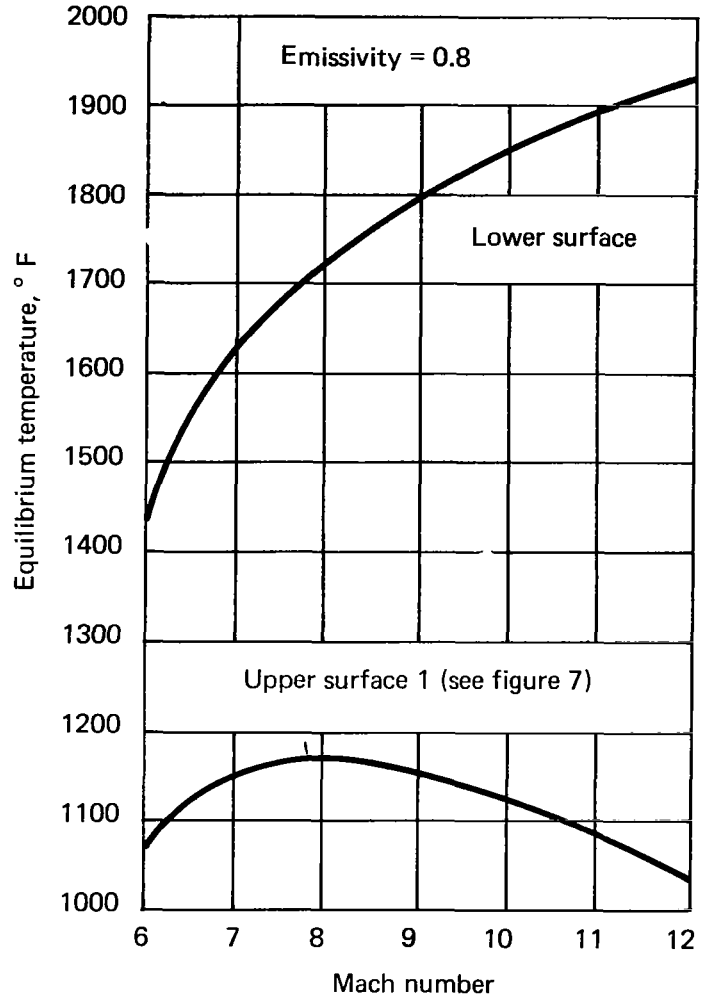


Figure 11. Radiation equilibrium temperatures for flat wing surfaces.

* The heat flux distribution in the region where the cylindrical and flat sections merge is not accurately represented in figure 12. However, the representation of figure 12 was considered sufficiently precise for these preliminary studies.

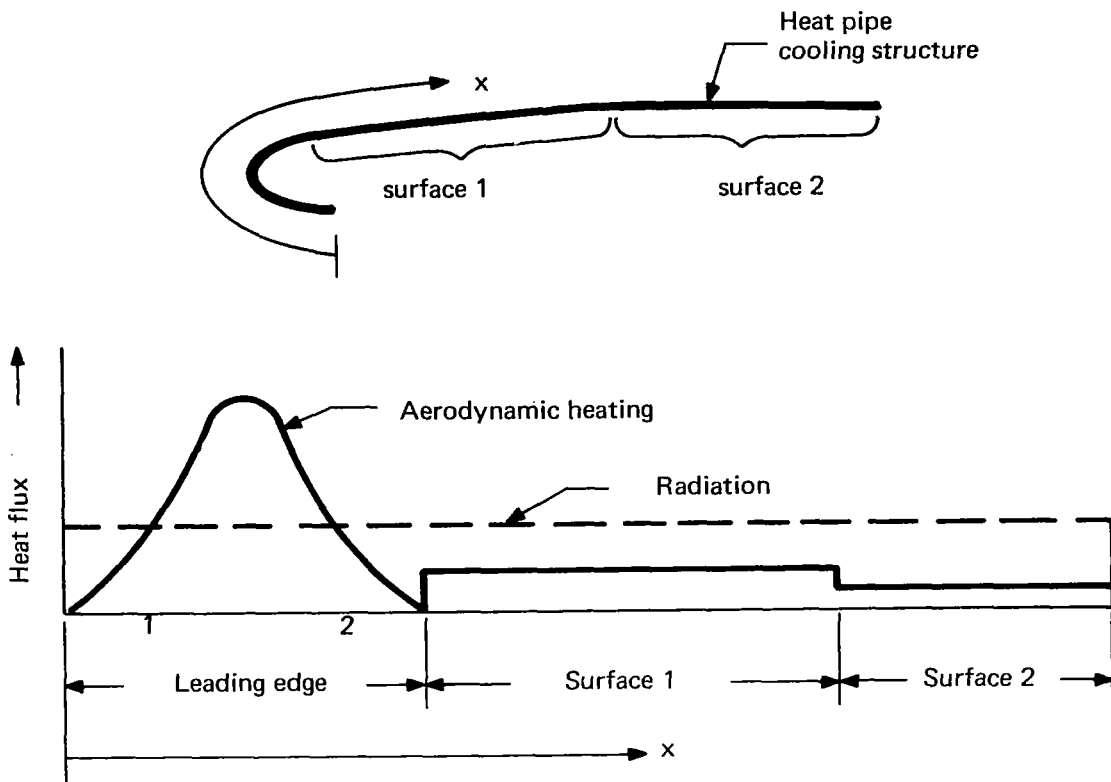


Figure 12. Heat flux distribution over surface of heat pipe cooling structure.

to determine the heat pipe heat load, does not vary strongly with the angle of attack. Therefore, the symmetrical distribution of figure 12, which corresponds to an angle of attack of 0° , was used in the heat load calculations.

The heat flux due to aerodynamic heating over each flat upper surface of the wing is assumed to be constant and equal to the heat flux at the point where the Reynolds number is equal to 10^6 . This generally occurs within a foot or so of the leading edge of the flat surface. (See table 5.) The heat flux actually diminishes continuously with distance from the leading edge.

The radiation heat flux (rate of heat rejection by radiation per unit surface area) is assumed to be constant over the entire length of the heat pipe cooling structure. This is equivalent to the assumption that the surface temperature of the heat pipe cooling structure is constant. Although the internal temperature of the heat pipe structure (i. e., the temperature of the heat pipe vapor) may be regarded as virtually constant, the surface temperature will

vary as the result of the temperature differences which are associated with the conduction of heat into and out of the heat pipe interior. This temperature difference is small over the heat rejection portion of the heat pipe structure (because the radiation heat flux is relatively small) and may be neglected. However, the temperature drop between the surface and the interior is significant over the heat input section, and is a maximum at the stagnation line, because of the high heat flux due to aerodynamic heating in that region.

Neglect of the higher surface temperature in the vicinity of the stagnation line underestimates the rate of heat loss by radiation from the leading edge and has the effect of overestimating the heat load of the heat pipe structure. However, when the stagnation line heat flux due to aerodynamic heating is large enough to cause an appreciable temperature drop through the wall and wick of the heat pipe structure, it is generally much larger than the radiation heat flux. The assumption of constant radiation heat load therefore results in a relatively small error in calculation of the heat pipe heat load.

The heat pipe heat load is obtained by integrating the net heat flux (that due to aerodynamic heating minus the radiation heat flux) over that portion of the wing surface for which the net heat flux is positive. The integration is carried out most readily along the surface coordinates x and $R\theta$, where x is the distance along the leading edge and $R\theta$ is the distance along the circumference of the circular section normal to the leading edge.

The heat pipe heat load Q is given by

$$Q = \frac{2 B R}{144 \cos \Lambda} \int_0^{\theta'} \left[q(\Lambda, \theta, R, T_w) - \epsilon \sigma T_w^4 \right] d\theta \quad (3)$$

where σ is the Stefan-Boltzmann radiation constant (0.476×10^{-12} Btu/ft²-sec-°R⁴), ϵ is the surface emissivity (0.8 from table 1), and the span B and leading edge radius R are expressed in inches. The integration limit θ' is the angle at which the bracketed term in equation (3) is equal to zero. With the aid of equation (1), it then follows that

$$\cos \theta' = \left[\frac{0.38 (T_w/1000)^4}{q(\Lambda, 0, R, T_w)} \right]^{2/3} \quad (4)$$

where $q(\Lambda, 0, R, T_w)$ is the stagnation line heat flux. In equation (4), numerical values have been substituted for the product $\epsilon \sigma$.

Upon substitution of equation (1) into equation (3), the heat pipe heat load per unit span width Q/B can be written

$$\frac{Q}{B} = \frac{R}{72 \cos \Lambda} \left[q(\Lambda, 0, R, T_w) \int_0^{\theta'} \cos^{3/2} \theta \, d\theta - 0.38 \theta' \left(\frac{T_w}{1000} \right)^4 \right] \quad (5)$$

The units of Q/B in equation (5) are Btu/sec-in. The angle θ' is obtained from equation (4), and is expressed in radians.

Curves of the heat load per unit span width are presented in figures 13, 14, and 15 as a function of heat pipe vapor temperature (approximately equal to the wing surface temperature away from the leading edge), Mach number, sweep angle, and leading edge radius. The first observation to be made from these figures is that the heat load decreases as the vapor temperature and sweep angle become larger, and increases as the Mach number and leading edge radius become larger. Thus, from the standpoint of minimizing the heat pipe load for a specified Mach number, small leading edge radii, large sweep angles, and high heat pipe vapor temperatures are desirable.

When the vapor temperature is equal to the stagnation line equilibrium temperature, the radiation heat flux will be equal to that due to aerodynamic heating, and the heat pipe heat load will drop to zero. The vapor temperatures at which leading edge cooling is no longer needed are equal to the radiation equilibrium temperatures of table 6.

The heat load varies from a minimum of about 0.05 Btu/in-sec at Mach 6 and $R = 0.25$ in. to a maximum of about 10 Btu/in-sec at Mach 12 and $R = 24$ in. These heat loads are well within the demonstrated capability of liquid metal heat pipes. For example, a sodium heat pipe with a diameter of 0.7 in. has operated at power levels up to 9.3 Btu/sec at a temperature of 1400° F (ref. 7). The maximum heat load transported by this heat pipe per unit diameter is $9.3/0.7 = 13.3$ Btu/in-sec.

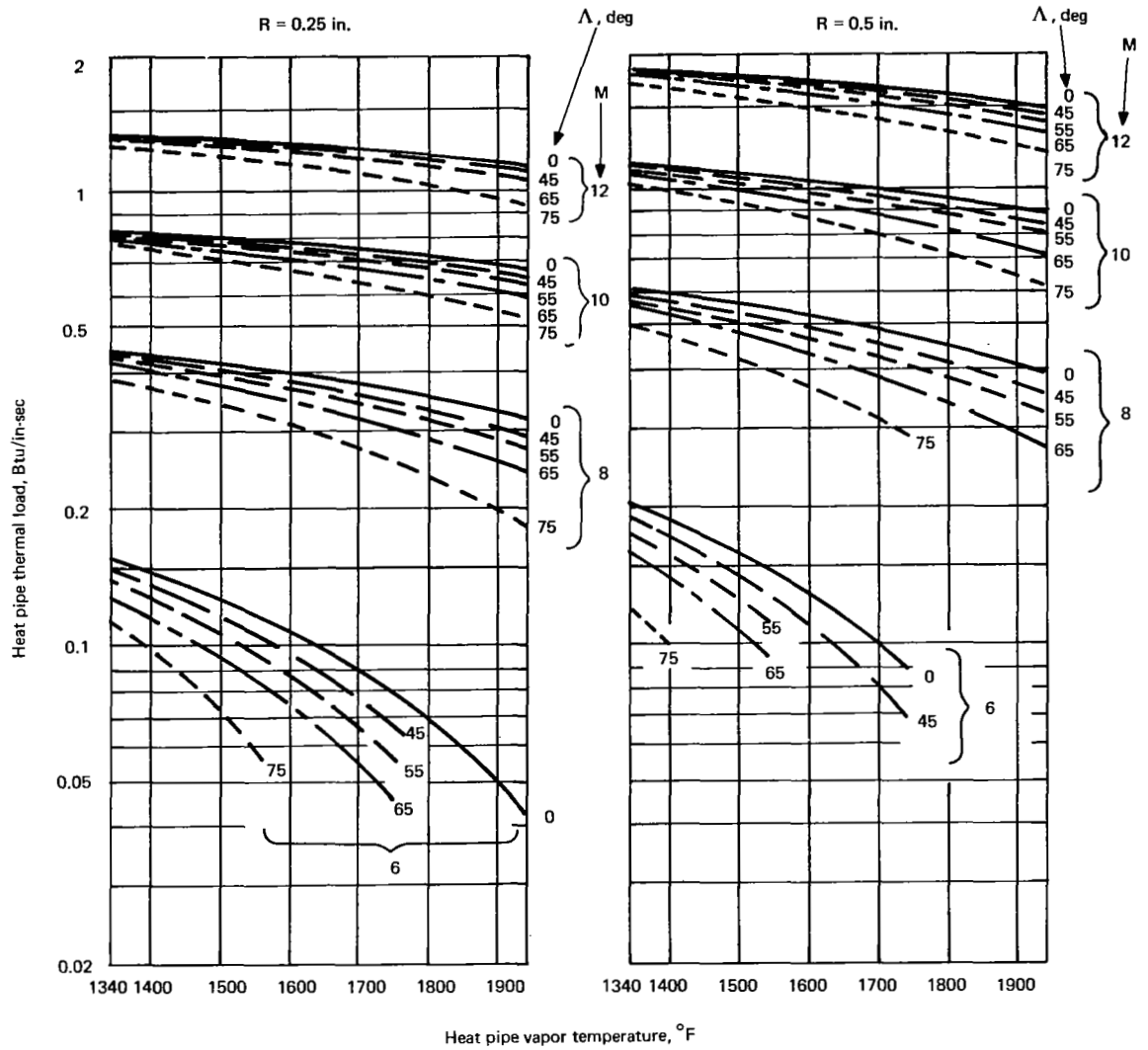


Figure 13. Heat pipe thermal load.

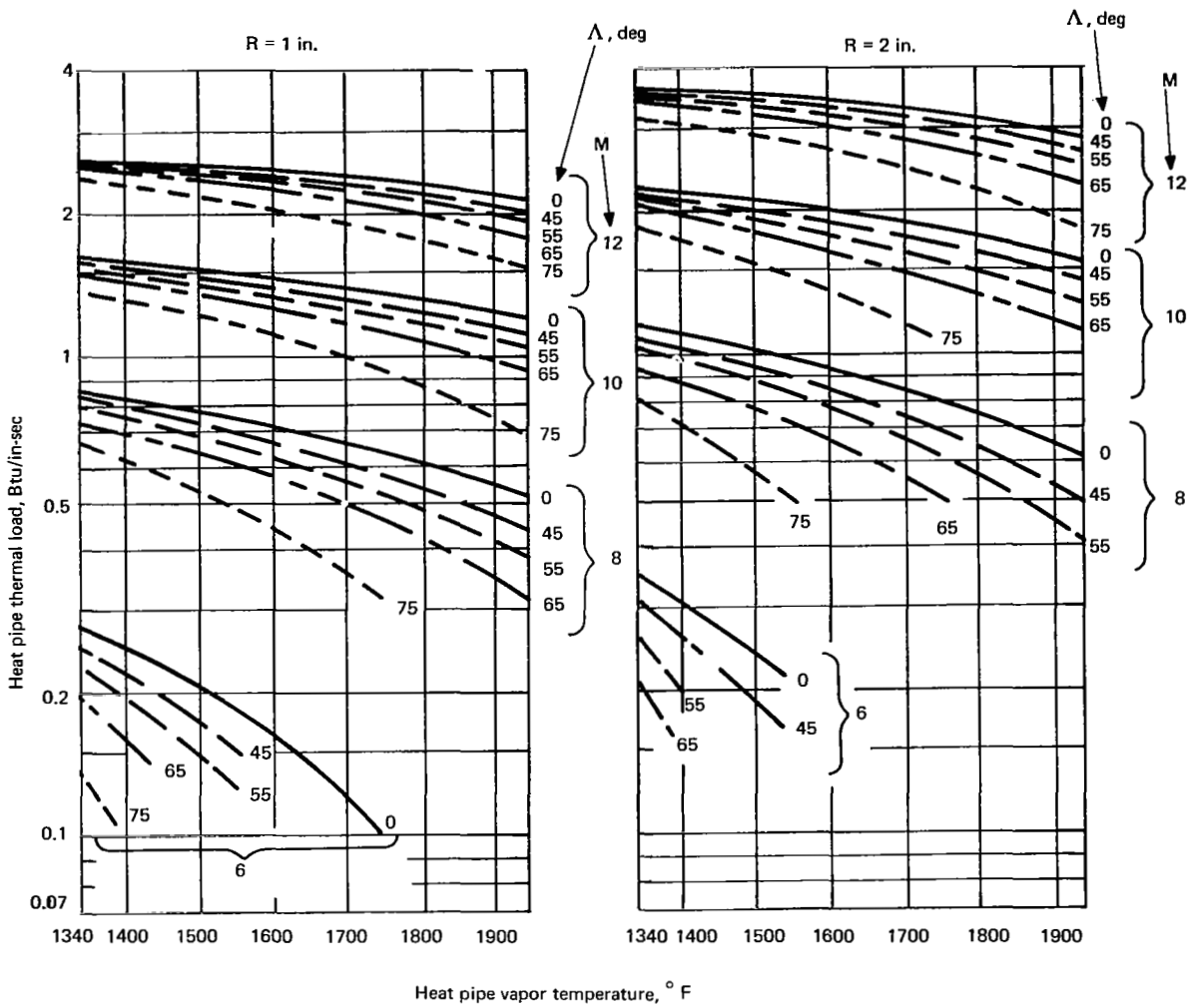


Figure 14. Heat pipe thermal load.

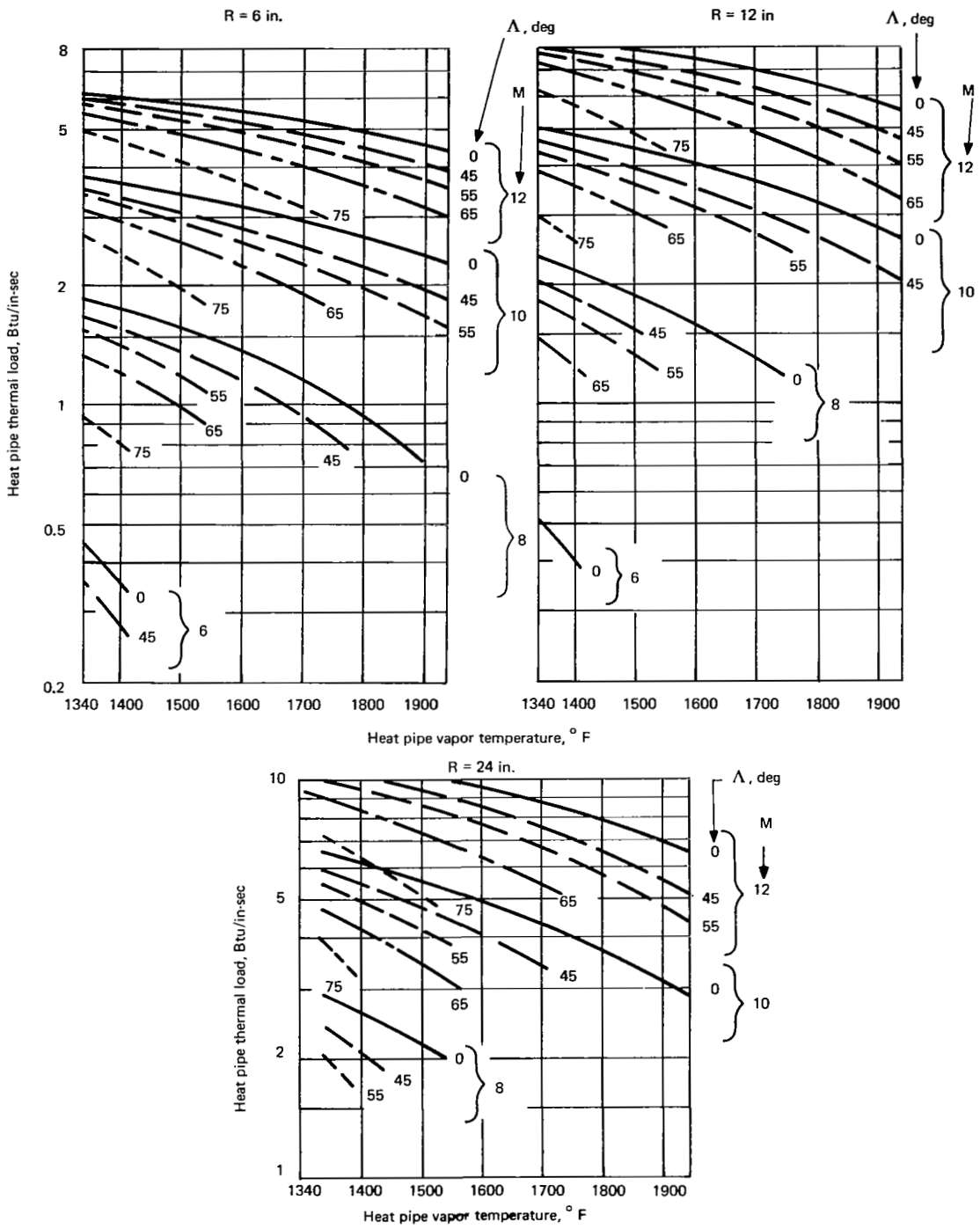


Figure 15. Heat pipe thermal load.

Maximum Surface Temperature

The maximum surface temperature exists at the stagnation line, and its magnitude depends on the thermal resistance between the surface and the heat pipe vapor as well as the stagnation line heat flux. The factors upon which the thermal resistance depends can only be established through detailed consideration of heat pipe design. In order to indicate the approximate maximum surface temperatures which are associated with the range of parameters used in the parametric study, one-dimensional temperature drop calculations at the stagnation line were carried out for a 20-mil-thick wall of Haynes 25, a 10-mil-thick wick assumed to have the thermal conductivity of liquid sodium, and a negligible thermal resistance at the liquid-vapor interface.

Results of the temperature drop calculations are given in figure 16. The maximum temperature T_m for a given heat pipe vapor temperature T_v ($\approx T_w$), leading edge radius R , sweep angle Λ , and Mach number may then be found by adding the temperature drop ΔT from figure 16 to T_v . The largest ΔT is on the order of 200°F and occurs at Mach 12, $R = 0.25 \text{ in.}$, and $\Lambda = 0^\circ$. With these conditions, the maximum surface temperature for a heat pipe vapor temperature of 1600°F would be about 1800°F . Materials selection and mechanical design of the heat pipe cooling structure would then be determined by conditions at 1800°F , despite the fact that the bulk of the structure was at 1600°F .

To take full advantage of the basically isothermal character of heat pipes, it would be preferable to select design conditions for which the temperature drop across the wall and wick at the stagnation line is of the order of 50°F or less. For example, the ΔT at Mach 12 would be reduced from 200°F to about 50°F by simultaneously increasing the sweep angle from 0 to 70° and the leading edge radius from 0.25 to 0.5 in.

Heat Pipe Length

The heat pipe length L is equal to the sum of the distance s around the curved leading edge plus the distance L_c along the flat upper surface over which the heat pipe structure extends, as is shown in figure 17. The distance s is given in table 3. The distance L_c is found by equating the rate of thermal radiation from the flat upper surfaces of the heat pipe cooling structure to the sum of the heat load Q_c transported from the leading edge and the aerodynamic heating rate Q_e on the flat surfaces.

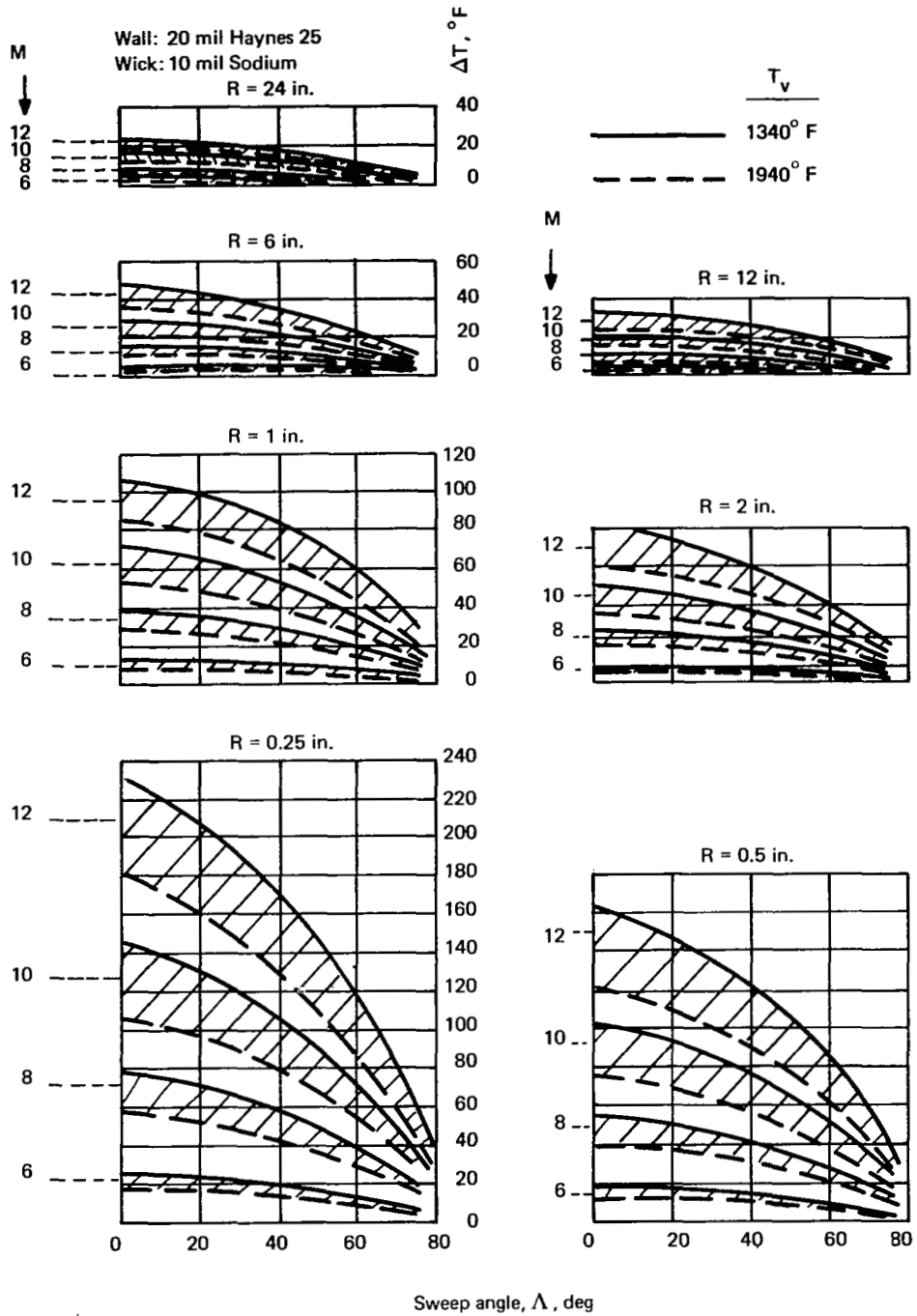


Figure 16. Temperature drop through wall and wick at stagnation line.

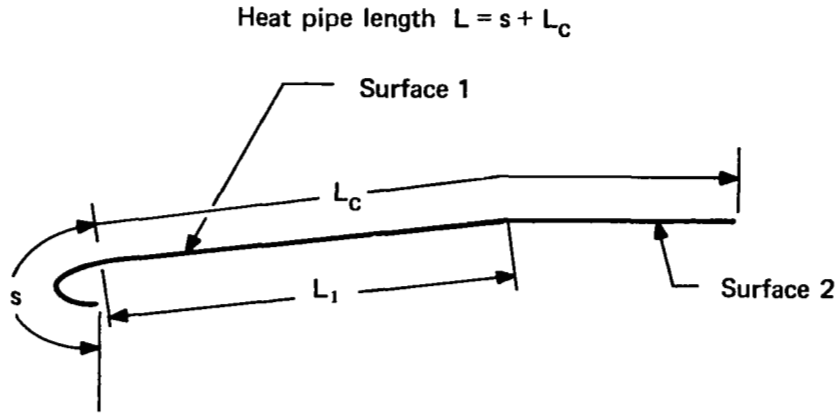


Figure 17. Heat pipe length in chordal plane.

The heat load Q_c is obtained from equation (5) by letting $\theta' = \pi/2$ radians (i. e., by integrating the net heat load over the entire surface of the rounded leading edge). Then, with Q_c in place of Q , equation (5) becomes

$$\frac{Q_c}{B} = \frac{R}{144 \cos \Lambda} \left[1.745 q(\Lambda, 0, R, T_w) - 1.192 \left(\frac{T_w}{1000} \right)^4 \right] \quad (6)$$

The heat flux due to aerodynamic heating on the flat surfaces is given by equation (2).

The following energy balances per unit span width may now be written.

$$\frac{0.38}{144} \left(\frac{T_w}{1000} \right)^4 L_c = \frac{h_1}{144} (T_{aw} - T_w) L_c + \left(\frac{Q_c}{B} \right), \quad L_c < L_1 \quad (7)$$

$$\frac{0.38}{144} \left(\frac{T_w}{1000} \right)^4 L_c = \frac{h_1}{144} (T_{aw} - T_w) L_1 + \frac{h_2}{144} (T_{aw} - T_w) (L_c - L_1) + \left(\frac{Q_c}{B} \right), \quad L_c \geq L_1 \quad (8)$$

In equations (7) and (8), L_1 and L_c are given in inches. The heat transfer coefficients h_1 and h_2 for surfaces 1 and 2 are given in table 5, and Q_c/B is obtained from equation (6). The length L_1 is given in table 3.

Upon solving the above equations for L_c ,

$$L_c = \frac{144 (Q_c/B)}{0.38 (T_w/1000)^4 - h_1 (T_{aw} - T_w)} \quad , L_c < L_1 \quad (9)$$

$$L_c = \frac{144 (Q_c/B) + (h_1 - h_2) (T_{aw} - T_w) L_1}{0.38 (T_w/1000)^4 - h_2 (T_{aw} - T_w)} \quad , L_c \geq L_1 \quad (10)$$

The results of the heat pipe length calculations are presented in figures 18, 19, and 20. The heat pipe length is plotted as a function of the maximum heat pipe temperature T_m instead of the heat pipe vapor temperature $T_v (\approx T_w)$ as was done for the heat pipe thermal load plots of figures 13, 14, and 15.* The curves of figures 18, 19, and 20 apply for a 20-mil-thick Haynes 25 wall and a 10-mil-thick sodium wick.

The heat pipe length L corresponding to a given vapor temperature T_v can be found by obtaining ΔT from figure 16, calculating $T_m = T_v + \Delta T$, and reading L from figure 18, 19, or 20.

Examination of figures 18, 19, and 20 shows that the heat pipe length increases with an increase in Mach number M and leading edge radius R , and decreases with an increase in sweep angle Λ and maximum heat pipe temperature T_m . Heat pipe lengths smaller than the peripheral length s around the leading edge were not calculated. This is why some of the curves do not extend over the full range of heat pipe temperatures.

* The plot of heat pipe length versus maximum temperature gives a more accurate picture of actual length requirements, since it is the maximum heat pipe temperature rather than the vapor temperature which will be established by material temperature limitations.

Wall: 20 mil Haynes 25
Wick: 10 mil sodium

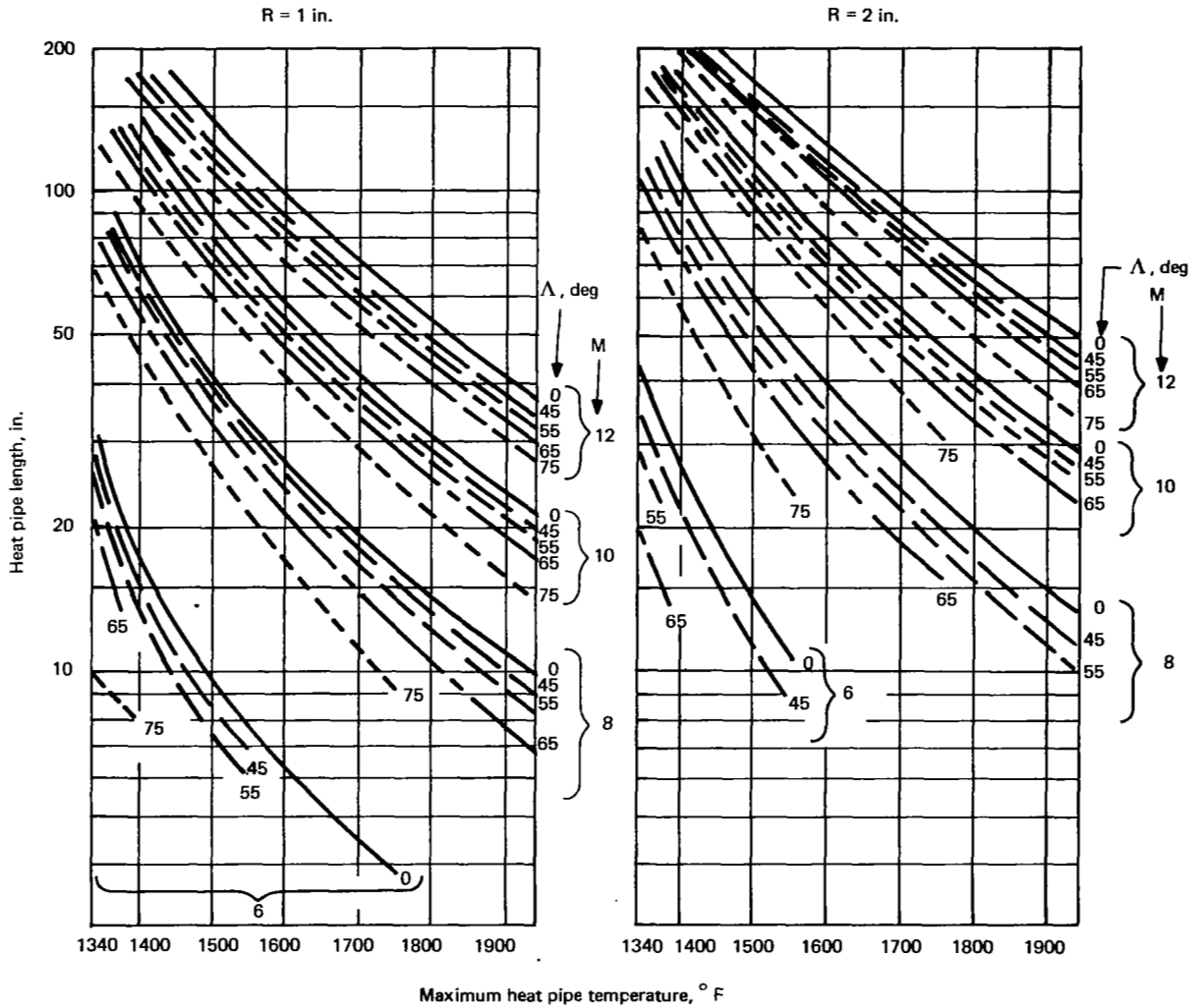


Figure 19. Heat pipe length.

Wall: 20 mil Haynes 25
 Wick: 10 mil sodium

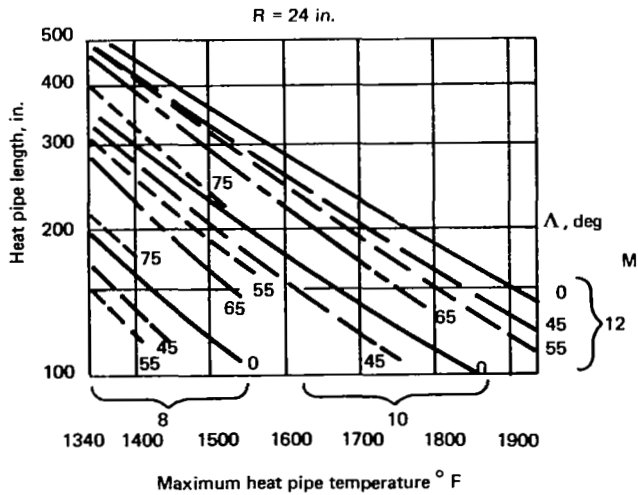
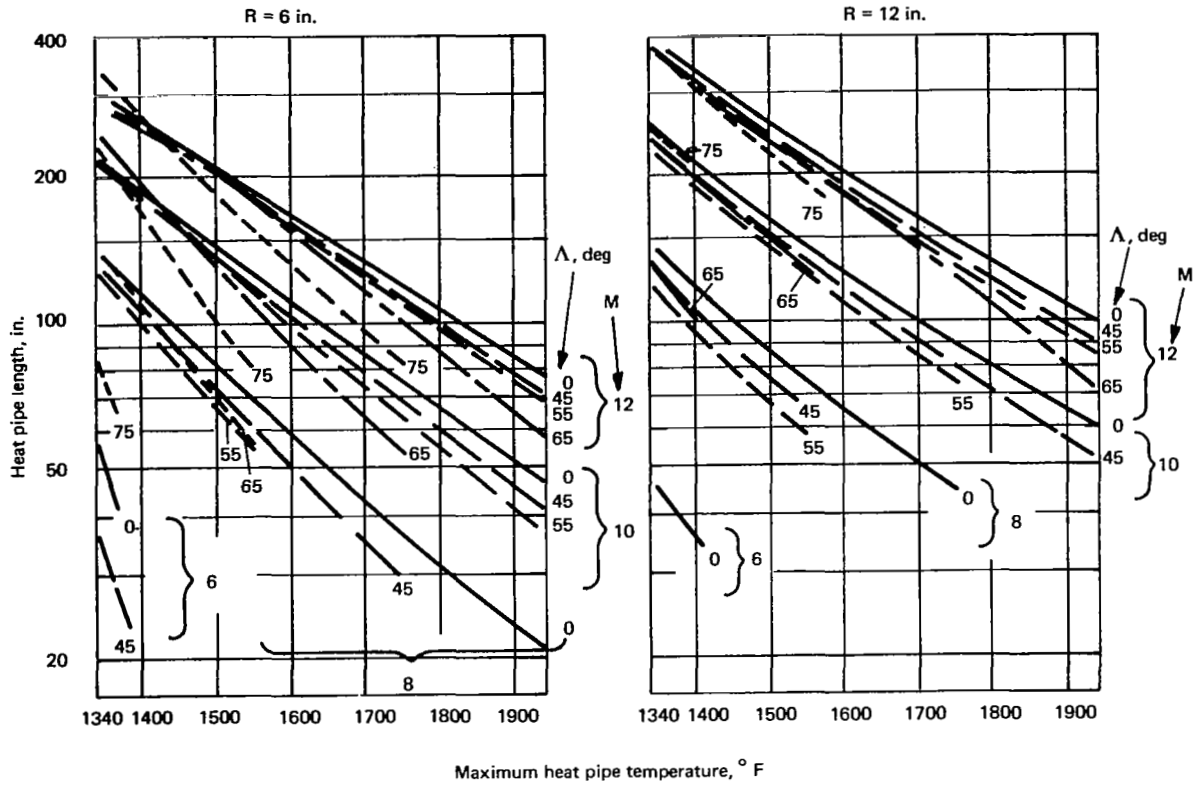


Figure 20. Heat pipe length.

The calculated heat pipe lengths range from a minimum of less than 2 in. for $M = 6$ and $R = 0.25$ in. to a maximum of 500 in. for $M = 12$ and $R = 24$ in. It is unlikely that the 500-inch-length would represent an actual design criterion, since it corresponds to $\Lambda = 0^\circ$ and $T_m = 1360^\circ$ F. A more reasonable design might specify $\Lambda = 65^\circ$ and $T_m = 1600^\circ$ F, for which the maximum heat pipe length at $M = 12$ and $R = 24$ in. is then 230 in. (19.2 ft). Since heat pipes almost 16 ft in length have already been constructed (ref. 8), the required heat pipe lengths for cooling hypersonic aircraft wings should be fabricable. Also, since the heat pipe lengths are a small fraction of the chord at $1/2$ the semispan (as is apparent from table 2), cooling protection can be provided over most of the wing span. If the wing tips were clipped at the minimum chord needed to accommodate the heat pipe length, full cooling protection could then be afforded over the entire wingspan.

It should also be noted that if the flow direction of the heat pipe fluid were to lie in a plane normal to the leading edge instead of in the chordal plane, the effective heat pipe length would be reduced by approximately $\cos \Lambda$. Thus, the heat pipe length of 19.2 ft mentioned in the previous paragraph would be reduced to 8.12 ft if the flow direction of the heat pipe were oriented normal to the leading edge.

PRELIMINARY DESIGN STUDIES

In the previous section, calculations of the heat load and heat pipe length were made for a wide range of Mach numbers, sweep angles, leading edge radii, and heat pipe vapor temperatures. The calculations were performed solely on the basis of aerodynamic heating rates, thermal radiation rates, and wing geometry. Further consideration of the design of heat pipe structures for cooling hypersonic aircraft wings requires that heat pipe characteristics be considered in some detail.

In this section, the selection of a heat pipe fluid and heat pipe fabrication materials are discussed first. Then, minimum heat pipe dimensions normal to the wing surface are estimated. Next, preliminary designs of heat pipe cooling structures for operation at Mach 8 are described. Finally, the effect of variations in design and operating criteria are considered.

Selection of Heat Pipe Fluid

As was stated earlier, an important first criterion for selection of a heat pipe fluid is that its vapor pressure lie approximately within the range of 1 to 100 psia at the contemplated operating temperature. In figure 21, the vapor pressures of four candidate heat pipe fluids are shown over the

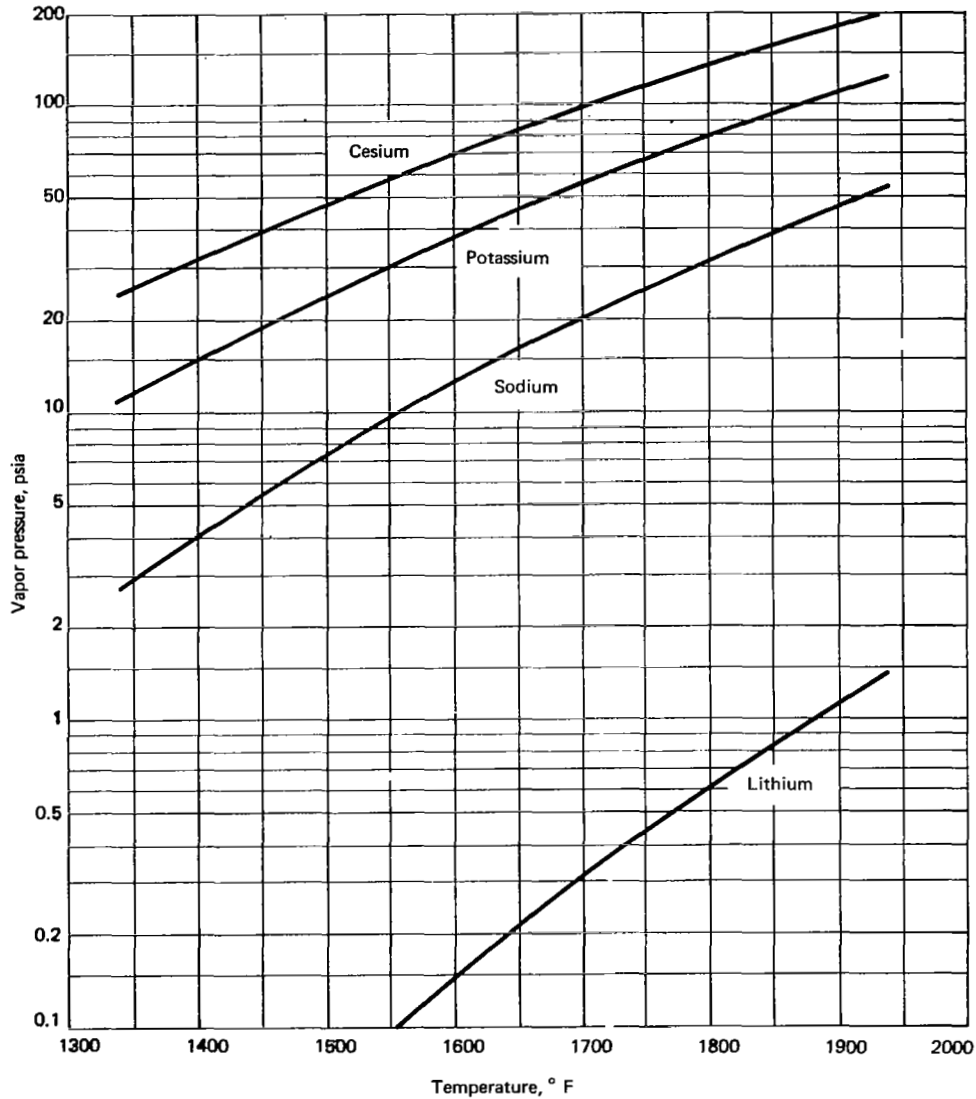


Figure 21. Vapor pressure of candidate heat pipe fluids.

temperature range 1340 to 1940° F. The vapor pressure of sodium meets the basic criterion over the entire temperature range. The vapor pressure of potassium lies between 1 and 100 psia from 1340 to 1870° F, while that of cesium meets the basic criterion between 1340 and 1700° F. The vapor pressure of lithium is less than 1 psia until the temperature reaches 1880° F. The curves of figure 21 indicate that sodium, potassium, and cesium are acceptable heat pipe fluids over most, if not all, of the temperature range of interest, while lithium is marginal except near the upper temperature limit.

Selection of the preferred heat pipe fluid for a particular application is best accomplished by comparing the fluid-dependent characteristics of a given heat pipe design for the various candidate fluids. Such a comparison was carried out for heat pipe design conditions which are typical of those expected for hypersonic cruise aircraft. The design conditions selected were:

Mach number	10
Leading edge radius	0.5 in.
Sweep angle	60 deg
Heat pipe vapor temperature	1540° F
Dynamic pressure	800 psf

For these conditions, figures 9, 13, 16, 18, and equation (1) may be used to obtain the following design data:

Stagnation line heat flux	0.660 Btu/in ² -sec
Heat load per unit span length	1.00 Btu/in-sec
Heat pipe length	39.0 in.

The following additional design assumptions were made:

Heat pipe cross-section	Circular
Heat pipe diameter	0.250 in.
Wall thickness	0.020 in.
Wick type	2 layer, with annular liquid flow channel
Flow channel thickness	0.010 in. (all liquid metal)
Thickness of inner wick layer	Negligible
Acceleration	0.5 g along heat pipe axis toward evaporator section
Wall material	René 41

Nucleation site radius for
initiation of boiling

1 micron

From the above data, the following additional heat pipe characteristics are immediately established:

Heat load*	0.250 Btu/sec
Vapor space diameter	0.190 in.
Axial heat flux (heat load per unit vapor space area)	8.83 Btu/in ² -sec
Temperature drop through wall at stagnation line	43.9° F

We now consider four heat pipes with the above characteristics, each of which has been loaded with one of the candidate heat pipe fluids: sodium, potassium, cesium, and lithium. We wish to establish the following for each heat pipe:

1. Whether the imposed heat load exceeds the sonic limit.
2. Whether the heat pipe is isothermal along its length.
3. The maximum permissible pore diameter at the liquid-vapor interface.
4. Whether heat pipe operation will be disrupted by boiling.
5. The maximum heat pipe temperature.
6. The vapor (internal) pressure.

For the specified operating conditions, heat pipe dimensions, and wall material, the six items of information listed above are all functions of properties of the heat pipe fluid.

Item 1 is determined by comparing the heat load with the sonic limit. If the heat load exceeds the sonic limit for a particular heat pipe fluid, heat pipe operation will be disrupted and the fluid is not suitable. If the heat load were

* Heat load = Heat load/unit span length x heat pipe diameter.

to exceed the sonic limit for all fluids, the vapor space area would have to be increased until the sonic limit for at least one candidate heat pipe fluid exceeded the heat load.

Item 2 is determined by calculating the ratio of the vapor pressure drop ΔP_v to the vapor pressure P_v . It can be established from the vapor pressure curves of figure 21 that the heat pipe vapor temperature will drop about 1.5 to 2° F for each per cent change in $\Delta P_v/P_v$. For practical purposes the heat pipe structure may be considered isothermal along its length if the temperature drop does not exceed 10° F, or if $\Delta P_v/P_v$ is less than 5 percent.

Item 3 is determined by consideration of the entrainment limit and the capillary pumping limit. For a given heat load, there is a critical pore diameter D_e above which the heat load will exceed the entrainment limit. For the same heat load, a minimum diameter of curvature D_c will develop in the wick pores at the liquid-vapor interface. This diameter of curvature cannot be smaller than the wick pore diameter D_p . Hence, in order to prevent disruption of heat pipe operation by either entrainment or tensile failure of the liquid-vapor interface, the pore diameter D_p cannot exceed the smaller value of D_e and D_c .

Item 4 is determined by consideration of the boiling limit. For a given heat load, there is a critical diameter of curvature D_b below which boiling will be initiated in the heat pipe liquid at the inner surface of the heat pipe wall. In order to avoid disruption of heat pipe operation by boiling, the actual diameter of curvature D_c must be larger than D_b .

Data and equations for the sonic limit, isothermal limit, entrainment limit, capillary pumping limit, and boiling limit are given in Appendixes B and C. These data and equations were used to determine the information required for items 1 through 4.

Items 5 and 6 are relatively straightforward, requiring no special knowledge of physical processes inside a heat pipe. The maximum temperature was found by adding the temperature drop through the heat pipe wall and wick at the stagnation line to the vapor temperature. The vapor pressure was obtained from the curves of figure 21.

The information required by items 1 through 6 is presented in table 7.

For lithium, the axial heat flux of 8.83 Btu/in²-sec is greater than the sonic limit. Lithium is therefore not a feasible heat pipe fluid for the specified heat pipe design and operating conditions, and was not considered further. For the other candidate fluids, the sonic limit is well above the axial heat flux. The vapor pressure drop is less than 1 per cent for the remaining candidate fluids,

TABLE 7. - COMPARISON OF CANDIDATE HEAT PIPE FLUIDS
(Vapor Temperature = 1540° F)

Fluid	Vapor pressure, psia	Sonic limit, Btu/in ² -sec	Vapor pressure drop, %	Pore dia no entrain, D _e , microns	Dia of curvature, D _c , microns	Dia of curv. no boiling, D _b , microns	Max. temp, ° F
Sodium	9.2	123.	0.614	276.	102.	2.02	1593
Potassium	29.0	236.	0.105	190.	51.2	2.30	1603
Cesium	55.0	208.	0.050	42.5	13.6	8.90	1618
Lithium	0.09	2.3	----	----	----	----	----

which indicates that heat pipes with these fluids will be isothermal in the axial direction within 1 to 2° F. However, the axial temperature drop is largest for sodium.

In every case, the diameter of curvature D_c is less than the maximum pore diameter D_e for no entrainment. Therefore, the pore diameter D_p cannot exceed D_c . With sodium, the heat pipe can function with wick pores as large as 102 microns, while the pore diameter cannot exceed 51 microns for potassium nor 13 microns for cesium. At the present time an effective pore diameter of 20 microns is about the minimum which is readily attainable. A cesium heat pipe would therefore present more difficult design and fabrication problems than either sodium or potassium heat pipes.

The minimum diameter of curvature D_b for no boiling is well below D_c for sodium and potassium, but within 5 microns of D_c for cesium. Because of uncertainties in the radius of nucleation sites where vapor bubbles are produced during boiling (a nucleation site radius of 1 micron was assumed in the calculation), the onset of boiling is a definite possibility for the cesium heat pipe, whereas the sodium heat pipe would be most resistant to boiling.

The maximum heat pipe temperature is lowest for sodium and highest for potassium, although the difference in temperature is not large. While the difference in vapor pressure is not significant in the present example, the difference may become very significant when the heat pipe cross-section is rectangular rather than circular, since the pressure must then be carried by bending in the heat pipe wall.

It can be concluded from the above analysis that lithium is not a suitable heat pipe fluid because of its low sonic limit. Cesium is not desirable because it requires a small wick pore diameter, the possibility of disruptive boiling exists, and its high vapor pressure will probably require a heavy containment structure in a practical design for wing cooling. Sodium and potassium both appear to be feasible heat pipe fluids. However, a sodium heat pipe is preferred because it is less prone to entrainment failure, larger wick pore diameters can be tolerated, sodium is less susceptible to boiling, and a lighter containment structure can be designed because of its lower vapor pressure.

These conclusions favoring sodium as the most appropriate heat pipe fluid were reached for a specified set of design and operating conditions which are believed to be reasonably representative of conditions likely to be encountered for a hypersonic cruise aircraft. If design and/or operating conditions depart significantly from those which were specified in this evaluation, the conclusions could require modification.

For example, at a lower Mach number and/or larger leading edge radius, where the stagnation line heat flux is significantly lower, the nonboiling criterion would be less limiting on cesium. At heat pipe vapor temperatures close to the lower temperature limit of 1340° F, the sodium heat pipe could have a significant axial temperature drop, in which case potassium could well be the preferred heat pipe fluid. At heat pipe vapor temperatures approaching the upper temperature limit of 1940° F, the sonic limit of lithium is about 50 Btu/in²-sec, well above the design axial heat flux. Lithium might then be considered as a possible alternate to sodium.

Selection of Heat Pipe Materials

The heat pipe wall and wick should be compatible with liquid sodium, the recommended heat pipe fluid, and preferably should be constructed from the same material. In addition, the wall material should be readily fabricable, and have adequate strength and oxidation resistance at contemplated operating temperatures.

Candidate alloys. - Five alloys have been considered for use in the wing structure of hypersonic cruise aircraft: the superalloys René 41, Haynes 25, and TD-NiCr, and the refractory alloys Ta-10W and Cb752 (ref. 9). When both strength and oxidation resistance are taken into account, the useful upper temperature limit of the superalloys for extended operation is around 1600° F, although TD-NiCr may be considered for temperatures as high as 2000 to 2200° F. The refractories may be useful to temperatures of 3000° F, but will

more likely be limited to 2400° F by temperature limitations of necessary oxidation-resistant coatings. (Higher temperatures may be permissible if experienced for relatively short periods or if confined to localized areas.)

The suitability of these alloys for use in the heat pipe cooling structure will now be considered. While high temperature operation substantially reduces the heat pipe length and, to a lesser extent, the heat load, there is a strong incentive to operate at temperatures at which superalloys are feasible. By limiting heat pipe temperatures to 1600 to 1800° F, the as-yet-unresolved problem of finding reliable, long-term oxidation resistant coatings for the refractory alloys is avoided, and the good strength and oxidation-resistant characteristics of the superalloys may be utilized to their best advantage. Therefore, only René 41, Haynes 25, and TD-NiCr will be considered further for heat pipe cooling structures. The composition of these alloys is given in table 8, and their physical properties are given in table 9.

Compatibility with sodium. - In addition to the property data of table 9, the compatibility of the listed alloys with the sodium heat pipe fluid is of major concern. Extended tests of liquid sodium in static capsules, rocking capsules, and thermal convection loops at temperatures up to 1500° F and testing periods up to 1000 hr have demonstrated the basic compatibility of sodium with nickel-base alloys and stainless steel (ref. 11). Corrosive attack is generally limited to light intergranular penetrations to depths of 1 to 2 mils, and is believed to result from the presence of oxides of sodium. If the oxygen content of the sodium is maintained below 10 ppm, corrosion effects are generally minimal.

Limited corrosion tests of cesium in TD-Ni refluxing capsules have been conducted at 1800° F for up to 500 hr (ref. 12). Since the corrosion effects of cesium are qualitatively similar to those of sodium, and TD-Ni is similar to TD-NiCr, these tests provide some indication of the compatibility of sodium and TD-NiCr. The test results showed that although corrosion was not extensive, metallic crystallites were found in the bottom of the capsules. Also, it appeared that some of the thoria dispersoid near the liquid metal-vapor interface in the reflux capsules had been lost. Some type of reaction between the thoria and liquid metals is thus indicated.

At temperatures above 1300° F, mass transfer effects become significant in sodium loops when temperature differences exceed 60° F. Mass transfer is believed to occur via the following mechanism. In the hot section of the loop, the container material dissolves in liquid sodium and is transported through the loop. In colder regions of the loop, the container material comes out of solution and is deposited on adjacent surfaces. The continuing accumulation of solid deposits in the cooler regions can eventually restrict or even block the flow of liquid sodium. Mass transfer increases with the temperature difference, the flow rate, and the oxygen content of sodium, and occurs at a significantly

TABLE 8. - COMPOSITION OF CANDIDATE HEAT PIPE ALLOYS

Material	Constituents, wt %											
	Ni	Co	Cr	W	C	Mn	Fe	Ti	Mo	Al	ThO ₂	Other
René 41	Bal	1	19		0.1		3	3	10	1.5		
Haynes 25	11	Bal	20	16.4	0.07	1.4	1.6					0.3Si
TD-NiCr	Bal		17-23		0.1						1.5-3	0.02S

TABLE 9. - PROPERTIES OF CANDIDATE HEAT PIPE ALLOYS (ref. 10)

Property	René 41			Haynes 25			TD-NiCr		
	Temperature, ° F								
	1400	1600	1800	1400	1600	1800	1400	1600	1800
Creep strength (0.5%/1000 hr), psi	25 000 ^b	2000 ^b	1400 ^b	12 000	4600	2000 ^a	13 000	9000	7000
Oxidation penetration, mils									
1000 hr	0.4	2.2	4.5	0.4	0.9				0.6
10 000 hr (extrap)	1.2	7.0	11.0	0.5	1.5				1.8
Modulus of elasticity, psi x 10 ⁻⁶	22.5	18.0	9.0	22.5	19.0	14.0	14.0	11.5	9.0
Thermal conductivity, Btu/hr-ft-°F	12.3	13.3	14.3	13.7	15.2	16.7	13.8	14.7	15.4
Specific heat, Btu/lb-°F	0.147	0.160	0.173	0.110	0.112	0.116	0.135	0.142	0.150
Emissivity (oxidized surface)	0.87	0.87	0.87	0.84	0.86	0.88	0.70	0.72	0.74
Density, lb/in ³	0.298			0.330			0.306		

^a Estimated.

^b Heat treated 2150° F (1/2 hr), air-cooled, and aged 1650° F (4 hr).

greater rate with nickel-base alloys such as Inconel and Hastelloy than with stainless steel. Mass transfer rates in Haynes 25, a cobalt-base alloy, are also much lower than for the above nickel-base alloys (ref. 13), and hence can be expected to be appreciably lower than in the nickel-base alloys René 41 and TD-NiCr.

In an isothermal liquid metal heat pipe, mass transfer may still occur as a result of the continuous distillation and condensation of the heat pipe fluid. When the heat pipe vapor condenses, it is pure and uncontaminated, and hence can dissolve container material. The condensate along with its solute then flows toward the evaporator, or heat input, end of the heat pipe. Upon evaporation of the liquid metal, the dissolved container material will then come out of solution and accumulate in the evaporator section of the wick. The same transport mechanism can also lead to the concentration of liquid metal oxides in the evaporator section and consequent intensification of liquid metal oxide corrosion.

Mass transfer may also occur as a consequence of the radial temperature gradients across the wick thickness. These temperature gradients could result in dissolution of container material from the hotter wall and its disposition on cooler portions of the wick at the evaporator section, and vice versa at the condenser section.

Mass transfer in liquid metal heat pipes should be much less pronounced than in all-liquid-metal flow systems because of the much lower flow rate which is required in a heat pipe to transfer a specified amount of heat. However, mass transport can be expected to become more significant with an increase in temperature (because of increased dissolution rates and solubility limits), operating time, (because of the increase in the total mass transport), and surface heat flux (because of the increase in the temperature drop across the heat pipe wick).

Longevity tests of liquid sodium and potassium heat pipes have confirmed that operation for thousands of hours is possible without adverse effects from mass transfer or oxide corrosion, even with nickel-base alloys. Some of these tests are summarized in table 10. In all of the tests neither the heat transfer rate nor the heat pipe temperature distribution changed measurably with time. Internal examination of the potassium-nickel heat pipe whose operation was terminated after 10 000 hr revealed negligible evidence of mass transfer. However, some corrosion typical of that caused by liquid metal oxides was observed in the wick at the evaporator section.

Gaseous diffusion. - All of the above tests were conducted in vacuum or in an inert gas atmosphere. Little lifetime data is available for heat pipes operating in air. However, there are indications that the diffusion of gas

TABLE 10. - LIFETIME OF SODIUM AND POTASSIUM HEAT PIPES (ref. 14)

Heat pipe fluid	Vessel Material	Temperature, °F	Heat transfer rate, Btu/sec	Operating life, hr	Status, Sept. 1969
Sodium	Hastelloy X	1320	0.19	20 000	Continuing
Sodium	316 Stainless	1420	0.28	4 000	Continuing
Sodium	Nickel	1470	0.19	8 200	Continuing
Potassium	Nickel	1110	1.14	10 000	Terminated
Potassium	Nickel	1110	1.66	38 000	Continuing ^a

^a Test still continuing as of Sept. 1970. Personal communication with Y. Eastman, RCA, Lancaster, Pa.

through the heat pipe wall into the interior can adversely affect heat pipe operation for some operating conditions. Such diffusion is undesirable for the following reasons: the accumulation of noncondensable gas could shorten the effective heat pipe length; the formation of gas bubbles in the heat pipe liquid could result in localized boiling and hot spots in the evaporator section of the wick; and the formation of large gas bubbles in the wick could impede the flow of liquid or disrupt the liquid-vapor interface, leading to drying out of the wick and overheating in the evaporator section.

Experiments in air with a 316 stainless flow loop containing liquid potassium have shown that nitrogen can diffuse through the container wall at a significant rate at 1500° F (ref. 4).

It has also been shown that hydrogen can rapidly diffuse through the wall of a sodium-stainless steel heat pipe, causing a cessation of capillary pumping and overheating of the evaporator section under some circumstances.* The hydrogen is believed to result from the reduction of water vapor in the air by the heat pipe surface. Hence, the presence of moisture in the atmosphere seems to be a prerequisite for the onset of heat pipe burnout due to hydrogen diffusion. This premise was verified in an experiment in which the heat pipe was first surrounded with argon saturated with water vapor. Disruption of heat pipe operation, as evidenced by a rise in the temperature of the evaporator section, occurred rapidly. Normal operation was then restored by surrounding

* Personal communication with J. Kemme, Los Alamos Scientific Laboratory, Los Alamos, N. Mex.

the heat pipe with dry gas, thus allowing the accumulated hydrogen to diffuse out of the heat pipe.

The rate of hydrogen diffusion into the heat pipe was greatly reduced by pre-oxidizing the exterior surface of the heat pipe, presumably because the oxide formed a diffusion barrier as well as eliminating the presence of metallic reducing agent at the heat pipe surface. Diffusion would probably also be inhibited by fabricating the heat pipe wall from an alloy with constituents such as zirconium or titanium which would tend to react with the diffusing gaseous species.

While hydrogen diffusion can apparently be expected in any heat pipe exposed to moist air, adverse effects on heat pipe operation have only been observed with relatively thick two-layer wicks with an all-liquid flow annulus. For example, while severe effects were noted with a 17-mil-thick flow annulus, effects were minimal with a 10-mil-thick annulus and negligible with single-layer wicks.

At expected cruise altitudes of 90 000 to 120 000 ft, the atmospheric pressure is on the order of 0.01 atmosphere or less, and the moisture content of the atmosphere is quite low. (The pressure at the stagnation line is about 0.1 atmospheres, however.) Therefore, for a given heat pipe temperature, diffusion rates of gases from the atmosphere through the walls of the heat pipe cooling structure should be much lower than at sea level. The exterior surface of the heat pipe structure will also be preoxidized in order to increase its emissivity, thus further inhibiting diffusion.

Materials selection. - Since it appears that the heat pipe cooling structure will cover only a small fraction of the total wing surface, and the difference in weight of structures fabricated from each of the candidate materials is not likely to be large, strength and weight were not prime factors in the materials selection process. Instead, major emphasis was placed on compatibility of the structural material with the sodium heat pipe fluid and with the atmosphere at expected operating temperatures.

On a materials compatibility basis, TD-NiCr would have to be considered as the least desirable of the three candidate materials. In addition to the experimental evidence previously cited which suggests that the dispersed thoria can react with liquid metals, it does not seem prudent to use a structural material with an oxygen-bearing constituent to contain a liquid metal whose corrosion behavior is very sensitive to its oxygen content. Even if the thoria were to be nonreactive with liquid sodium, the feasibility of its presence is questionable, since adequate wetting of a metal surface by liquid sodium is dependent on the surface being oxide free. Inadequate wetting of wick and inner

wall surfaces could substantially reduce the capillary pumping heat transport limit and the boiling heat transport limit.

The choice of structural material then lies between René 41 and Haynes 25. From the compatibility standpoint, Haynes 25 is preferred because it is a cobalt-base alloy and hence is less subject to mass transfer in liquid sodium than the nickel-base René 41, and in addition is more oxidation-resistant than René 41. Although René 41 is stronger and has a lower density than Haynes 25, a lighter structure will not necessarily result with René 41 because the thickness of sections exposed to the atmosphere would have to be increased to offset the greater oxidation penetration. (See table 9.)

Also, Haynes 25 has a higher thermal conductivity than René 41 and a lower specific heat. The higher thermal conductivity will result in lower maximum structural temperatures, while the lower specific heat can result in more rapid heating of the heat pipe structure during the climb to cruising altitude (if the product of specific heat and total structural mass is lower for Haynes 25). A rapid increase in the heat pipe temperature during startup is desirable to minimize or prevent possible startup problems.

On the basis of the above considerations, Haynes 25 was selected as the preferred heat pipe structural material, with René 41 as a reasonable alternate.

Minimum Thickness of Heat Pipe Cooling Structure

One of the most important questions related to the feasibility of heat pipe cooling is whether the heat pipe cooling structure can be accommodated within the confines of the wing profile. To answer this question, an investigation of the minimum heat pipe thickness required for effective leading edge cooling was carried out. The investigation was performed for conditions approximating those encountered during hypersonic cruise flight, but detailed design configurations were not considered.

Assumptions. - Minimum thicknesses were determined for the most extreme heating conditions of interest in this study, which correspond to a Mach number of 12 and a sweep angle of 0° . Circular heat pipes with the same length in the chordal plane and heat load per unit span as are required for leading edge cooling were used for the calculations. The heat pipes were assumed to be straight, and were subjected to an acceleration of 0.5 g along the axis from the condenser to the evaporator end.

The latter assumption overestimates the static liquid pressure drop due to acceleration, since for the actual wing geometry the distance between the condenser end and the leading edge, rather than the entire heat pipe length, determines the maximum static liquid pressure drop. The overestimate is small for the smaller leading edge radii, on which primary design interest is centered.

Sodium was used as the heat pipe fluid. A two-layer wick was used, consisting of a 10-mil-thick liquid sodium flow annulus and a porous inner wick layer of negligible thickness. Haynes 25 was used for the heat pipe wall, whose thickness was taken to be 20 mils.

Analytical approach. - The basic objective of the study was to calculate the minimum heat pipe diameter D for which the following criteria would be satisfied:

1. Vapor pressure drop does not exceed 10 percent. (The axial drop in vapor temperature is then less than 20° F.)
2. The wick pore diameter D_p is not smaller than 20 microns.
3. Boiling does not occur in the heat pipe wick.

The first criterion was established from the isothermal heat transport limit, the second from the entrainment and capillary pumping limits, and the third from the boiling limit. Equations and data needed to calculate these limits are given in Appendixes B and C.

For a specified leading edge radius and heat pipe vapor temperature, and with the above assumptions, the heat pipe diameter D and the vapor space diameter D_v are the only unknown heat pipe dimensions. The two diameters are related by

$$D_v = D - 2(t_w + t_c) \quad (11)$$

where t_w is the wall thickness, t_c is the wick thickness, and dimensions are given in inches. Since $t_w = 0.020$ in. and $t_c = 0.010$ in., equation (11) takes the form

$$D_v = D - 0.060 \quad (11a)$$

The axial heat flux ξ can then be expressed as

$$\xi = \frac{(Q/B)D}{\frac{\pi}{4} D_v^2} = \frac{(Q/B) D}{\frac{\pi}{4} (D - 0.060)^2} \quad (12)$$

where Q/B is the heat load per unit span length in Btu/in-sec and ξ is the axial heat flux in Btu/in²-sec. Upon solving equation (12) for D ,

$$D = \left(0.060 + 0.637 \frac{Q/B}{\xi} \right) \left[1 + \sqrt{1 - \left(\frac{1}{1 + 10.6 \frac{Q/B}{\xi}} \right)^2} \right] \quad (13)$$

The heat pipe diameter was calculated from equation (13) for the largest axial heat flux ξ for which the three criteria cited above are satisfied simultaneously.

Results. - Results of the calculations are given in figure 22, where the minimum heat pipe diameter is shown as a function of the heat pipe vapor temperature and the leading edge radius. In order for the heat pipes to conform to the leading edge geometry, the minimum heat pipe diameter must be less than the leading edge radius. Figure 22 shows this to be the case for all leading edge radii equal to or greater than 0.25 in. at vapor temperatures greater than 1370° F. Thus, heat pipes can be accommodated within the wing structure for leading edge radii as small as 0.25 in. While the latter statement applies specifically for the circular heat pipes used in the analysis, it is generally valid for heat pipes of other than circular cross-section, heat pipe diameter being roughly equivalent to the dimension normal to the wing surface.

For Mach numbers less than 12 and sweep angles greater than 0°, the minimum heat pipe diameters will be smaller than those of figure 22. Therefore, it can be concluded that for most hypersonic design and cruise conditions of interest, the heat pipe cooling structure can readily be accommodated within

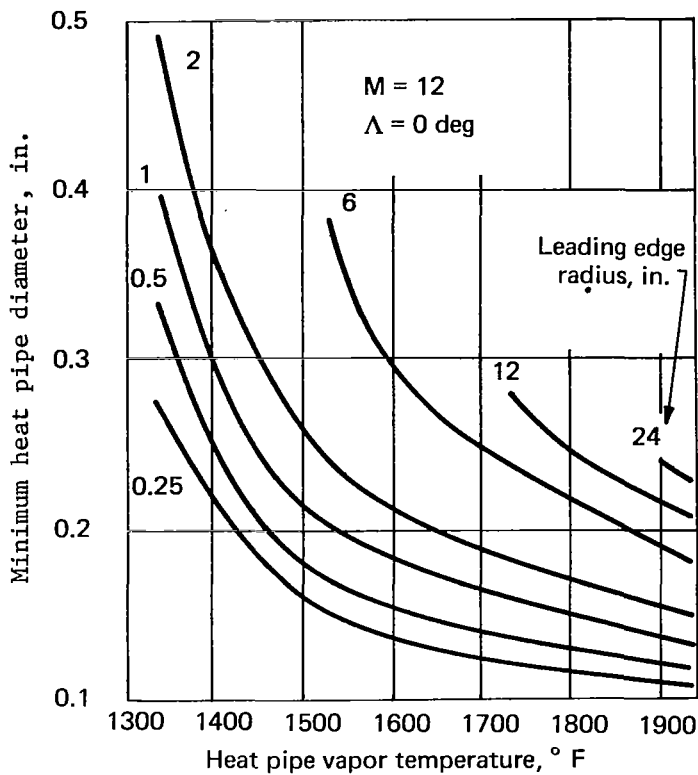


Figure 22. Minimum heat pipe diameter.

when $R = 24$ in., the vapor temperature should exceed $\approx 1850^\circ \text{F}$.

It must be emphasized that the conclusions regarding operating temperature for the larger leading edge radii are not definitive, since for these larger radii, wing geometry has an important influence on the required heat pipe diameter. The reason that the diameters of figure 22 become quite large for the larger radii is that the associated heat pipe lengths are large. As a result, the static liquid pressure drop due to the assumed 0.5 g axial acceleration can become so high that the maximum pressure difference between the vapor and liquid can no longer be sustained by surface tension, even when the vapor pressure drop is zero. (see figure 4).

For the actual wing, the maximum static liquid pressure drop is determined by the distance between the condenser end of the heat pipe structure and the leading edge, rather than by the entire heat pipe length (as was assumed for the calculations of figure 22). Hence, the static liquid pressure drop for the actual wing will be smaller than has been calculated, and actual heat pipe diameters will be smaller than those shown in figure 22. The difference in heat pipe diameters is small for leading edge radii less than 2 in., but is quite significant for radii of 6 in. and larger.

the wing profile. Further, the minimum thickness of the structure may well be determined by fabrication and dimensional tolerance considerations rather than by heat transport limits.

It can be seen from figure 22 that the minimum heat pipe diameter starts to increase rapidly as the heat pipe vapor temperature decreases. For leading edge radii of 6 in. and larger, high operating temperatures are necessary in order to avoid excessive heat pipe diameters. For example, when $R = 6$ in., the vapor temperature should exceed $\approx 1500^\circ \text{F}$; when $R = 12$ in., the vapor temperature should exceed $\approx 1700^\circ \text{F}$; and

When the sweep angle is greater than 0° , the liquid static head and hence the required heat pipe diameters can be reduced further by orienting the heat pipe axis along the normal to the leading edge instead of parallel to the direction of acceleration.

Design for Mach 8, 65 Degree Sweepback Wing

The preliminary design of a heat pipe cooling structure has been carried out, subject to the criteria of table 11.

TABLE 11. - CRITERIA FOR PRELIMINARY DESIGN OF HEAT PIPE COOLING STRUCTURE

Mach number	8
Dynamic pressure	800 psf
Leading edge radius	0.5 in.
Sweep angle	65 deg
Angle of attack	7 deg
Vertical acceleration	1.0 g (upward)
Horizontal acceleration	0.5 g (forward)
Heat pipe fluid	Sodium
Heat pipe vapor temperature	1540° F
Wall and wick material	Haynes 25
Minimum gage structural thickness	0.020 in.

Additional design data corresponding to the criteria of table 11 are given in table 12. Data are also given for leading edge radii of 0.25 and 1 in. because designs for these radii are considered in a subsequent section.

Initial design studies were carried out for the 0.5-inch-leading-edge-radius wing. The first step was the determination of the overall length of the heat pipe cooling structure.

TABLE 12. - ADDITIONAL DESIGN DATA

Leading edge radius, in.	Stagnation heat flux, Btu/ft ² -sec	Heat load, Btu/in-sec	Heat pipe length, L_p , in.	Leading edge periphery, s, in.
0.25	60.5	0.358	15.0	1.37
0.5	42.9	0.468	20.3	2.75
1.0	30.2	0.594	26.7	5.50

Overall length. - In the design concepts which were studied, the portion of the nose over which the heat pipe cooling structure extends was considered to be a separate structural entity, to be mechanically fastened to the primary wing structure. As is shown in figure 23, the heat pipe structure extends over a portion of the lower wing surface, so that the entire nose section is essentially isothermal. If the radiation equilibrium temperature T_e of the lower wing surface is higher than the heat pipe vapor temperature T_v , there will be a net increase to the heat pipe load which requires that the heat rejection length L_c be extended by the distance L_e , as shown in figure 23. If T_e is lower than T_v , the length L_l of the lower wing surface represents additional heat rejection surface which permits a reduction in the heat rejection length L_c on the

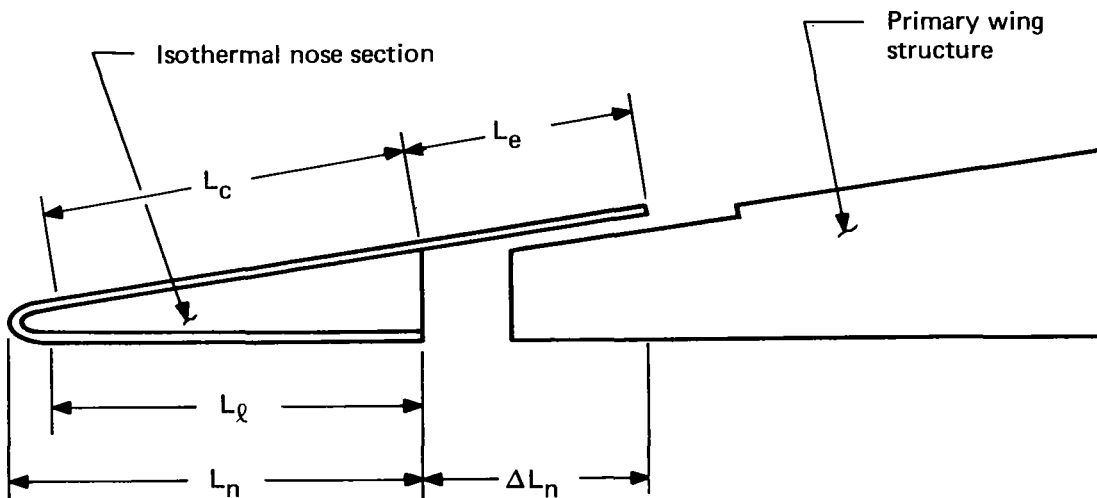


Figure 23. Design concept for heat-pipe-cooled, isothermal nose section.

upper surface. If T_e is equal to T_v , the lower surface of the nose section is adiabatic, and L_c is unchanged by the presence of the added heat pipe length L_ℓ .

For the case when T_e of the lower wing surface is higher than T_v , the longer the length L_n of the isothermal nose section, the larger will be the required increment L_e in the heat rejection length. The length L_n should be sufficient to facilitate assembly of the nose section to the primary wing structure, but not so long that the increase L_e in the heat rejection length becomes excessive.

The heat load per unit span length Q_ℓ/B on the lower edge of the isothermal nose section can be obtained from equation (9) or (10), with L_ℓ used in place of L_c and Q_ℓ/B used in place of Q_c/B . A negative value for Q_ℓ/B denotes a net input of heat to the heat pipe cooling structure. The required increment L_e in the heat rejection length is then given by

$$L_e = \frac{Q_\ell/B}{Q_c/B} L_c \quad (14)$$

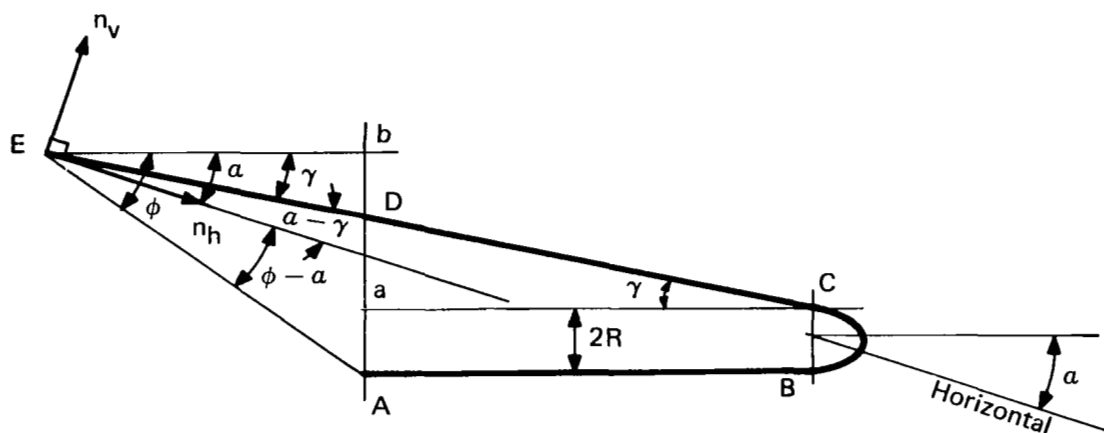
For purposes of this study, the length L_ℓ was assumed to be equal to $L_c \cos \gamma$. The geometry of the nose section is then as shown in figure 24. From figure 24 and the information which has already been developed, the nose section geometry can be defined completely. In figure 25, the nose section lengths L_n and $L_n + \Delta L_n$ along the chord at Mach 8 and Mach 10 are shown as a function of heat pipe vapor temperature for a leading edge radius of 0.5 in., a sweep angle of 65° , and an angle of attack of 7° . L_n is the chordal length if heat pipe cooling were provided for the rounded leading edge only, while ΔL_n is the required increment in L_n when the lower surface of the nose section is also cooled.

It can be seen from figure 25 that, at Mach 8, an extension of the heat pipe cooling structure beyond the nose section is required until the lower surface equilibrium temperature of 1720°F is reached. At Mach 10, the heat pipe cooling structure must be extended beyond the isothermal nose section until the lower surface equilibrium temperature of 1855°F is reached. At the proposed heat pipe vapor temperature of 1540°F , the chordal lengths L_n and ΔL_n are:

M	$L_n, \text{ in.}$	$\Delta L_n, \text{ in.}$	$L_n + \Delta L_n, \text{ in.}$
8	18.66	14.40	33.06
10	36.4	51.4	87.8

The lengths of the isothermal nose section and of the extension to the heat pipe cooling structure appear to be quite reasonable at Mach 8, but may be somewhat unwieldy at Mach 10. The overall length in the chordal direction may be reduced by an increase in the heat pipe vapor temperature and/or a reduction in the isothermal nose length.

From figure 25, the overall length at Mach 10 can be reduced to 33 in. (the length at Mach 8 and 1540° F) by raising the heat pipe vapor temperature



$$\begin{aligned} ED &= L_e \\ DC &= L_c \\ AB &= L_\ell \end{aligned}$$

$$\begin{aligned} aD &= DC \sin \gamma \\ bD &= ED \sin \gamma \\ bE &= ED \cos \gamma \\ bA &= bD + aD + 2R \\ AD &= aD + 2R \\ \tan \gamma &= \frac{bA}{bE} \end{aligned}$$

$$EA = \sqrt{(bE)^2 + (bA)^2}$$

Figure 24. Geometry of nose section.

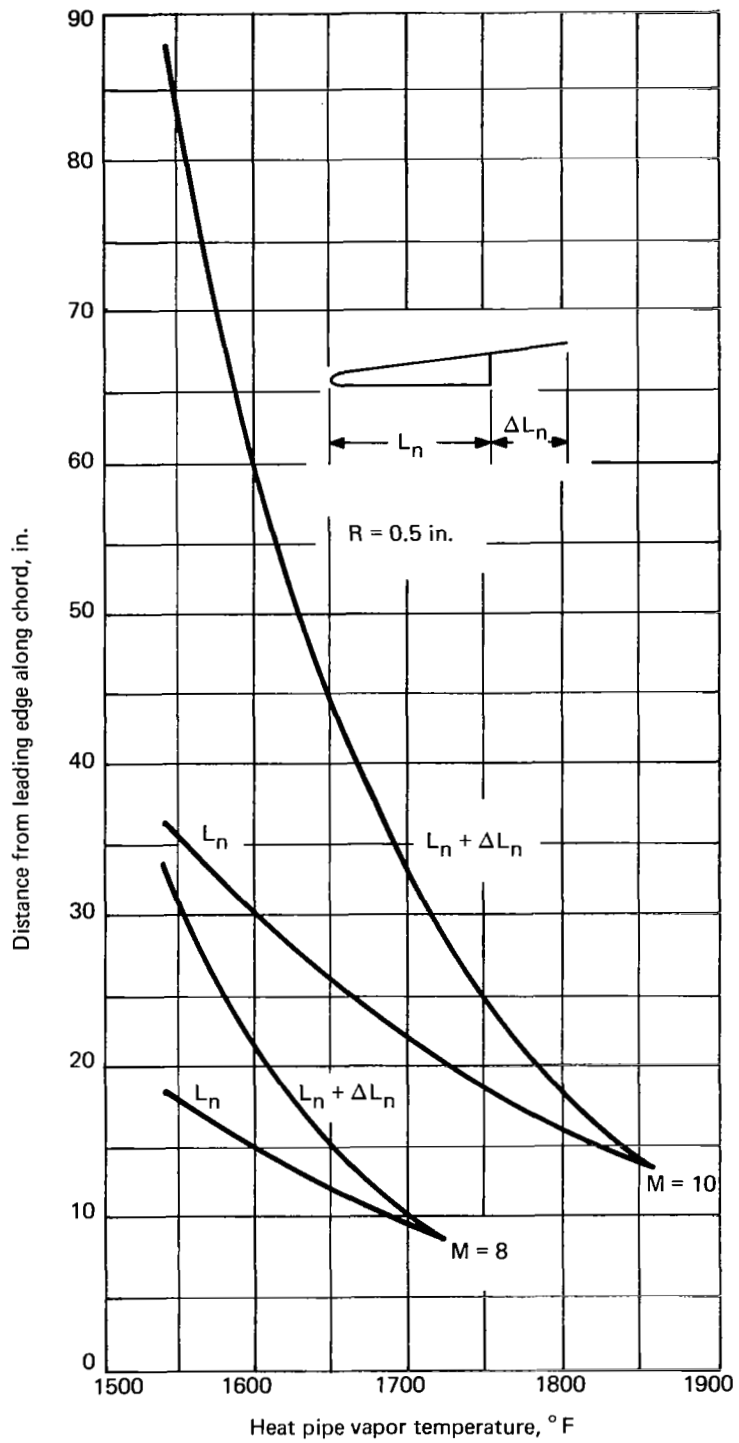


Figure 25. Length of nose section vs. heat pipe vapor temperature.

to 1700° F. If, at Mach 10 and 1540° F, the chordal length of the isothermal nose section were reduced to 18.6 in. (the isothermal nose section length at Mach 8 and 1540° F), the chordal length ΔL_n of the extension would be cut in half. The overall chordal length would then be the sum of the length L_n for cooling the rounded leading edge plus one-half the length increment ΔL_n , or $36.4 + 25.7 = 62.1$ in. The design of the heat pipe cooling structure for operation at Mach 10 will be considered in more detail subsequently.

Cross-sectional dimensions. - The next step in the design of the Mach 8 heat pipe cooling structure was the determination of cross-sectional dimensions. The cross-sections which were considered are shown in figure 26. The circular cross-section was included primarily for reference purposes. In rectangular cross-section B, the wick structure lines only the interior surface of the outer wall. In rectangular cross-section C, the wick lines all the interior surfaces of the heat pipe structure. The wick is of the two-layer type, consisting of a liquid sodium flow channel adjacent to the wall and an inner wick layer adjacent to the vapor space. The liquid sodium flow channel may be open, with liquid sodium filling the entire volume, or porous, with liquid sodium occupying the voids between the solid elements of a porous metallic filler.

Primary design consideration was given to the heat pipe structure as a double-walled shell around the periphery of the nose section. The vapor space is then confined between the inner and outer walls of the rectangular sections, as is shown in figure 26.

On the basis of the previously-described minimum-thickness studies and considering minimum dimensions to which the heat pipe structure could reasonably be fabricated, a vapor space thickness H_v of 0.200 in. was specified. Because both the internal and external pressures to which the heat pipe structure will be exposed are moderate, the minimum gage thickness of 0.020 in. was specified for the Haynes 25 walls and supporting ribs. The thickness t_p of the porous inner wick layer was taken to be 0.010 in.

The remaining unspecified dimensions are the vapor space width W_v (for the rectangular sections), the flow channel width t_a , and the pore diameter D_p of the inner wick layer. The width W_v was established from stress and deflection requirements, and the width t_a and diameter D_p were established from heat pipe heat transport limits. The wick friction factor K for the porous liquid sodium flow channel and its effective capillary pore diameter D_a represent additional design variables.

Stress and Deflection. - The walls of the heat pipe cooling structure will be subjected to stress and deflection because of the pressure difference between the interior and exterior of the structure. Since the direction and the

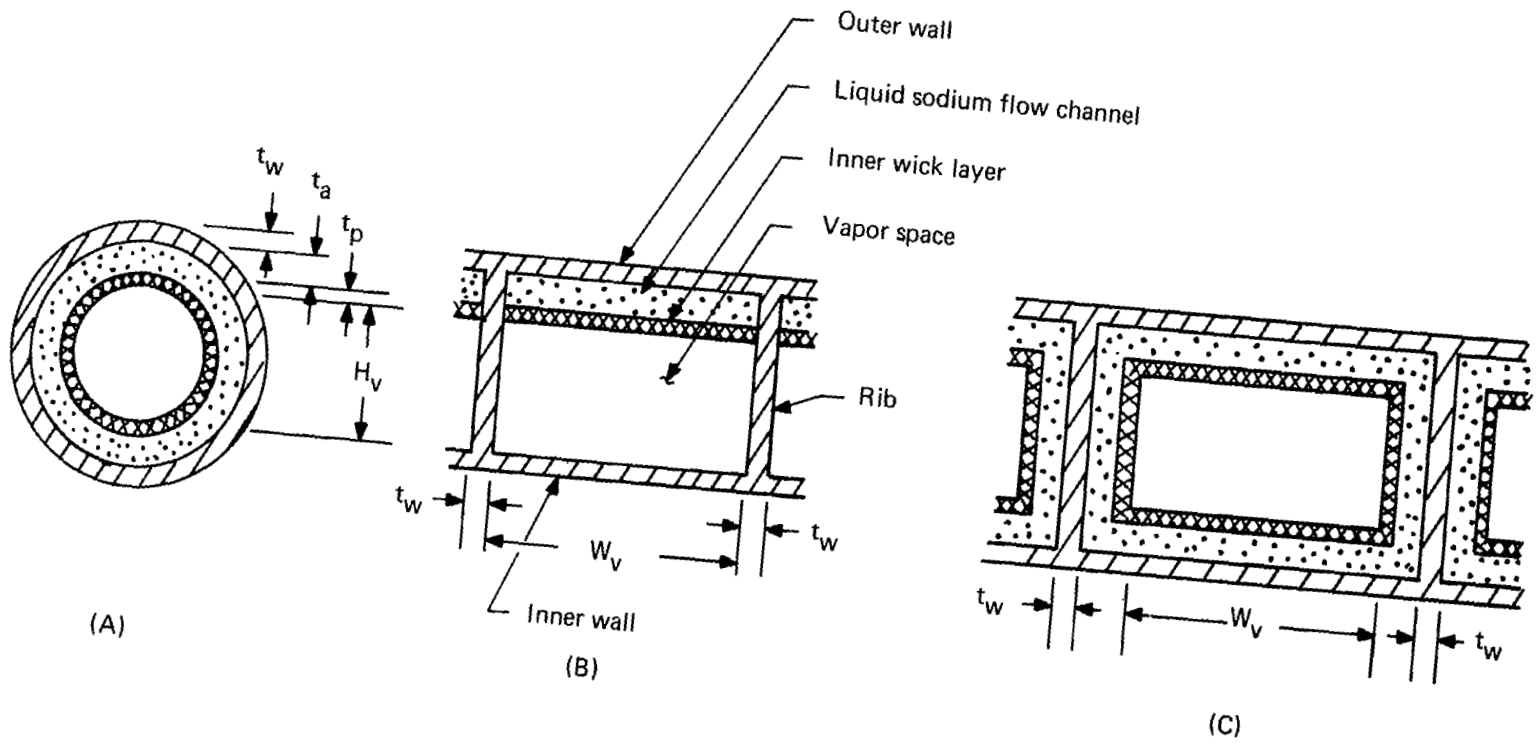


Figure 26. Cross-sections for heat pipe cooling structure.

magnitude of the pressure differential are quite different during cruise and when the aircraft is on the ground, both conditions must be considered. The internal pressure P_i and the external pressure P_o for ground and cruise conditions are listed below.

Pressure	Ground	Cruise (refs. 5, 6)	
		Stagnation Line	Flat Surface
P_o , psia	14.7	1.87	0.12
P_i , psia	0	9.2	9.2
$P_o - P_i$, psia	14.7	-7.33	-9.1

For the circular cross-section, the wall hoop stress was calculated from the equation

$$s = \left(\frac{\bar{r}}{t_w} \right) (P_o - P_i) \quad (15)$$

where t_w is the wall thickness and \bar{r} is the mean wall radius.

The pressure difference P_b required to buckle the heat pipe wall was calculated from the equation (ref. 15)

$$P_b = \frac{E}{4(1 - \nu^2)} \left(\frac{t_w}{\bar{r}} \right)^3 \quad (16)$$

where E is the modulus of elasticity and ν is Poisson's ratio (assumed to be 0.3).

For the rectangular sections, the stress in the ribs was calculated from the equation (ref. 16),

$$s = \frac{W}{t_w} (P_o - P_i) \quad (17)$$

where W is the centerline distance between ribs.

The bending stress in the inner and outer heat pipe walls was calculated from the standard beam formula (ref. 16)

$$s = \frac{M}{I} \left(\frac{t_w}{2} \right) \quad (18)$$

where M is the bending moment, I is the moment of inertia of the wall cross-section about its centerline, and t_w is the wall thickness. The walls were assumed to have fixed ends at points of contact with the ribs. For these conditions, it can be shown that the maximum bending stress from equation (18) takes the form

$$s = \left(\frac{W}{t_w} \right)^2 \frac{(P_o - P_i)}{2} \quad (19)$$

The pressure differential P_b which is required to buckle the ribs of the heat pipe structure can be expressed in the form (ref. 15)

$$P_b = \frac{\pi^2}{3} E \left(\frac{t_w}{H} \right)^2 \left(\frac{t_w}{W} \right) \quad (20)$$

where H is the rib height.

The maximum deflection y of the heat pipe walls can be expressed in the form (ref. 15)

$$\frac{y}{W} = 0.0312 \left(\frac{P_o - P_i}{E} \right) \left(\frac{W}{t_w} \right)^3 \quad (21)$$

The rib centerline width W was calculated from equation (21) for the case where $y/W = 0.001$.

Data for Haynes 25 which is needed for the stress and deflection calculations at the cruise heat pipe temperature of $\approx 1540^\circ \text{F}$ can be estimated from table 9. Needed room temperature data for calculations while the hypersonic aircraft is on the ground are: $E = 34.2 \times 10^6 \text{ psi}$, yield stress = 67 000 psi.

The calculation of W from equation (21) yielded the following results.

	<u>W, in.</u>
Ground (room temp)	0.841
Cruise (1540° F)	0.832

On the basis of these results, the vapor space width for the rectangular sections was specified to be 0.800 in. With this width, the maximum fractional deflection of the walls will be less than 0.001 for cross-section B of figure 26, and somewhat more than 0.001 for cross-section C (depending on the as-yet-to-be specified thickness t_a of the liquid flow channel).

A summary of the stress calculations, in which W and H were given the approximate values of 0.800 in. and 0.200 in. respectively, is presented in table 13.

TABLE 13. - STRESS CALCULATIONS FOR HEAT PIPE COOLING STRUCTURE

	Cylindrical cross-section	
	Ground (Room temp)	Cruise (1540° F)
Max. wall stress (hoop stress), psi	-84.5 ^a	52.4
Buckling pressure, psi	49 500	29 700
	Rectangular sections	
	Ground	Cruise
Max. rib stress, psi	-588 ^a	364
Max. wall bending stress, psi	11 730	7 270
Rib buckling pressure, psi	28 200	16 900

^a Minus sign denotes compressive stress.

It is evident that buckling will not be a problem, since pressure differentials necessary for buckling are well in excess of 10 000 psi while the maximum available pressure difference $P_o - P_i$ is 14.7 psi. Similarly, the hoop and rib stresses are well below the yield stress of 67 000 psi at room temperature and the stress of 7000 psi for 0.5% creep/1000 hr at 1540° F.

The most critical stress condition is the bending stress in the walls of the rectangular sections. At room temperature the bending stress is about 1/6 of the yield stress. However, at 1540° F the bending stress and creep stress are comparable. Over an operating period of several thousand hours, some plastic deformation of the most highly stressed wall fibers could develop. Whether such deformation would be acceptable from a design standpoint is a question which was not resolved during this preliminary study. If desired, the bending stress can be reduced by an increase in the wall thickness and/or a decrease in the rib-to-rib spacing.

Wick design. - The remaining design factors to be established are the characteristics of the liquid flow channel and the inner wick layer. (The thickness t_p of the inner wick layer has already been specified.) Determination of these factors requires detailed consideration of heat pipe heat transport limits.

Liquid static pressure drop: The initial information required is the magnitude of the liquid static pressure drop $\Delta P_{\ell s}$ which is produced by acceleration. The pressure drop $\Delta P_{\ell s}$ may be calculated from the equation

$$\Delta P_{\ell s} = w_{\ell} \ell (n_v \cos \Omega_v + n_h \cos \Omega_h) \quad (22)$$

where w_{ℓ} is the liquid specific weight in lb/in^3 , ℓ is the straight-line distance from the condenser end of the heat pipe cooling structure to some other point along the heat pipe length in inches, n_v is the vertical acceleration in number of g's, n_h is the horizontal acceleration in number of g's, Ω_v is the angle between the vertical acceleration vector and the line segment ℓ , and Ω_h is the angle between the horizontal acceleration vector and the line segment ℓ .

The relation of the acceleration vectors to the geometry of the wing cross-section is shown in figure 24. The end of the condenser section is at point E. The vertical acceleration is taken as positive when directed upward and as negative when directed downward. The horizontal acceleration is taken as positive when directed in the direction of flight and as negative when directed opposite to the flight direction. The angles Ω_v and Ω_h

are positive in the counterclockwise direction and negative in the clockwise direction.

As will be shown later, the liquid pressure drop between the condenser end at point E of figure 24 and points C (the evaporator-condenser interface) and A (the beginning of the evaporator section) are of primary interest. From the relationships presented in figure 24 and previously developed geometrical data, it can be established that the length of line segment EC is 32.0 in. and that the length of line segment EA is 14.90 in.

During and in the vicinity of cruise flight, the aircraft may be subjected to a variety of acceleration - angle of attack combinations. These various combinations, along with the resulting liquid static pressure drop (or rise) between line segments EC and EA of figure 24, are given in table 14. A negative value for the pressure drop in table 14 denotes a pressure rise.

TABLE 14. - STATIC LIQUID PRESSURE DROP IN HEAT PIPE DUE TO ACCELERATION

Case	Angle of attack, deg	Vertical accel., #g's	Horizontal accel., #g's	Pressure drop, psi	
				Segment EC ^a	Segment EA ^a
A	7	1.0	0.0	0.0274	-0.0570
B	7	1.0	0.5	0.461	0.1432
C	7	1.0	-0.5	-0.408	-0.258
D	0	-0.5	0.0	0.0394	0.0527
E	14	2.0	0.0	0.266	-0.0155

^a See figure 24.

Case A represents the basic steady-state cruise design condition. Cases B and C represent transient situations in which the aircraft undergoes horizontal acceleration or deceleration while cruising. Case D is representative of the transient condition encountered during noseover, and Case E represents conditions encountered during a banking maneuver. The largest static liquid pressure drops occur for case B, and hence were used in the design calculations.

Diameter of curvature at liquid-vapor interface: The next step in the design procedure was to calculate the diameter of curvature D_c at the

liquid-vapor interface which is required if surface tension is to balance the maximum difference between the vapor and liquid pressures. The pore diameter D_p of the inner wick layer must be less than D_c . The calculations were performed for an open liquid flow channel and for liquid flow channels filled with five representative porous wick materials. The properties of the porous wick materials are listed in table 15.

TABLE 15. - PROPERTIES OF POROUS WICK MATERIALS (ref. 17)

Identif. Number	Type	Mean fiber or wire dia., mils	Porosity	Wick friction factor, mils ⁻²	Mean pore dia., microns ^a
H11	Sintered fiber (430 S.S.)	1.3	0.887	1.180	190
H12	Sintered fiber (430 S.S.)	1.3	0.807	3.30	129
M7	50-mesh sintered screen (Ni)	9.	0.625	0.974	609
M8	100-mesh sintered screen (Ni)	4.5	0.585	4.21	263
M10	200-mesh sintered screen (Ni)	2.2	0.651	8.35	126

^a Based on capillary rise experiments with water, using oxidized samples. Perfect wetting assumed.

In table 15, the identification numbers refer to specific wick test samples from which the indicated data were obtained. The "H" numbers designate sintered fiber samples, and the "M" numbers designate sintered wire screen samples. The wick friction factor is the inverse of the permeability, and is used in the calculation of the liquid pressure drop through the wick material.

Using the methods of Appendix B, the diameter of curvature D_c was calculated as a function of liquid channel thickness t_a for the cross-sections of figure 26. The calculation was performed first for an open liquid flow channel. Results for the porous flow channels were then obtained using the following relation, which is derivable from Appendix B.

$$t_{ap} = \frac{K}{8} t_a^3 \quad (23)$$

In equation (23), t_{ap} is the thickness of a porous flow channel with wick friction factor K for which the liquid pressure drop is the same as that of an open flow channel of thickness t_a . Once a curve of t_a versus D_c was available for a heat pipe with an open liquid flow channel, a similar curve for a porous flow channel could be obtained for a given heat pipe by simply plotting t_{ap} obtained from equation (23) for a specific t_a against the D_c corresponding to that t_a .

Since the liquid static pressure drop is larger at the evaporator-condenser interface than at the beginning of the evaporator section (as Case B of table 14 shows), it is possible that the minimum diameter of curvature may occur at the evaporator-condenser interface. In the calculations, D_c was evaluated at both the evaporator-condenser interface and the beginning of the evaporator section, and the smaller value was used as the basis for design.

In figures 27, 28, and 29, the liquid flow channel thickness is shown as a function of the minimum diameter of curvature and flow channel type for the three cross-sections of figure 26. It is evident that, for a given diameter of curvature, the open flow channel is the thinnest, followed by the porous flow channels containing 50-mesh screen (M7) and sintered fibers (H11). The H11 porous flow channel was selected for further consideration along with the open channel.

The H11 channel was selected over the M7 flow channel because, as can be seen from table 15, the H11 material is more porous, is composed of much finer structural elements (1.3-mil fibers versus 9-mil wires for the M7 screen), and has about 1/3 the mean pore diameter. Since the density of metallic fibers and wires is much higher than that of the sodium which fills the pores, a flow channel of the higher porosity H11 material will weigh less than that of the lower porosity M7 material of approximately the same thickness. Because of the relative coarseness of its wires, the flow channel comprised of M7 wire mesh must have a minimum thickness of 18 mils (one layer of mesh), and will probably require a thickness several times greater in order to obtain a flow channel with reproducible flow characteristics and minimum edge effects. The H11 fibers, on the other hand, are only 1.3 mils in diameter, and a flow channel containing this material can be much thinner while still retaining good homogeneity and reproducibility.

Finally, because of its smaller pore size, the H11 sintered fiber channel can support a vapor-liquid pressure difference three times greater than can be supported by the M7 wire mesh. This property is normally not of consequence because it is the inner wick layer, rather than the liquid flow channel, where a surface tension barrier between vapor and liquid must be provided. However, it can be important if the liquid sodium column should be disrupted by some external disturbance during heat pipe operation. The

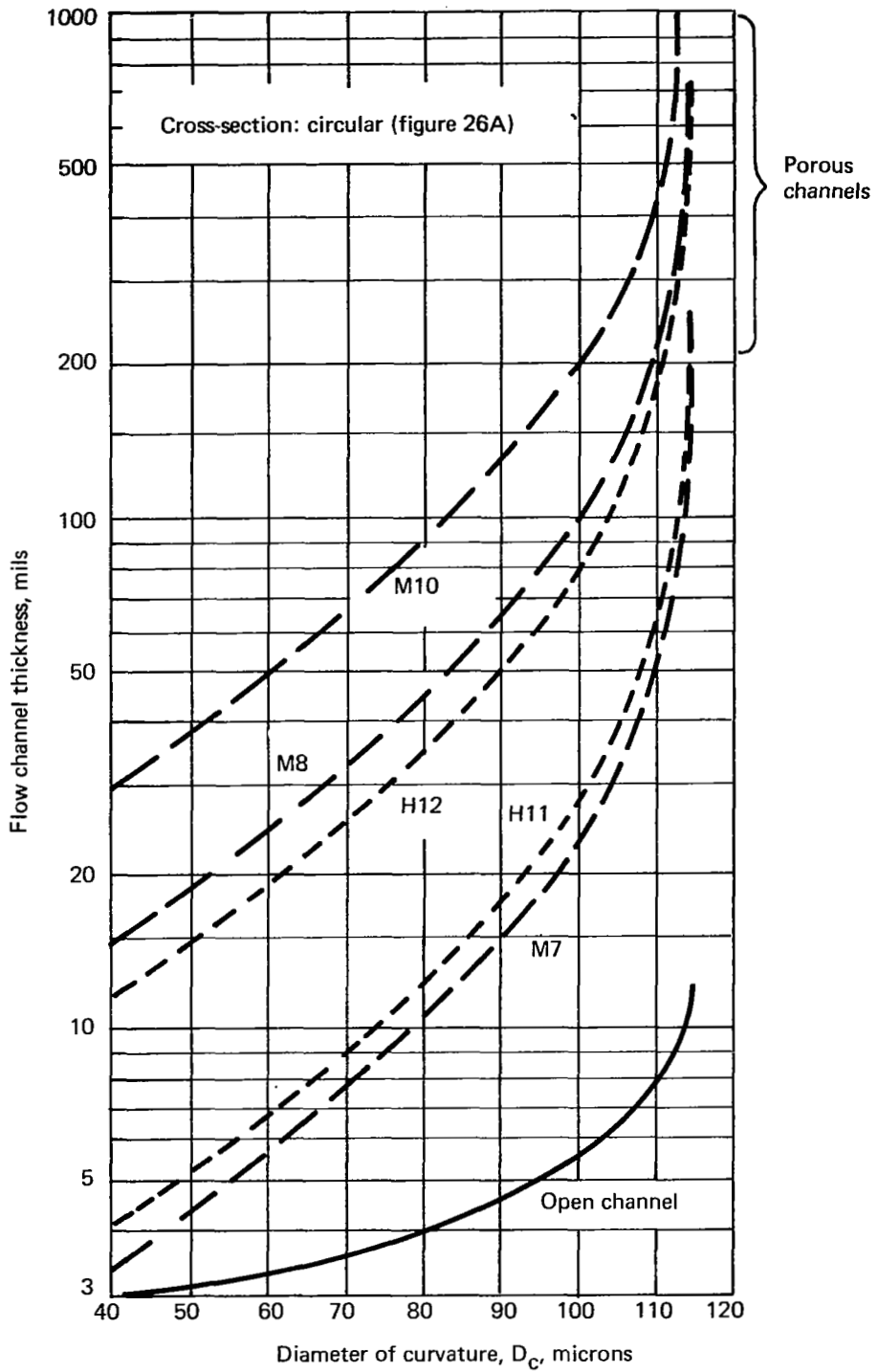


Figure 27. Liquid flow channel thickness for various wick types.

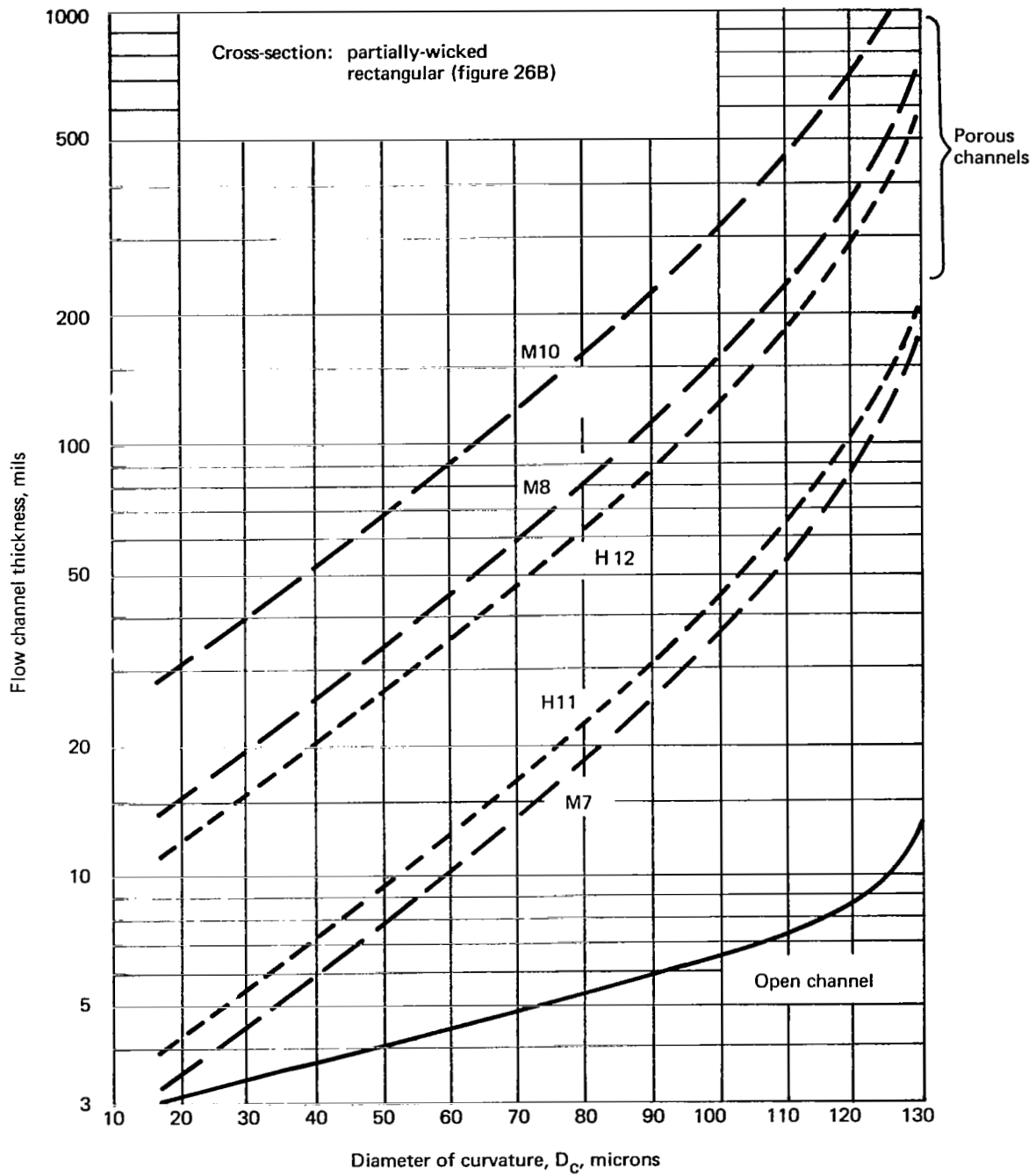


Figure 28. Liquid flow channel thickness for various wick types.

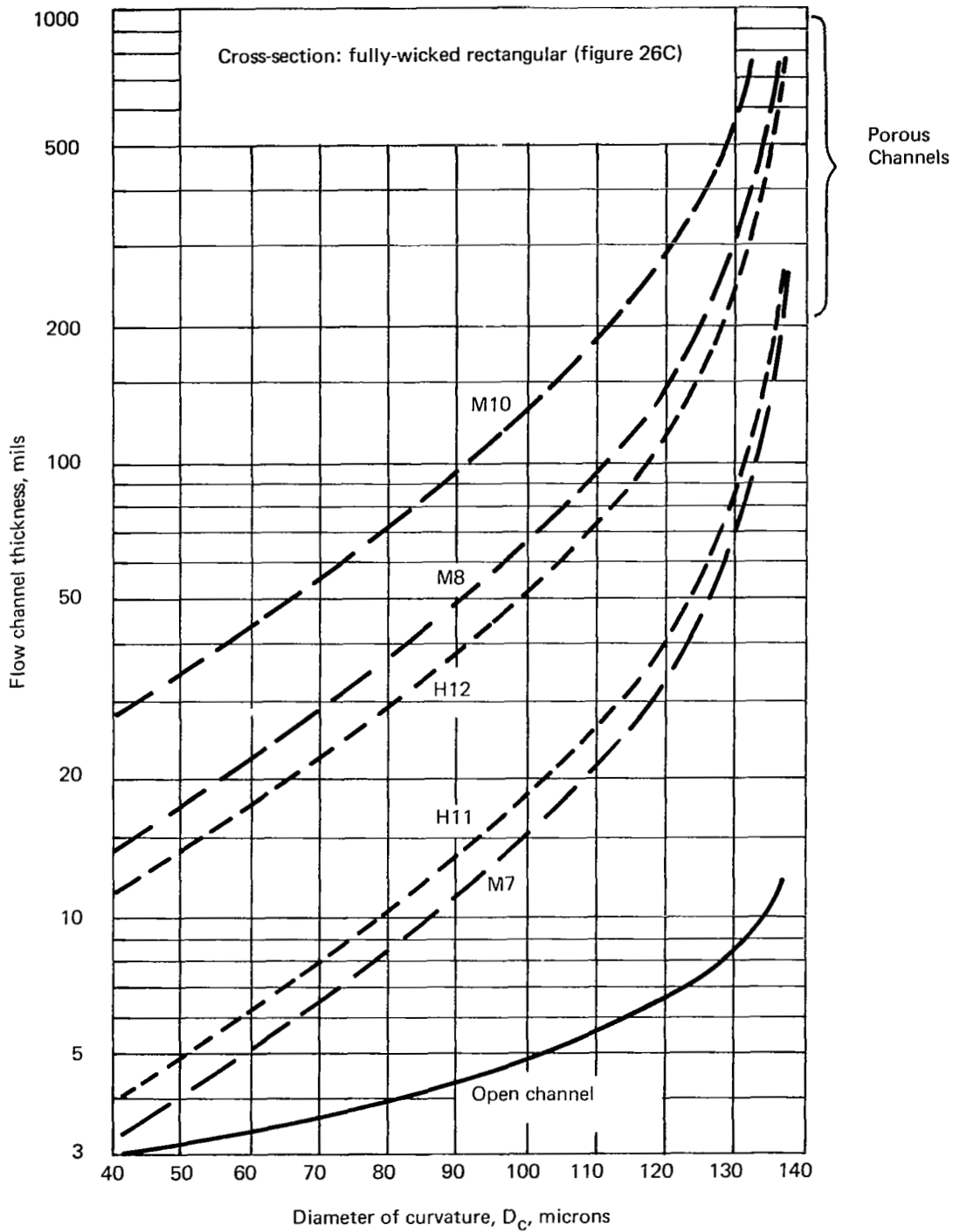


Figure 29. Liquid flow channel thickness for various wick types.

liquid-vapor interface would then extend into the liquid flow channel, and the channel with the finer pores would then refill with liquid more quickly under more severe operating conditions.

It was estimated that the minimum flow channel thickness for ease of fabrication and good dimensional reproducibility would be 9 mils for the open channel and 30 mils for the H11 sintered fiber flow channel. Then, from figures 27-29, the minimum diameter of curvature D_C will lie in the range of 113 to 132 microns for the open flow channel and in the range of 88 to 114 microns for the H11 sintered fiber channel. These curvatures will be achievable if the pore diameter in the 10-mil-thick inner wick layer is less than the minimum diameter of curvature of 88 microns. This requirement is readily met by fabricating the inner wick layer from three layers of 200-mesh screen, whose spacing between wires is about 70 microns. Thus, both open and porous liquid flow channels appear to be feasible, and the same wick characteristics can be used for each of the heat pipe cross-sections of figure 26.

Additional calculations confirmed that for all of the cross-sections, the axial (chordwise) temperature drop along the heat pipes is negligible, and that entrainment and boiling limits would not be encountered. Results of the wick design calculations are summarized in table 16.

Temperature drop: The total wick temperature drop (through both the inner wick layer and the liquid flow channel) was calculated to be $8.6^\circ F$ for the 9-mil open flow channel and $17.8^\circ F$ for the 30-mil porous flow channel. In the wick temperature drop calculations, the thermal conductivity of the sodium-filled porous wicks was obtained by weighting the thermal conductivity of the liquid and solid components by the volume fraction occupied by each component. A porosity of 0.65 was used for the 200-mesh inner wick layer. The porosity of the H11 sintered fiber flow channel is given in table 15.

Selection of Cross-Section. - The weight per unit surface area of heat pipe cooling structures with 9-mil open flow channels and 30-mil porous flow channels is given in table 17.

The rectangular cross-section of figure 26B is seen to yield the lowest weight for either flow channel type, followed by the rectangular cross-section of figure 26C and the circular cross-section of figure 26A. Since the circular cross-section is the heaviest and in addition would present serious fabrication problems (in attempting to bend the circular heat pipe to form a 0.5-inch-radius leading edge), it will not be considered further.

On the basis of weight, the cross-section of figure 26B would be preferred. However, with this cross-section the wick only covers a portion of the interior

TABLE 16. - SUMMARY OF WICK DESIGN CALCULATIONS

Cross-section	Liquid flow channel	Vapor pressure drop, %	Max. $P_v - P_l$, psi	Dia. curvature, microns	Min. pore dia. for entrain., microns	Max. dia. curvature for boiling, ^a microns
Circular (fig. 28A)	9-mil, open	2.44	0.609	113	378	2.02
	30-mil, H11	2.44	0.674	102	378	2.06
Rect. (fig. 28B)	9-mil, open	0.57	0.569	121	1070	2.02
	30-mil, H11	0.57	0.782	88	1070	2.06
Rect (fig. 28C)	9-mil, open	0.60	0.520	132	983	2.02
	30-mil, H11	0.60	0.600	114	983	2.06

^a Based on nucleation site radius of 1 micron.

surface of the heat pipe structure. While this should not present any problem during steady-state operation, some condensation may occur on the interior unwicked walls during startup, when the interior of the heat pipe structure is cooler than the portion adjacent to the wing surface. It is expected that this condensate will eventually find its way into the wick, in which case the effect on heat pipe operation would be minimal. However, the feasibility of the partially-wicked cross-section would have to be demonstrated experimentally. For purposes of this design study, it was assumed that the partially-wicked design is feasible. If the partially-wicked design should not be feasible then the rectangular section of figure 26C can be used, at the expense of a 14 percent weight increase with the 9-mil open flow channel and a 32 percent weight increase with the 30-mil porous flow channel.

Selection of flow channel. - Next, the selection of the flow channel type was considered. For the selected rectangular cross-section of figure 26B, the heat pipe structure is about 4 percent heavier with the 30-mil porous flow channel than with the 9-mil open flow channel. However, the porous flow channel can withstand a greater vapor-liquid pressure differential, which could

TABLE 17. - WEIGHT PER UNIT SURFACE AREA OF HEAT PIPE DESIGNS

Cross-section	Liquid flow channel	Weight, lb/ft ²
Circular (fig. 26A)	9-mil, open	3.34
	30-mil, H11	3.85
Rect. (fig. 26B)	9-mil, open	2.38
	30-mil, H11	2.49
Rect. (fig. 26C)	9-mil, open	2.72
	30-mil, H11	3.29

be important to restoration of normal operation if the liquid column were to be disrupted by an external disturbance. For the porous channel, the maximum pressure difference $P_v - P_l$ in psi which can be sustained is given by

$$P_v - P_l = 8480 \frac{\sigma}{D_a} \quad (24)$$

where σ is the surface tension in lb/ft and D_a is the mean pore diameter in microns. For the open flow channel, the maximum $P_v - P_l$ which can be sustained is given by

$$P_v - P_l = 4240 \frac{\sigma}{t_a} \quad (25)$$

where t_a is the channel thickness in microns.

Since $\sigma(1540^\circ \text{ F}) = 0.0081 \text{ lb/ft}$, $D_a = 190 \text{ microns}$, and $t_a = 9 \text{ mils} = 228 \text{ microns}$, the use of equations (24) and (25) yields $P_v - P_l = 0.361 \text{ psi}$ for the porous flow channel and $P_v - P_l = 0.150 \text{ psi}$ for the open flow channel. Thus, the porous channel can withstand a pressure difference almost 2-1/2 times larger than the open channel, although neither channel can withstand the design pressure difference of 0.569 psi for the open channel and 0.782 psi for the porous channel. (See table 16.)

The design pressure differences are based on the assumption that the hypersonic aircraft is undergoing a forward acceleration of 0.5g. If the liquid sodium column were to be disrupted, the column could be restored to its full length by reducing the forward acceleration. If the acceleration were reduced to zero, the liquid static pressure drop would then drop from 0.461 psi (as shown in table 14) to 0.027 psi. The maximum $P_v - P_l$ to be sustained by surface tension would drop from 0.569 psi to 0.135 psi for the open channel and from 0.782 psi to 0.348 psi for the porous channel. Thus, in the absence of forward acceleration both the open and horizontal flow channels would have the capability to maintain pressure equilibrium across the liquid-vapor interface of a completely filled wick.

On the basis of the above considerations both the open and porous flow channels are feasible, with little apparent difference between them. The 30-mil H11 porous flow channel was selected in preference to the 9-mil open flow channel because flow through the thicker channel is less sensitive to dimensional tolerances, and the channel probably can be fabricated more easily. Also, the open channel may be disrupted more readily by gaseous diffusion.

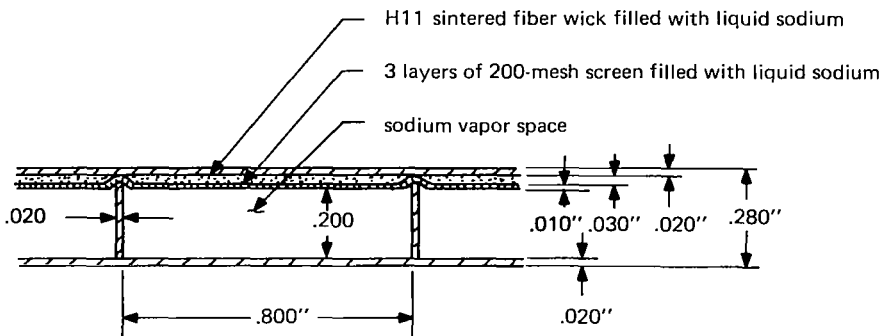
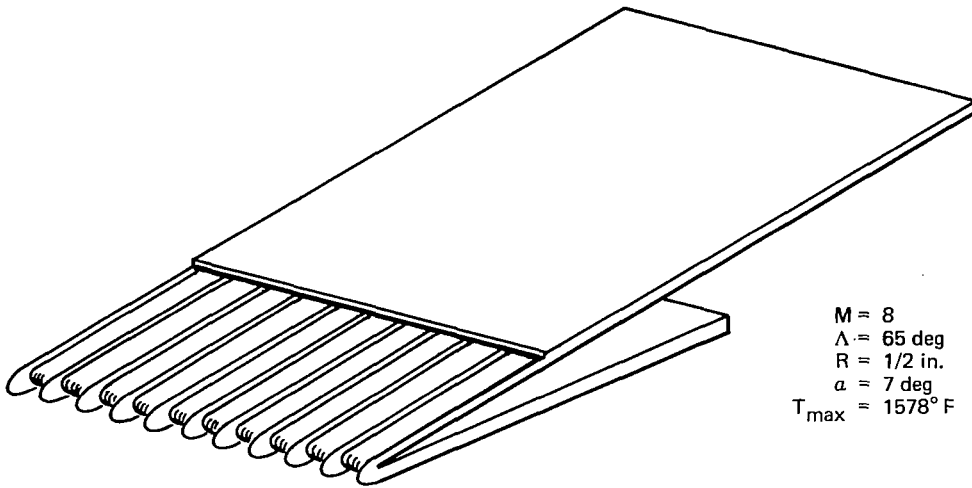
Final design. - The resulting design for the heat pipe cooling structure is shown in figure 30. The total length in the chordal direction is 33.06 in., and the maximum height of the structure is 3.90 in. The first 18.66 in. of chordal length constitutes an isothermal nose section. The last 14.40 in. constitutes the extension to the heat rejection length which is needed to reject heat added along the lower surface of the isothermal nose section. The overall thickness of the heat pipe structure is 0.280 in.

The structure is basically a double-walled shell which has been shaped to conform to the wing profile. The width of the structure in the spanwise direction will be determined by detailed fabrication considerations. It was not determined whether the heat pipe shell has sufficient strength and rigidity to stand alone, or whether internal supporting ribs might be needed. Thermal insulation would be used in the indicated locations to minimize thermal interactions between the heat pipe cooling structure and the adjacent primary wing structure.

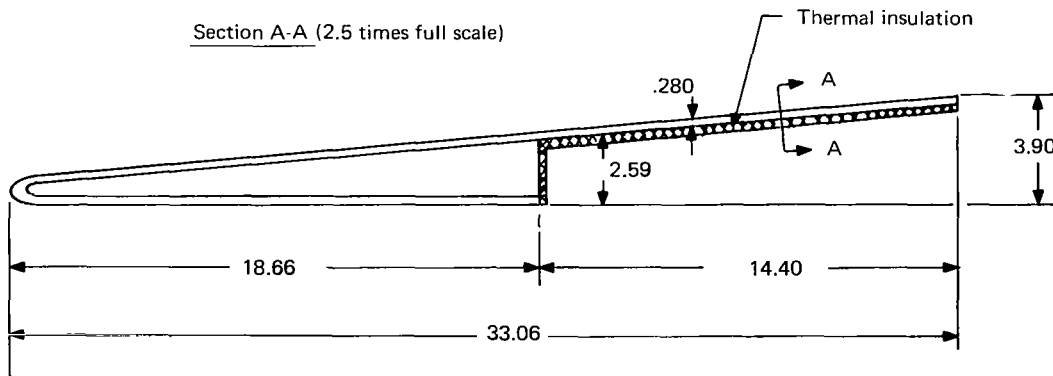
The maximum temperature at the stagnation line of the heat pipe cooling structure is 1578° F. This may be compared with the equilibrium temperature of 2465° F for an uncooled leading edge. (See table 6.)

An estimate of the maximum thermal stress in the heat pipe wall at the stagnation line was made using the formula

$$s = E \alpha \Delta T_w \quad (26)$$



Section A-A (2.5 times full scale)



Material: Haynes 25
 Scale: 1/5
 Dimensions are in inches

Figure 30. Design of heat pipe cooling structure for leading edge.

where α is the linear expansion coefficient and ΔT_w is the temperature drop through the heat pipe wall. Using $E = 20.5 \times 10^6$ psi, $\alpha = 8.8 \times 10^{-6}$ in./in. - °F, and $\Delta T_w = 19.8^\circ\text{F}$, the calculated thermal stress is 3580 psi. This figure is well below the stress of 7000 psi which is required for 0.5% creep/1000 hr at 1540° F in Haynes 25. Thus, plastic deformation due to thermal stress should be quite small.

In table 18, the major design parameters of the heat pipe cooling structure are listed and compared with experimental data for sodium heat pipes of roughly comparable dimensions, construction, and operating temperature. The comparison generally confirms the feasibility of the heat pipe cooling structure design and indicates that the design requirements are well within the demonstrated heat pipe state-of-the-art. The last three entries are particularly significant in this regard. The design liquid static head is about 1/3 the liquid static head under which the heat pipe of reference 18 has been operated. The design surface heat flux is 1/2 to 1/5 of the experimental values, and the design axial heat flux is about 1/9 of the experimental values.

Design Modifications

In this section, design modifications necessary to accommodate several variations in design and operation conditions are considered.

Designs for leading edge radii of 0.25 and 1 inch. - The same design procedures which have been described for a heat pipe cooling structure with a leading edge radius of 0.5 in. were also employed in developing designs for leading edge radii of 0.25 and 1 in. The principal effect of leading edge radius was on the chordal length and structural weight, both factors increasing with the leading edge radius. There was also a relatively small effect on the maximum temperature, which decreases with an increase in the leading edge radius.

The internal design is the same for all three leading edge radii, with the following exceptions. For the 0.25-inch-radius wing, the 0.280-inch thickness of the heat pipe structural shell is too large to fit within the wing profile at the leading edge. Therefore, for this case the entire interior of the isothermal nose section should be used as the vapor space for the heat pipe fluid. (See figure 31.) For the 1-inch-radius wing, a finer-pored structure was used for the liquid flow channel in order to facilitate refilling of the channel should the liquid column become disrupted. To offset the increased friction factor associated with the finer-pored liquid flow channel, a somewhat thicker flow channel was used along with a finer-pored mesh in the inner wick layer.

TABLE 18. - COMPARISON OF HEAT PIPE DESIGN PARAMETERS WITH EXPERIMENTAL DATA (M = 8, $\Lambda = 65$ deg, R = 0.5 in.)

Parameter	Design of figure 30	Experimental data	
		Ref. 18	Ref. 7
Struct. material	Haynes 25	Stainless	Stainless
Working fluid	Sodium	Sodium	Sodium
Temperature	1540° F	1470° F ^a	1400° F ^a
Outer dimensions	0.280 in. x 0.820 in.	0.544 in. dia.	0.705 in. dia.
Vapor space dimensions	0.200 in. x 0.800 in.	0.448 in. dia.	0.537 in. dia.
Wick type	2-layer (one side)	2-layer	2-layer
Capillary layer:	3 layers 200-mesh screen	8 layers 400-mesh screen	1 layer fine-mesh screen
Thickness	10 mils	6.5 mils	3.6 mils
Pore dia.	≈70 microns	19 microns	10 microns
Liquid flow channel layer:	H11 sintered fibers	Crescent-shaped annulus	Grooved wall
Thickness	30 mils	5.9 mils (av)	29.5 mils
Length along axis	52.3 in.	54.0 in.	33.5 in.
Thermal power/cell	0.700 Btu/sec	6.06 Btu/sec	9.30 Btu/sec
Wall thickness	20 mils	35.4 mils	65.5 mils
Liquid static head	0.461 psi	1.47 psi ^b	?
Surface head flux	42.9 Btu/ft ² -sec	92.7 Btu/ft ² -sec	193 Btu/ft ² -sec
Axial heat flux	4.49 Btu/in ² -sec	38.5 Btu/in ² -sec	41.0 Btu/in ² -sec

^a Temp. on outside surface of condensing section.

^b Power level not known when subjected to liquid static head.

The major design parameters for the heat pipe cooling structure are given as a function of leading edge radius in table 19. The following parameters are common to each design: Mach number, 8; sweep angle, 65°; vapor temperature, 1540° F; heat pipe fluid, sodium; heat pipe material, Haynes 25; angle of attack, 7°; wedge angle, 5.1°. The cross-section used in all cases is that of figure 26B.

TABLE 19. - HEAT PIPE COOLING STRUCTURE DESIGN PARAMETERS
VERSUS LEADING EDGE RADIUS

Parameter	Leading edge radius, in.		
	0.25	0.5	1.0
Total chordwise length, in.	25.61	33.06	40.2
Chordwise length of isothermal nose section, in.	14.19	18.66	23.6
Maximum thickness, in.	2.78	3.90	5.43
Heat pipe length, in.	40.1	52.3	64.6
Heat rejection length, in.	25.13	32.0	37.9
Vapor space width, in.	0.8	0.8	0.8
Vapor space depth, in.	Variable ^a	0.2	0.2
Wall thickness, in.	0.020	0.020	0.020
Flow channel:			
Thickness, in.	0.030	0.030	0.040
Material	H11 sint. fiber	H11 sint. fiber	H12 sint. fiber
Inner wick layer:			
Thickness, in.	0.010	0.010	0.010
Material	200-mesh screen	200-mesh screen	400-mesh screen
Overall thickness, in.	0.280	0.280	0.290
Maximum temperature, ° F	1595	1577	1570
Weight/unit surface area, lb/ft ²	2.48	2.49	2.84

^a Occupies entire interior of isothermal nose section.

Use of entire internal volume for vapor space. - As was pointed out above, it may be necessary to use the entire internal volume of the isothermal nose section in order to accommodate the heat pipe cooling structure in wings with small leading edge radii. Even where the leading edge is large enough to accommodate a shell-like pipe structure over the entire periphery of the leading edge, use of the entire internal wing volume may still be preferable.

The weight of the heat pipe cooling structure for the wing with a leading edge radius of 0.5 in. was recalculated for the design of figure 31. The following changes resulted from modification of the shell-type design of figure 30.

1. The inner skin was eliminated in the isothermal nose section.

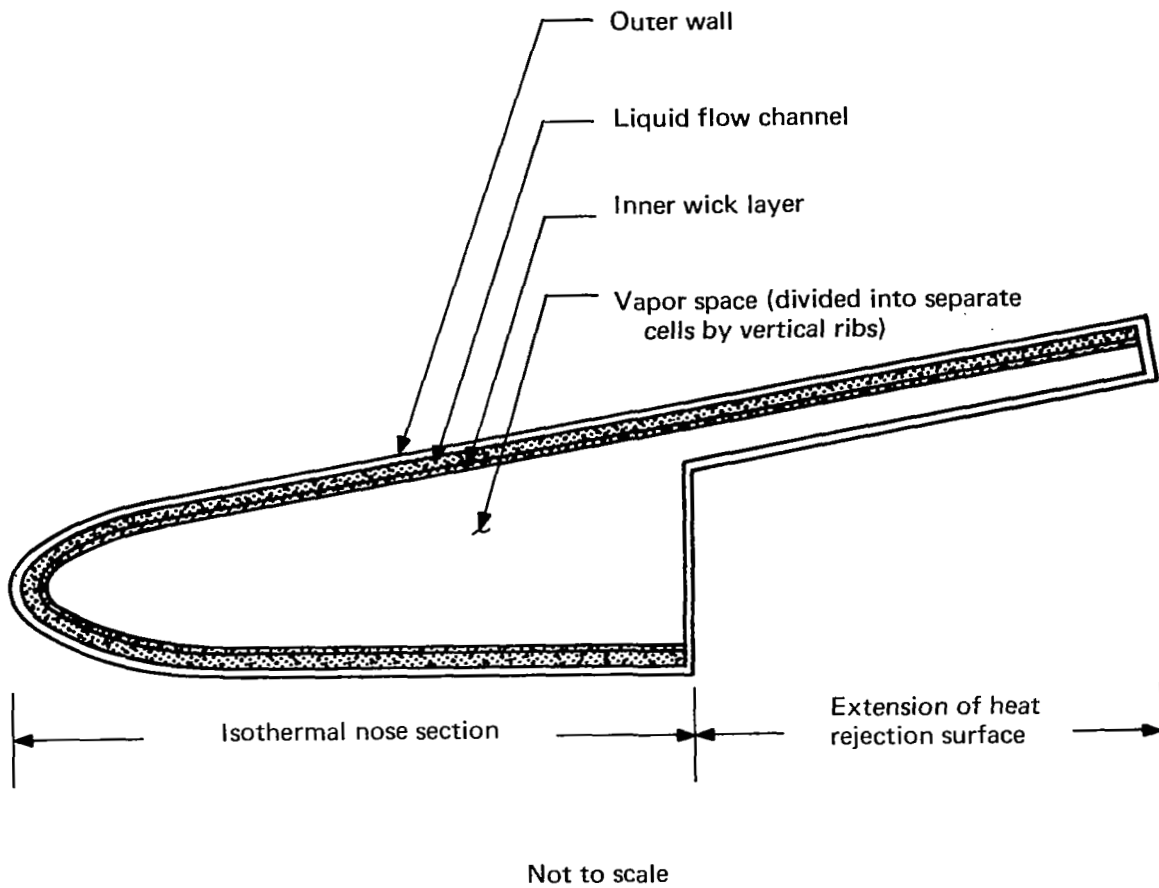


Figure 31. Cross-section of heat pipe cooling structure for which vapor space occupies entire internal volume.

2. The supporting ribs were extended over the full wing depth in the isothermal nose section.
3. A 0.020-inch-thick closure plate was added to the rear of the isothermal nose section.

The weight of the design configuration of figure 31 was calculated to be 2.39 lb/ft², compared with 2.49 lb/ft² for the shell design of figure 30. Thus, a weight saving of about 4 per cent results from permitting the heat pipe vapor to fully occupy the internal volume of the isothermal nose section.

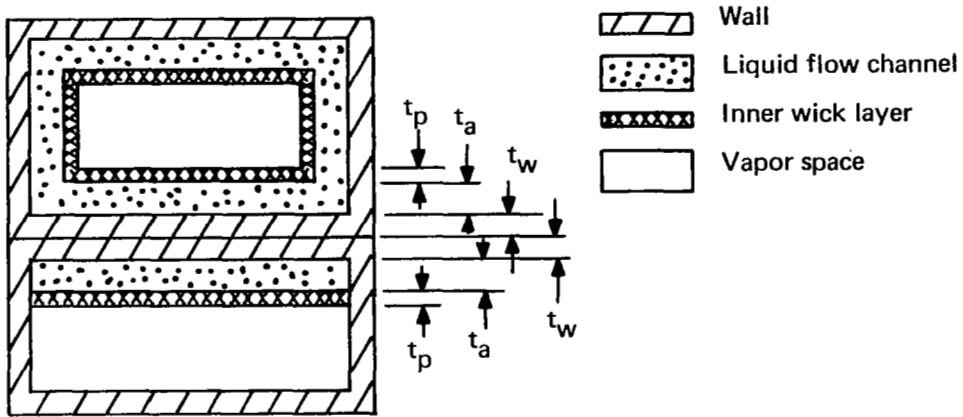
The heat transport capacity of the modified design of figure 31 is comparable to or larger than that of the shell-type heat pipe structure. The vapor pressure drop will be much smaller in the isothermal nose section because of the smaller mean flow velocity and smaller mean flow length, but the vapor pressure drop is already quite small in the shell-type design. The liquid pressure drop is unchanged, but could be reduced by lining the ribs with wicking material to reduce the mean velocity and mean flow length of the liquid condensate while returning to the leading edge and lower surface of the isothermal nose section. The additional wicking material would add weight and fabrication complexity, however.

Separate extension of heat pipe cooling structure. - In the designs which have been considered thus far, the extension of the heat pipe cooling structure, which is needed to reject heat absorbed along the lower surface of the isothermal nose section, is integral with the main structure. Another possibility is to fabricate the isothermal nose section and the extension separately and then to braze overlapped portions of the two sections together. In addition to possible simplification of the fabrication process, the use of two separate overlapping heat pipe structures reduces the liquid static pressure drop, which in some cases may permit the use of a coarser-pored wick structure.

A schematic of a heat pipe cooling structure with a separate overlapping extension is shown in figure 32. While the main part of the structure utilizes a partially wicked interior of the type shown in figure 26B, the extension employs a fully wicked interior of the type shown in figure 26C. A fully wicked structure is necessary for the extension because heat is added along the interior surface of the extension which lies along the overlap, and is rejected along the exterior surface.

The overlapped structure of figure 32 will be heavier than the continuous structure of figure 30 for the following reasons:

1. The weight of the overlapped portion of the extension represents a direct weight increment.
2. The temperature of the overlapped extension will be lower because of the added thermal resistance of the wick structures in the overlapped section, requiring increased length (and hence weight) of the extension to dissipate heat by radiation.
3. The fully wicked structure used in the overlapped extension of figure 32 is heavier than the partially wicked structure which is used in the extension of the continuous heat pipe cooling structure of figure 30.



Section A-A (enlarged)

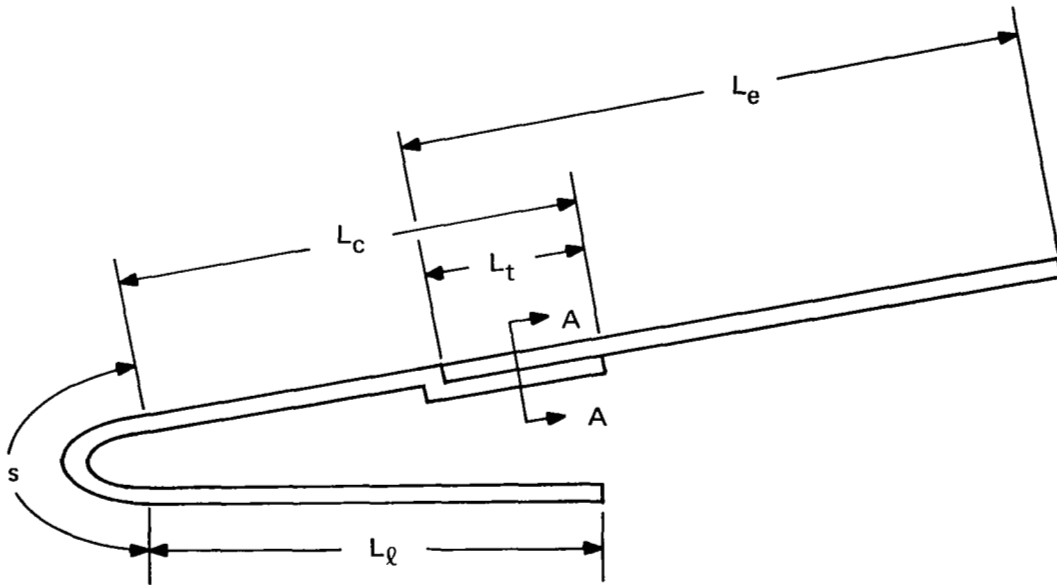


Figure 32. Heat pipe cooling structure with overlapped extension.

A weight optimization study of an overlapped heat pipe cooling structure was carried out using the basic characteristics of the design shown in figure 30. The separate extension was assumed to have a wick structure identical to that of figure 30, but which covers the entire interior surface in the manner of figure 26C.

The geometry for the overlapped heat pipe cooling structure is shown in figure 32. The heat to be rejected from the extension length L_e is equal to the heat absorbed over the distance L_l of the lower surface plus the fraction L_t/L_c of the heat which is absorbed over the distance s of the leading edge. The remainder of the heat absorbed by the leading edge is rejected over the distance $L_c - L_t$. The heat rejection temperature over the distance $L_c - L_t$ is approximately equal to the heat pipe vapor temperature T_v in the isothermal nose section. The heat rejection temperature over the extension length L_e is equal to $T_v - \Delta T$, where ΔT is the temperature drop between the heat pipe vapor in the isothermal nose section and in the extension. The temperature drop ΔT can be expressed as

$$\Delta T = \left[\frac{(Q/B)_l + (Q/B)_s (L_t/L_c)}{L_t} \right] \left(\frac{t_p + t_a}{k_c} + \frac{t_w}{k_w} \right) \quad (27)$$

The bracketed term in equation (27) represents the heat flux over the overlapped length L_t .

The extension length L_e can be obtained from equation (9). This equation, in terms of the heat load and temperature of the separate extension, takes the form

$$L_e = \frac{144 \left[(Q/B)_l + (Q/B)_s (L_t/L_c) \right]}{0.380 \left[(T_v - \Delta T)/1000 \right]^4 - h_l \left[T_{aw} - (T_v - \Delta T) \right]} \quad (28)$$

The extension length L_e was calculated as a function of the overlapped length L_t from equations (27) and (28) for a leading edge radius of 0.5 in., using the cross-section of figure 26B for the nose section and the cross-section of figure 26C for the extension. The input parameters, listed below, are the same as were used in arriving at the continuous heat pipe structural design of figure 30.

$$\begin{aligned}
(Q/B)_l &= 0.386 \text{ Btu/in. -sec} \\
(Q/B)_s &= 0.468 \text{ Btu/in. -sec} \\
L_c &= 17.55 \text{ in.} \\
t_p &= 0.010 \text{ in.} \\
t_a &= 0.030 \text{ in.} \\
t_w &= 0.020 \text{ in.} \\
k_c &= 29.2 \text{ Btu/hr-ft-}^\circ\text{F} \\
k_w &= 13.0 \text{ Btu/hr-ft-}^\circ\text{F} \\
T_v &= 2000^\circ\text{R} \\
T_{aw} &= 4470^\circ\text{R} \\
h_l &= 9.56 \times 10^{-4} \text{ Btu/ft}^2\text{-sec-}^\circ\text{R}
\end{aligned}$$

The results of the calculations are shown in figure 33. It can be seen that the minimum extension length of 20.6 in. occurs for an overlap length of 2.5 in. Since the extension length for the continuous heat pipe cooling structure is 14.48 in., the use of an overlap results in an increase in the extension length of at least 6.12 in., or 42.3 percent. The temperature drop ΔT at the optimum overlap length of 2.5 in. is 45.4° F.

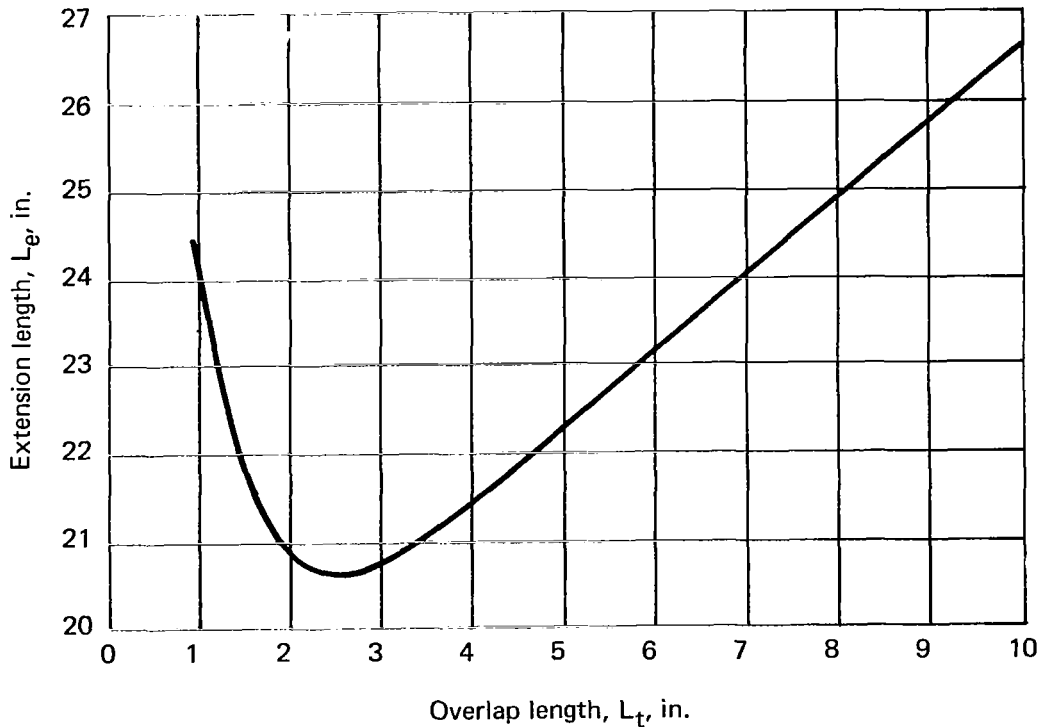


Figure 33. Extension length of heat pipe cooling structure vs. overlap length.

The total weight of the structure was obtained using the weight data of table 17 for the rectangular sections of figures 26B and 26C with 30 mil, H11 porous liquid flow channels. The data of table 17 were calculated for a total heat pipe length of 52.3 in. The weight of the overlapped heat pipe cooling structure per unit span length was found from the formula

$$\frac{W}{A} = \left(\frac{L_l + s + L_c}{52.3} \right) \left(\frac{W}{A} \right)_B + \frac{L_e}{52.3} \left(\frac{W}{A} \right)_C \quad (29)$$

where $(W/A)_B$ is the weight per unit surface area of the 52.3-inch-long continuous heat pipe structure using the rectangular section of figure 26B, and $(W/A)_C$ is the weight per unit surface area of the 52.3-inch-long structure using the rectangular section of figure 26C.

Using the following data,

$$\begin{aligned} L_l + s + L_c &= 37.5 \text{ in.} \\ L_e &= 20.6 \text{ in.} \\ (W/A)_B &= 2.49 \text{ lb/ft}^2 \\ (W/A)_C &= 3.29 \text{ lb/ft}^2 \end{aligned}$$

the total weight per unit span length is found to be 3.08 lb/ft². The overlapped structure is at least 23.9 percent heavier than the continuous structure of figure 30. The continuous structure is therefore the preferred design as long as the greater unbroken heat pipe length does not result in fabrication difficulties or an excessive static liquid pressure drop.

Effect of angle of attack on design. - The design of the heat pipe cooling structure was carried out for the conditions of Case B in table 14, since this resulted in the largest static liquid pressure drop. The angle of attack for Case B was 7°, the vertical acceleration was 1 g, and the horizontal acceleration was 0.5 g. In this section the design which evolved from Case B will be checked for adequacy of performance when subjected to the conditions of Cases D and E in table 14.

The angle of attack strongly influences aerodynamic heating on the flat surfaces of the heat pipe cooling structure and, to a lesser extent, influences the static liquid pressure drop. While the angle of attack also affects the aerodynamic heating distribution over the rounded leading edge of the heat pipe cooling structure, the total heat input over the leading edge is relatively

insensitive to the angle of attack. In the analysis to be considered here, only the effect of angle of attack on the aerodynamic heating rates for the flat wing surfaces is considered in detail.

The heat transfer coefficients for the upper and lower flat surfaces of the heat pipe cooling structure are given in table 20 as a function of the angle of attack. The heat transfer coefficients were calculated according to the methods of Appendix A. From table 20, it is evident that the heating rate on the upper flat surface decreases with an increase in the angle of attack, while the reverse is true for the heating rate on the lower flat surface.

TABLE 20. - HEAT TRANSFER COEFFICIENTS FOR FLAT WING SURFACES VERSUS ANGLE OF ATTACK

Angle of attack, deg	Heat transfer coefficient, Btu/ft ² -sec-°R	
	Upper surface	Lower surface
0	0.00216	0.00131
7	0.000956	0.00375
14	0.000286	0.00905

The heat pipe vapor temperature T_v (approximately equal to the temperature of the flat wing surfaces) for angles of attack other than the design value of 7° can be found by equating the sum of the heat load which is incident on the rounded leading edge and the flat surfaces to the thermal radiation rate from the flat surfaces. For the design of figure 30, the equality can be expressed as

$$0.468 + h_l (4470 - T_v) \frac{17.48}{144} + h_u (4470 - T_v) \frac{32.0}{144} = 0.380 \left(\frac{T_v}{1000} \right)^4 \frac{49.48}{144} \quad (30)$$

In equation (30), each term has the unit Btu/in-sec. The heat load of 0.468 Btu/in-sec on the rounded leading edge corresponds to a heat pipe vapor temperature of 1540° F. Although the leading edge heat load varies slowly with temperature, it was considered independent of T_v for purposes of this analysis.

For an angle of attack of 0° (corresponding to Case D of table 14) equation (30) yields a value of 1540° F for T_v , which is coincidentally the same as the heat pipe vapor temperature for the design angle of attack of 7° . Moreover, on the lower surface the radiation heat flux exceeds the heat flux due to aerodynamic heating, so that the lower surface now represents an additional heat dissipation surface instead of contributing to the heat pipe heat load. The heat pipe heat load is then only that due to aerodynamic heating of the rounded leading edge, and hence has dropped from the design value of $0.854\text{ Btu/in. -sec}$ to 0.468 Btu/in.-sec . Moreover, for Case D the static liquid pressure drop has dropped from 0.461 psi to 0.039 psi at the evaporator-condenser interface and from 0.1432 psi to 0.0527 psi over the entire heat pipe length.

Since both the heat pipe heat load and the static liquid pressure drop are well below the design values (which are based on Case B), the heat pipe design of figure 30 should operate under the conditions of Case D with little change in temperature and with a greater margin between the actual heat load and heat transport capacity.

For an angle of attack of 14° (corresponding to Case E of table 14), equation (30) yields a value of 1750° F for T_v , which is 210° F higher than the design temperature of 1540° F . The higher temperature is due to more intense aerodynamic heating of the lower surface of the isothermal nose section. As a result, the heat pipe heat load increases from the design value of 0.854 Btu/in.-sec to 1.85 Btu/in.-sec . The calculated temperature of 1750° F is an equilibrium value, to be approached only after the Case E operating conditions have persisted for some time. A transient analysis to determine the heat pipe temperature as a function of time after a change of operating conditions from Case B to Case E was beyond the scope of this study. It is possible that the increased temperature encountered for Case E would be acceptable if the time spent under the conditions of Case E represented a small fraction of the total flight time.

The heat pipe temperature for Case E can be reduced through adoption of one or more of the following design alternatives.

1. Reduction of the angle of attack below 14° .
2. An increase in the length of the heat pipe extension to make available more heat rejection surface.
3. A reduction in the length of the lower surface of the isothermal nose section to reduce the heat pipe heat load.

As an example, the operating temperature could be reduced to 1540° F if the length of the lower surface were reduced from 17.48 in. to 9.35 in., as may be established from equation (30). The isothermal nose section would then have a length of about 11 in. instead of almost 19 in. This reduced length would probably still be feasible from the fabrication and wing assembly standpoints. However, the heat pipe heat load at 1540° F would still be 1.53 Btu/in-sec, about 80 percent higher than the design value. The higher heat load will probably result in higher internal pressure drops, despite the smaller static liquid pressure drop which is encountered for Case E. As a result, some redesign might be necessary, most probably consisting of an increase in the thickness of the liquid flow channel and/or a decrease in the pore size of the inner wick layer. Whether such design modifications would actually be required depends on the duration of the Case E operating conditions and on whether the angle of attack need be as large as 14°.

Operation of Mach 8 design at Mach 10. - The reasonable dimensions and adequate thermal performance of the Mach 8 design appear to represent a good departure point for investigation of Mach 10 designs. Therefore, it was decided to evaluate the adequacy of the Mach 8 design of figure 30 at Mach 10. The evaluation was carried out for the cruise conditions defined by Case B of table 14. The design equations and procedures used in the evaluation are the same as those which were employed in the design of the Mach 8 heat pipe cooling structure.

Heat pipe vapor temperature: The lengths L_c needed for rejection of heat absorbed by the rounded leading edge and L_e needed for rejection of heat absorbed by the lower surface of the isothermal nose section were calculated as a function of heat pipe vapor temperature for operation of the heat pipe cooling structure at Mach 10. The lengths s of the rounded leading edge and L_l of the lower surface were held constant and equal to the s and L_l of the Mach 8 design of figure 30. In figure 34, L_c and the total heat rejection length $L_c + L_e$ are plotted as a function of the heat pipe vapor temperature, along with the total heat pipe heat load. From figure 34, the temperature for which $L_c + L_e$ is equal to 32.0 in., the total heat rejection length of the Mach 8 design, is found to be 1684° F. Thus, if the Mach 8 design is placed in a Mach 10 flow field, the heat pipe vapor temperature will increase from 1540° F to 1684° F. Also, from figure 34, the heat load per unit span length is 1.300 Btu/in-sec, compared to 0.854 Btu/in-sec at Mach 8.

Maximum heat pipe temperature: The maximum temperature drop between the exterior surface and the heat pipe vapor at the stagnation line was calculated to be 60.9° F. Of this total temperature drop, 28.8° F occurs through the heat pipe wall and 32.1° F through the heat pipe wick. The maximum temperature of the heat pipe cooling structure is the sum of the vapor

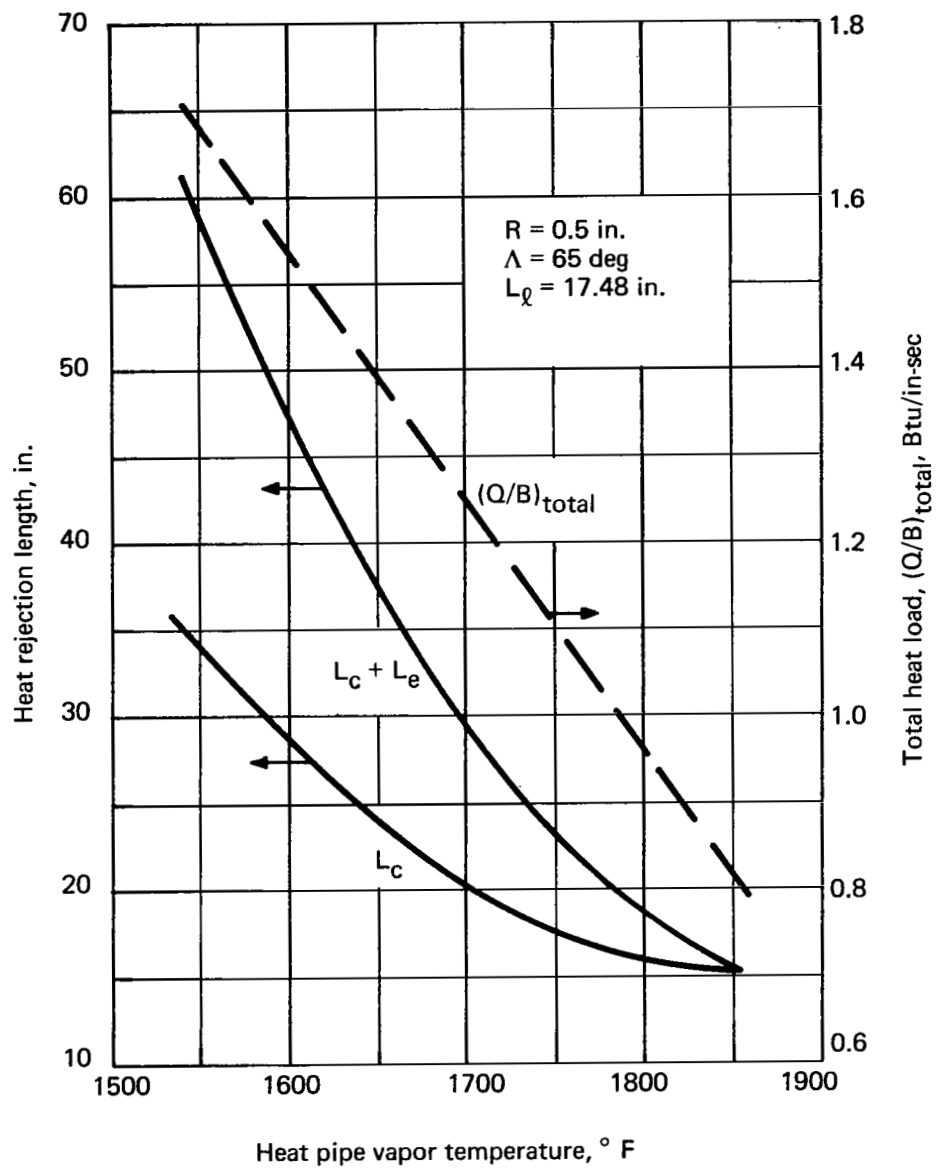


Figure 34. Heat rejection lengths and heat pipe heat load at Mach 10.

temperature and the maximum temperature drop, and is equal to $1684 + 60.9 = 1745^\circ \text{ F}$.

Stress and deflection: At 1684° F , the vapor pressure of sodium is 18.7 psi, compared to 9.2 psi at 1540° F . Thus, the stress environment at Mach 10 is more severe, while the allowable stress is reduced because of the higher operating temperature. At the mean wall temperature of 1730° F (at the stagnation line), the stress in Haynes 25 for 0.5% creep/1000 hr was estimated to be 2500 psi.

The maximum bending stress in the heat pipe outer wall was calculated to be 14 900 psi, a clearly excessive figure. Therefore, modification of the rib spacing and/or wall thickness was necessary to reduce the bending stress. A reduction in the rib spacing (vapor space width) from 0.8 in. to 0.3 in. lowered the bending stress to 2100 psi, which was considered to be a reasonable design value. The maximum wall deflection is then only 0.037 mil, also an acceptable figure, and the tensile stress in the ribs is only 282 psi. Thus, the first design modification required in the Mach 8 design for use at Mach 10 was a reduction in the vapor space width to 0.3 in.

The thermal stress in the stagnation line region was estimated to be 4200 psi. Although the thermal stress is higher than the creep stress, the thermal stress calculation is believed to be conservative. More detailed examination of the thermal stress problem was beyond the scope of the present study.

Heat transport limits: The ability of the Mach 8 design to carry the increased heat load at Mach 10 was determined by consideration of the heat transport limits.

Application of the capillary pumping limit equation resulted in a minimum diameter of curvature of 68.8 microns at the liquid-vapor interface. Since this figure is lower than the minimum pore diameter of about 70 microns in the 200-mesh screen of the inner wick layer, operation at Mach 10 will require a finer-pored mesh. Several layers of 400-mesh screen, for which the spacing between wires is about 40 microns, will be a satisfactory replacement for the 200-mesh screen.

The vapor pressure drop was found to be negligible, which indicates that the heat pipe cooling structure is quite isothermal over its length. From the entrainment limit equation, it was found that entrainment would not occur if the pore diameter at the liquid-vapor interface were smaller than 717 microns. Since the pore diameter of the 400-mesh screen is about 40 microns, entrainment will not be a problem at Mach 10.

From the boiling limit equation, it was established that boiling will not occur in the heat pipe cooling structure if the minimum diameter of curvature exceeds 2.2 microns. This calculation was based on the assumption that the radius of nucleation sites is 1 micron. Since the boiling limit decreases at a rather significant rate with temperature, a second, more conservative calculation was made using a nucleation site radius of 7 microns. This value was estimated to be an upper limit on the nucleation site radius, based on actual heat transfer data for a sodium heat pipe.* The resulting minimum diameter of curvature for no boiling with nucleation site radii of 7 microns was 41.9 microns. Since even this conservatively calculated value is well below the actual minimum diameter of curvature of 68.8 microns, it may be concluded that heat pipe operation at Mach 10 will not be disrupted by boiling.

Weight: The closer rib spacing which was found necessary to avoid excessive bending stress in the heat pipe wall will result in a heavier heat pipe cooling structure. The calculated weight per unit surface area of the Mach 8 design with a rib spacing of 0.3 in. was 2.92 lb/ft², an increase of 17 percent over the weight of the unmodified Mach 8 design with a rib spacing of 0.8 in.

Conclusions: The Mach 8 heat pipe cooling structure design of figure 30, whose maximum temperature is 1578° F, will attain a maximum temperature of 1745° F when operated at Mach 10. The following design modifications are required for Mach 10 operation.

1. The spacing between ribs must be reduced from 0.8 in. to 0.3 in. to avoid excessive bending stress in the wall of the heat pipe structure. As a result, the structural weight increases by 17 per cent.
2. The 200-mesh screen in the inner wick layer must be replaced with 400-mesh screen to avoid breakdown of the liquid-vapor interface.

Further examination of the thermal stress level in the stagnation region is required before the suitability of the Mach 8 design for operation at Mach 10 can be established.

TRANSIENT BEHAVIOR OF HEAT PIPE COOLING STRUCTURE

In this section the transient behavior of the heat pipe cooling structure is examined while a hypersonic aircraft climbs to cruise speed and altitude.

* Unpublished calculation by author.

The purpose of the investigation was to determine the adequacy of the steady-state design under the transient conditions encountered during the climb phase of flight. First, the temperature history of the heat pipe cooling structure was calculated. Then the actual heat loads were compared with heat transport limits throughout the transient period. The effect of the expansion of liquid sodium during startup was also considered. The transient analysis was performed for the heat pipe cooling structure design of figure 30.

Input Data

The initial step in the analysis was to determine the stagnation line heat flux as a function of time. The following climb schedule was specified.

1. The climb transient starts at Mach 2 and 40 000 ft.
2. The aircraft climbs with a forward acceleration of 16.1 ft/sec^2 (0.5 g), and is subjected to a dynamic pressure of 2000 psf, until Mach 8 is reached.
3. The aircraft then continues to climb at a constant Mach number of 8 to cruising altitude, at which the dynamic pressure is 800 psf. The climb rate is equal to that when Mach 8 is first reached.

The elapsed time at a given Mach number during the horizontal acceleration period was obtained by dividing the velocity increment by the acceleration. After Mach 8 is reached, the time is a linear function of altitude (as determined by the constant climb rate). The data used in determining the transient input data are given in table 21.

The heat flux $q(0, 0, 1, T_o)$ in table 21 is the stagnation line heat flux at the reference wall temperature T_o for a sweep angle of 0° and a leading edge radius of 1 in. The stagnation line heat flux for a sweep angle of 65° and a leading edge radius of 0.5 in. (the design conditions of figure 30) is 0.6 times $q(0, 0, 1, T_o)$, as may be established from equation (1) with $T_w = T_o$.

In figure 35 the altitude, Mach number, and stagnation line heat flux corresponding to the specified climb schedule and the data of table 21 are shown as a function of time. At Mach 2 and 40 000 ft (the start of the transient), the heat flux is $0.005 \text{ Btu/in}^2\text{-sec}$. The cruise Mach number of 8 is reached 368 seconds later at an altitude of 86 000 ft, when the heat flux peaks at $0.545 \text{ Btu/in}^2\text{-sec}$. The aircraft then climbs at the rate of 66.5 ft/sec while the Mach number remains constant, and reaches the cruising altitude of

TABLE 21. - INPUT DATA FOR TRANSIENT CALCULATIONS (refs. 5, 6)

Mach no.	Dynamic pressure, psf	Velocity, ft/sec	Altitude, ft	Adiabatic wall temp., °R	Ref. wall temp., T ₀ , °F	Heat flux, q(0, 0, 1, T ₀) Btu/in ² -sec
2	< 2000	1936	40 000	696	80	0.00750
3	2000	2904	44 500	1062	80	0.0365
6	2000	5840	73 510	2940	1540	0.264
8	2000	7852	85 800	4560	1540	0.911
8	1400	7894	93 640	4600	1540	0.702
8	800	7960	105 825	4620	1540	0.500

105 000 ft after 650 seconds. At this point the heat flux has dropped to the steady-state design value of 0.298 Btu/in²-sec.

Transient Analysis

A simplified model for calculating the temperature history of the heat pipe cooling structure was devised. The model is in general accord with experimental observations of transient heat pipe behavior.

Experimental observations. - It has been observed that when heat is added at the design rate to a liquid metal heat pipe which is at room temperature, the temperature of the heated zone increases rapidly and approaches the steady-state value. At the same time a well-defined front between the heated and unheated zones moves into the unheated zone at a slower rate. When the front eventually reaches the end of the heat pipe, the entire heat pipe is at relatively uniform temperature. The temperature then continues to rise until the steady-state value is reached.

Cotter (ref. 19) has attributed the observed transient behavior to the fact that the vapor pressure of the heat pipe fluid is initially so low that molecular flow conditions prevail. Until the vapor pressure of the heated zone reaches a level where continuum flow can exist, heat transfer from the heated zone to the adjacent unheated zone proceeds quite slowly via axial conduction through the heat pipe wall and wick.

Once continuum flow has been established in the hot zone, heat transfer occurs via the highly efficient process of evaporation and condensation. Hot

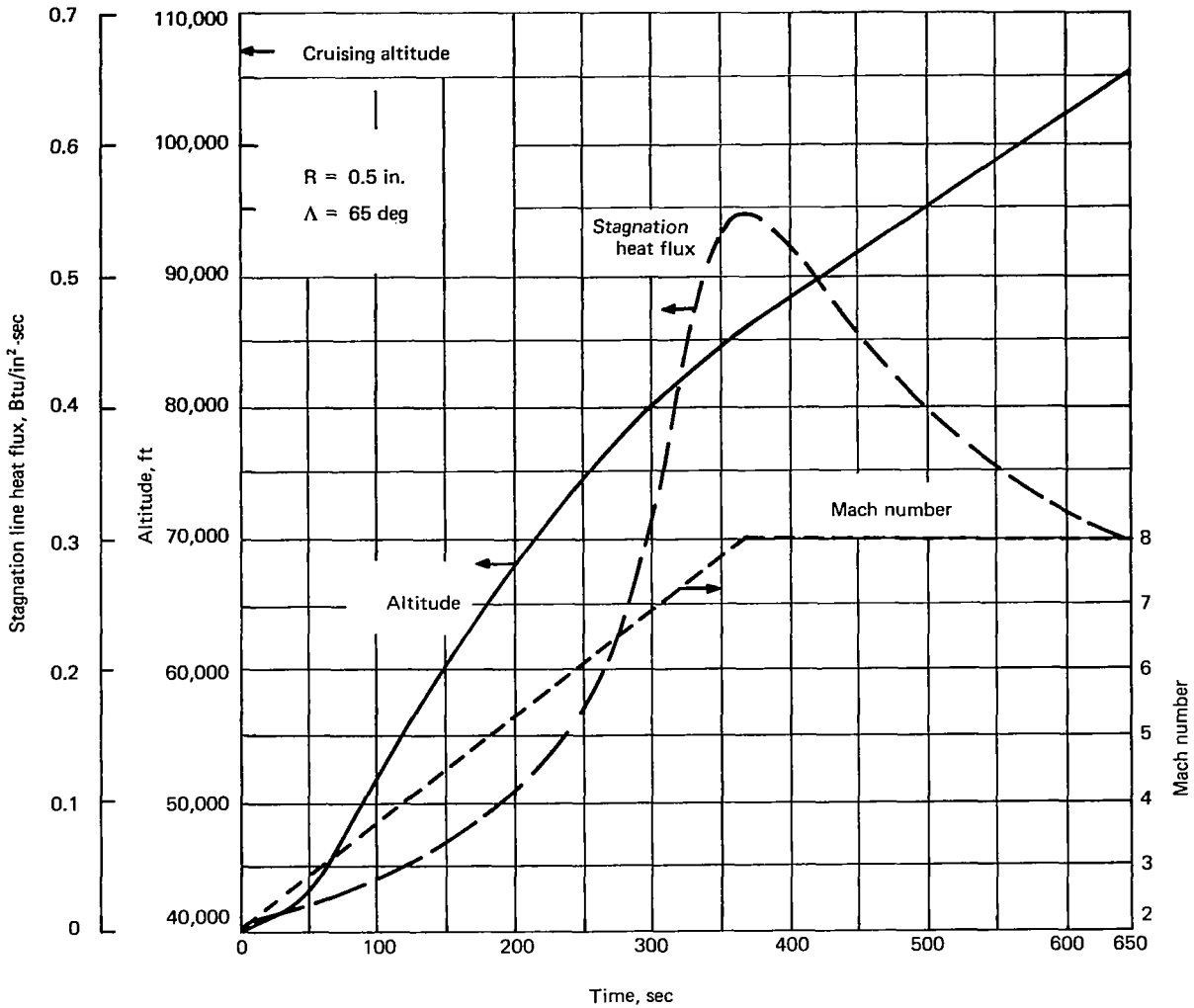


Figure 35. Altitude, Mach number, and stagnation heat flux vs. time to cruise conditions.

vapor from the heated zone then flows into the unheated zone at a rate which is limited by the sonic velocity of the vapor. Condensation occurs so rapidly at the interface between the hot and cold zones that there is little vapor penetration into the cold zone. As a result, a relatively well-defined front divides the two zones. Once the front has reached the end of the unheated zone of the heat pipe, continuum flow exists over the entire heat pipe length. The entire heat pipe is then at relatively uniform temperature, which continues to rise until the steady state is reached.

Description of transient model. - The model which was used as the basis for the transient calculations is shown in figure 36. Overall dimensions are the same as those of figure 30. The span distance of 0.820 in. is equal to the rib-to-rib centerline spacing. The x_1 coordinate represents the location of the continuum wave front in the upper leg of the heat pipe cooling structure; the x_2 coordinate represents the location of the continuum wave front in the lower leg. The wave fronts are assumed to separate a constant temperature continuum region (behind the wave fronts) from constant temperature molecular flow regions (preceding the wave fronts). Heat transfer is assumed to occur only through the outer surface of the heat pipe cooling structure. All other surfaces are assumed to be perfectly insulated. Temperature gradients normal to the outer surface are assumed to be negligible.

Volumetric heat capacity: The volumetric heat capacity C per unit of heat pipe length is defined as

$$C = w_w c_w A_w + w_l c_l A_l \quad (31)$$

where C is in Btu/in-°F, the subscript w refers to the Haynes 25 wall and wick, the subscript l refers to the sodium heat pipe liquid, w is the

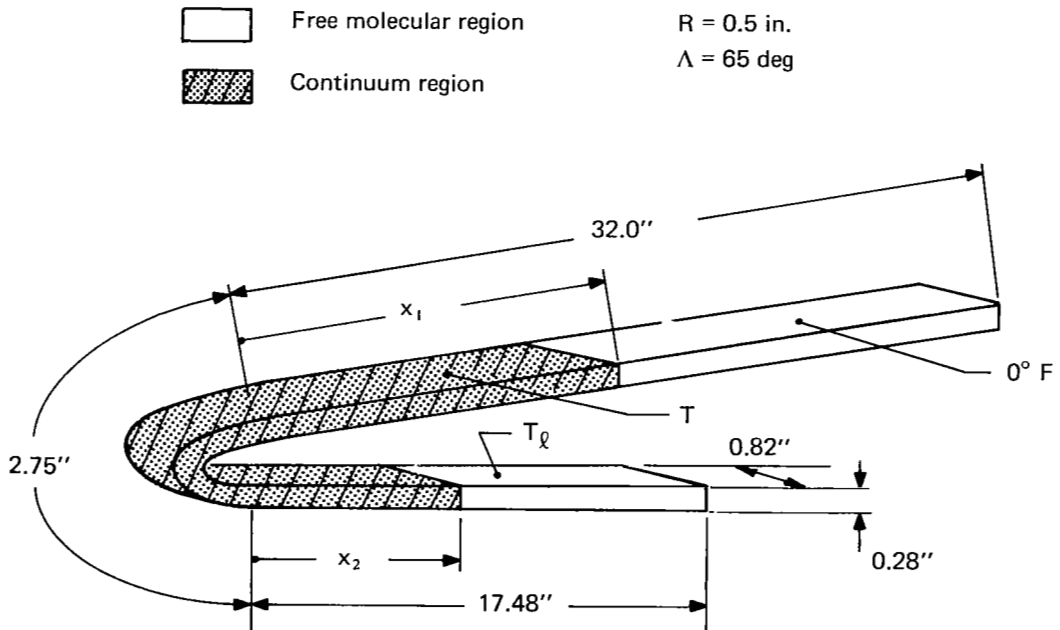


Figure 36. Model for analysis of transient temperature of heat pipe cooling structure.

specific weight in lb/in³, c is the specific heat in Btu/lb-°F, and A is the cross-sectional area in inches. It can be shown that the mean cross-sectional area in the elliptical nose section is about 35 per cent larger than in the remainder of the heat pipe cooling structure. Therefore, for the nose section,

$$C_n = 1.35 C \quad (32)$$

The volumetric heat capacity was evaluated using the data of tables 9, 15, 19, and the liquid metal property data from Appendix C. Material properties at a temperature of about 800° F were used. The calculated values were:

$$\begin{aligned} C &= 0.001616 \text{ Btu/in-}^\circ\text{F} \\ C_n &= 0.00218 \text{ Btu/in-}^\circ\text{F} \end{aligned}$$

Since sodium is a solid below its melting point of 208° F, the volumetric heat capacity C below the melting point and the effect of melting must be considered. At a mean temperature of about 120° F, C was calculated to be 0.001701 Btu/in-°F, which is about 5 per cent larger than the mean value used for liquid sodium. It was also determined that the heat required to melt the sodium per unit heat pipe length is 0.0452 Btu/in. This quantity of heat is equal to the heat required to increase the temperature of the cold heat pipe by $0.0452/0.001701 = 26.6^\circ \text{ F}$.

Thus, the heat required to melt the sodium is only a small fraction of the total involved during the climb transient, when the heat pipe temperature must be increased by about 1500° F. In the simplified transient analysis employed here, the melting of sodium was neglected and the calculated values of C and C_n for liquid sodium were used over the entire temperature range under consideration.

Heat transfer rates: In the process of carrying out the transient calculation, it is necessary to utilize net heat transfer rates to or from the leading edge, the lower leg, and the upper leg of the heat pipe cooling structure. These heat transfer rates are equal to the integral of the difference between the aerodynamic heating heat flux and the radiation heat flux over the surface of the section under consideration.

For the leading edge and the lower leg of the heat pipe cooling structure, the aerodynamic heating rate exceeds the radiation rate, and there is a net heat input rate to the structure. The net heat input rate at the leading edge was

approximated by multiplying the aerodynamic heating rate Q_p at a given time by the ratio of the steady state net-to-aerodynamic heating rates. This ratio is equal to 0.760. The net heat input rate at the nose is then given by

$$Q_{in} = 0.760 Q_p \quad (33)$$

The heating rate Q_p was calculated from equations (1) and (5), using the heat flux data of table 21. In equation (5) the second (radiation) term in the brackets was neglected, θ' in the integral was given the value $\pi/2$ radians, and the span width B was given the value of 0.82 in. In equations (1) and (5), T_w was taken to be equal to the reference temperature T_o .

The net heating rate Q_{il} on the lower leg of the heat pipe cooling structure was approximated by multiplying Q_{in} by the ratio of the steady state net heating rate on the lower leg to that on the nose section. This ratio is equal to 0.825. Thus,

$$Q_{il} = 0.825 Q_{in} \quad (34)$$

The heating rate per unit length of the lower leg was assumed to be equal to Q_{il}/L_l and independent of the distance x_2 from the leading edge. The length of the lower leg L_l is equal to 17.48 in.

On the upper leg of the heat pipe cooling structure, the radiation rate exceeds the aerodynamic heating rate. The net heat rejection rate $Q_{ru}(x_1)$ over the length x_1 of the upper leg was approximated by multiplying the radiation rate $Bx_1 q_r$ by the ratio of the steady state net heat rejection rate to the steady state radiation rate. This ratio is equal to 0.632. Thus,

$$Q_{ru}(x_1) = 0.632 Bx_1 q_r = 0.00137 \left(\frac{T}{1000} \right)^4 x_1 \quad (35)$$

In equation (35), B is the rib-to-rib spacing (0.82 in.), x_1 is in inches, T is in $^{\circ}R$, and $Q_{ru}(x_1)$ is in Btu/sec. Heat transfer is assumed to be negligible over the distance $L_u - x_1$, where L_u is the length of the upper leg. The value of L_u is 32.0 in.

The transient calculation also requires the use of the sonic heat transport limit Q_s . The sonic heat transport limit for sodium is given as a function of temperature in table 22. The sonic heat transport limit was obtained by multiplying the axial sonic heat flux by the vapor space cross-sectional area of 0.160 in². The axial sonic heat fluxes at 1300° F and above in table 22 were obtained from reference 2; the remaining axial sonic heat fluxes were obtained from reference 18.

TABLE 22. - SONIC HEAT TRANSPORT LIMIT FOR SODIUM VERSUS TEMPERATURE

Temperature, °F	Axial sonic heat flux, Btu/in ² -sec	Sonic heat transport rate, Btu/sec
932	0.732	0.122
1022	3.05	0.489
1112	7.63	1.22
1202	16.15	2.58
1300	26.5	4.24
1500	92.9	14.88
1700	265.	42.4
1900	530.	85.0
2100	1040.	166.7

Transient equations. - The climb transient involves four distinct phases. The transient equations for each phase are presented below.

Phase 1: During phase 1, the heat pipe vapor is in the free molecule regime throughout the vapor space, and the transfer of heat along the length of the heat pipe cooling structure is assumed to be negligible. The temperatures of the leading edge and the lower leg increase at different rates due to aerodynamic heating. The temperature of the upper leg is assumed to remain constant at the initial temperature of 0° F. Phase 1 continues until the temperature of the leading edge has reached the value T_c at which continuum flow is assured.

Although there is no sharp line of demarcation between the free molecular and continuum flow regimes, continuum flow is generally considered to be established when the mean free path λ is substantially less than the minimum dimension of the flow container. For purposes of this analysis, the temperature

T_c at which continuum flow is assured was assumed to be that at which $\lambda = 0.01 H_v$, where H_v is the minimum vapor space dimension of 0.2 in. Phase 1 is assumed to be completed when the temperature of the leading edge reaches T_c .

From kinetic theory, the product $w_v \lambda$ is independent of gas pressure. For the saturated heat pipe vapor, $w_v \lambda$ is also independent of the saturation temperature T_v . The product $w_v \lambda$ may be evaluated from the equation (ref. 20)

$$w_v \lambda = \mu_v \left(\frac{\pi M}{2 g R T} \right)^{1/2} \quad (36)$$

where M is the molecular weight (23 for sodium vapor), R is the universal gas constant, g is the acceleration of gravity, T_v is the absolute saturation temperature, μ_v is the vapor viscosity, w_v is the vapor specific weight and λ is the mean free path. Equation (36) was evaluated at $T_v = 2000^\circ R$, for which $\mu_v = 1.50 \times 10^{-5}$ lb/ft-sec. The resulting value for $w_v \lambda$ was 9.05×10^{-9} lb/ft². Then, letting $\lambda = 0.01 H_v = 1.67 \times 10^{-4}$ ft, $w_v = 5.41 \times 10^{-5}$ lb/ft³. From a graph of sodium vapor density versus temperature, $T_v = 870^\circ F$. Thus, continuum flow is assured when $T_v \geq 870^\circ F$. For calculational purposes, phase 1 was assumed to continue until the leading edge was equal to $900^\circ F$.

The phase 1 equations for calculating the temperature T of the leading edge and T_ℓ of the lower leg are:

$$T = \frac{\int_0^t \dot{Q}_{in} dt}{C_n s} \quad (37)$$

$$T_\ell = \frac{\int_0^t \dot{Q}_{i\ell} dt}{C L_\ell} \quad (38)$$

In the above equations, the nose section peripheral length s of the leading edge is 2.75 in., and the length L_ℓ of the lower leg is 17.48 in. The temperatures T and T_ℓ are in $^\circ F$.

Phase 2: During phase 2, a continuum front moves into the upper and lower legs from the leading edge. At time t , the front is located at x_1

in the upper leg and at x_2 in the lower leg. The temperature behind the continuum front is T . Ahead of the front, the temperature is 0°F in the upper leg and T_f in the lower leg. Phase 2 continues until the continuum front in the lower leg has traveled the distance L_f .

The transient equations for phase 2 were derived from separate energy balances for the evaporator region and for the condensing regions in the upper and lower legs. An additional energy balance is made for the free molecular region of the lower leg.

The evaporator region includes the nose section plus the region of the lower leg behind the continuum front. The appropriate energy balance is

$$\left[Q_{in} + x_2 (Q_{if}/L_f) \right]_i \Delta t = (C_n s + C_{x_2,i}) (T_{i+1} - T_i) + 2 Q_{s,i} \Delta t$$

or

$$T_{i+1} = T_i + \frac{\left[Q_{in} + x_2 (Q_{if}/L_f) - 2 Q_s \right]_i}{C_n s + C_{x_2,i}} \Delta t \quad (39)$$

Equation (39) gives the temperature of the continuum region as a function of time. The subscript i denotes conditions at time t , and the subscript $i+1$ denotes conditions at time $t + \Delta t$.

The condenser region in the upper leg includes the length x_1 plus the differential length at the continuum front over which the temperature is raised from 0°F to T . The energy balance is

$$\left[Q_s - x_1 (Q_r/L_u) \right]_i \Delta t = C_{x_1,i} (T_{i+1} - T_i) + C_{T_i} (x_{1,i+1} - x_{1,i})$$

or

$$x_{1,i+1} = x_{1,i} + \frac{\left[Q_s - x_1 (Q_r/L_u) \right]_i}{C_{T_i}} \Delta t - \frac{(T_{i+1} - T_i)}{T_i} x_{1,i} \quad (40)$$

Equation (40) gives the position of the continuum front in the upper leg as a function of time.

The energy balance for the free molecular region of the lower leg is

$$(L_{\ell} - x_{2,i}) (Q_{i\ell}/L_{\ell})_i \Delta t = C (L_{\ell} - x_{2,i}) (T_{\ell,i+1} - T_{\ell,i})$$

or

$$T_{\ell,i+1} = T_{\ell,i} + \frac{(Q_{i\ell}/L_{\ell})_i}{C} \Delta t \quad (41)$$

Equation (41) gives the temperature of the free molecular region in the lower leg as a function of time.

The condenser region in the lower leg is confined to a differential length at the continuum front, over which the temperature is raised from T_{ℓ} to T . The energy balance is

$$Q_{s,i} \Delta t = C (T_i - T_{\ell,i}) (x_{2,i+1} - x_{2,i})$$

or

$$x_{2,i+1} = x_{2,i} + \frac{Q_{s,i}}{C (T_i - T_{\ell,i})} \quad (42)$$

Equation (42) gives the position of the continuum front in the lower leg as a function of time.

Phase 3: In phase 3, there is no longer a continuum front in the lower leg. The lower leg and the nose section now act as a single heat source, from which the vapor produced flows into the upper leg at the sonic heat transport rate. Phase 3 continues until the continuum region has filled the entire length of the heat pipe cooling structure (i.e., until $x_1 = L_u$).

For the nose section and the lower leg,

$$(Q_{in} + Q_{i\ell})_i \Delta t = (C_n s + C L_\ell) (T_{i+1} - T_i) + Q_{s,i} \Delta t$$

or

$$T_{i+1} = T_i + \frac{(Q_{in} + Q_{i\ell} - Q_{s,i})_i}{C_n s + C L_\ell} \Delta t \quad (43)$$

Equation (43) gives the temperature behind the continuum front as a function of time.

For the portion of the upper leg behind the continuum front,

$$[Q_s - x_l (Q_r/L_u)]_i \Delta t = C x_{l,i} (T_{i+1} - T_i) + C T_i (x_{l,i+1} - x_{l,i})$$

or

$$x_{l,i+1} = x_{l,i} + \frac{[Q_s - x_l (Q_r/L_u)]_i}{C T_i} \Delta t - \left(\frac{T_{i+1} - T_i}{T_i} \right) x_{l,i} \quad (44)$$

The above equation, which gives the position of the continuum front in the upper leg as a function of time, is identical in form to equation (40).

Phase 4: In phase 4, the uniform temperature continuum region extends over the entire length of the heat pipe cooling structure, and there is no longer any continuum front. Phase 4 continues until the temperature of the heat pipe cooling structure approaches the steady state value.

The heat balance now takes the form

$$(Q_{in} + Q_{i\ell} - Q_r)_i \Delta t = [C_n s + C (L_\ell + L_u)] (T_{i+1} - T_i)$$

or

$$T_{i+1} = T_i + \frac{(Q_{in} + Q_{il} - Q_r)_i}{C_n + C(L_l + L_u)} \Delta t \quad (45)$$

Equation (45) gives the continuum temperature (now the temperature of the entire heat pipe cooling structure) as a function of time.

Results of transient analysis. - The results of the transient analysis of the heat pipe cooling structure are shown in figure 37. Separate curves are plotted for the temperature of the leading edge and continuum region, the temperature of the free molecular region along the lower leg, and the position of the continuum fronts in the upper and lower legs.

Phase 1 is seen to cover a period of 150 sec, during which the leading edge temperature rises to 900° F and the temperature of the lower leg rises to 160° F. Phase 2 lasts from 150 to 275 sec. during which time the continuum region completely fills the lower leg and moves a distance of 6.8 in. into the upper leg. During the same time interval the continuum temperature has risen to 970° F. Just prior to its disappearance, the temperature of the free molecular region in the lower leg has risen to 740° F.

Phase 3 covers the interval from 275 to 350 sec. During this time, the continuum temperature increases to 1110° F as it completely fills the heat pipe cooling structure. Phase 4 extends from 350 to 790 sec. The temperature is now uniform over the entire heat pipe cooling structure. At 368 sec, which corresponds to the peak aerodynamic heating rate, the temperature has risen to 1300° F. The peak temperature of 1712° F is reached after 500 sec. At 650 sec, when the cruising altitude is reached, the temperature has dropped to 1585° F. At 790 sec the temperature approaches the steady state value of 1540° F.

According to figure 37, the temperature exceeds the steady state vapor temperature of 1540° F from 405 to 790 sec, a period of more than six min per flight. As a result, the internal (vapor) pressure will exceed the steady state value, resulting in higher stresses, and the creep rate will exceed that expected during steady state operation. Whether the increased stresses and creep rates encountered during a portion of the climb transient can be tolerated is beyond the scope of this preliminary study. If design changes are warranted, they will probably take the form of closer rib spacing and/or an increase in the rib and wall thicknesses. Alternately, the temperature excess can be reduced by adoption of a climb trajectory for which the dynamic pressure is smaller than the 2000 psf which was assumed in the transient analysis.

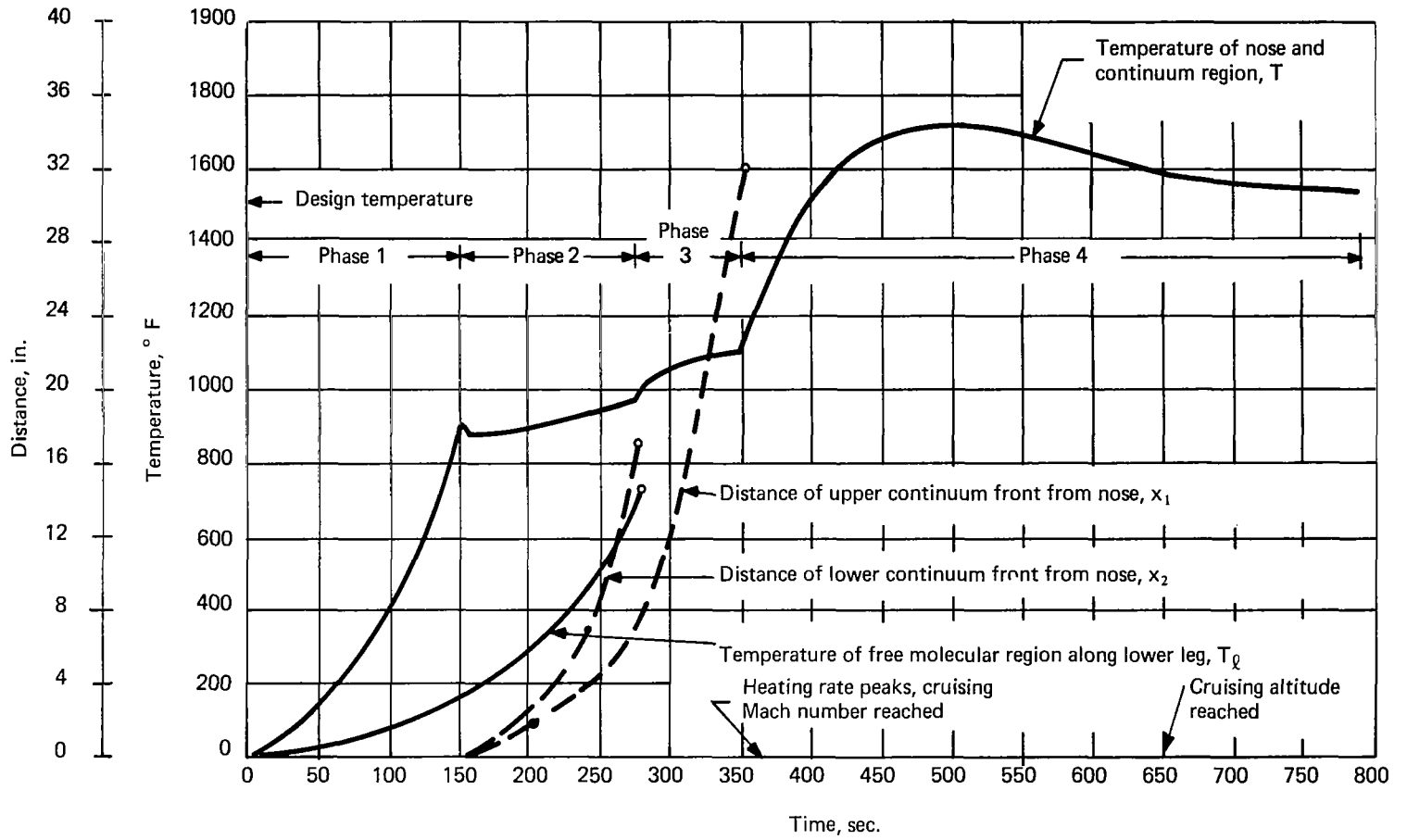


Figure 37. Transient behavior of heat pipe cooling structure during climb.

The large temperature gradient associated with the continuum wave front should also be examined with respect to thermal stress effects. Consideration of this problem was beyond the scope of this study.

Heat Transport Limits During Transient

Entrainment, boiling, and capillary pumping limits were calculated as a function of time and compared with actual heat transport rates to determine whether disruption of heat pipe operation was likely during the climb transient. In addition, vapor and liquid pressure drops were calculated as a function of time to provide further information about the stability of heat pipe flow and heat transport processes during the transient. The methods and data of Appendixes B and C were used in the calculations.

Entrainment limit. - If entrainment is not to occur, the rate of heat transport Q from the heat addition to the heat rejection section of the heat pipe cooling structure (i.e., the heat load) must not exceed the heat transport rate Q_e for entrainment. Before continuum flow has been fully established over the entire length of the heat pipe cooling structure, Q is equal to the sonic heat transport rate Q_s . After continuum flow has been fully established, Q is equal to the net rate of heat transfer from the leading edge to the upper leg. From figure 37, continuum flow is fully established at $t = 350$ sec, at which time the continuum temperature is 1110° F.

The appropriate equations for Q are then

$$\left. \begin{aligned} Q &= Q_{s,i} && , t \leq 350 \text{ sec} \\ Q &= (Q_{in} + Q_{il})_i - (C_n s + C L_\ell) \left(\frac{T_{i+1} - T_i}{\Delta t} \right) && , t > 350 \text{ sec} \end{aligned} \right\} (46)$$

In figure 38, the actual heat transport rate Q and the heat transport rate Q_e at which entrainment occurs are shown as a function of heat pipe temperature during the climb transient. Figure 38 indicates that Q exceeds Q_e between 1050 and 1110° F. (This temperature range corresponds to the time between 295 and 350 sec, according to figure 37.) Thus, heat pipe operation could possibly be disrupted by entrainment in the interval between 295 and 350 sec.

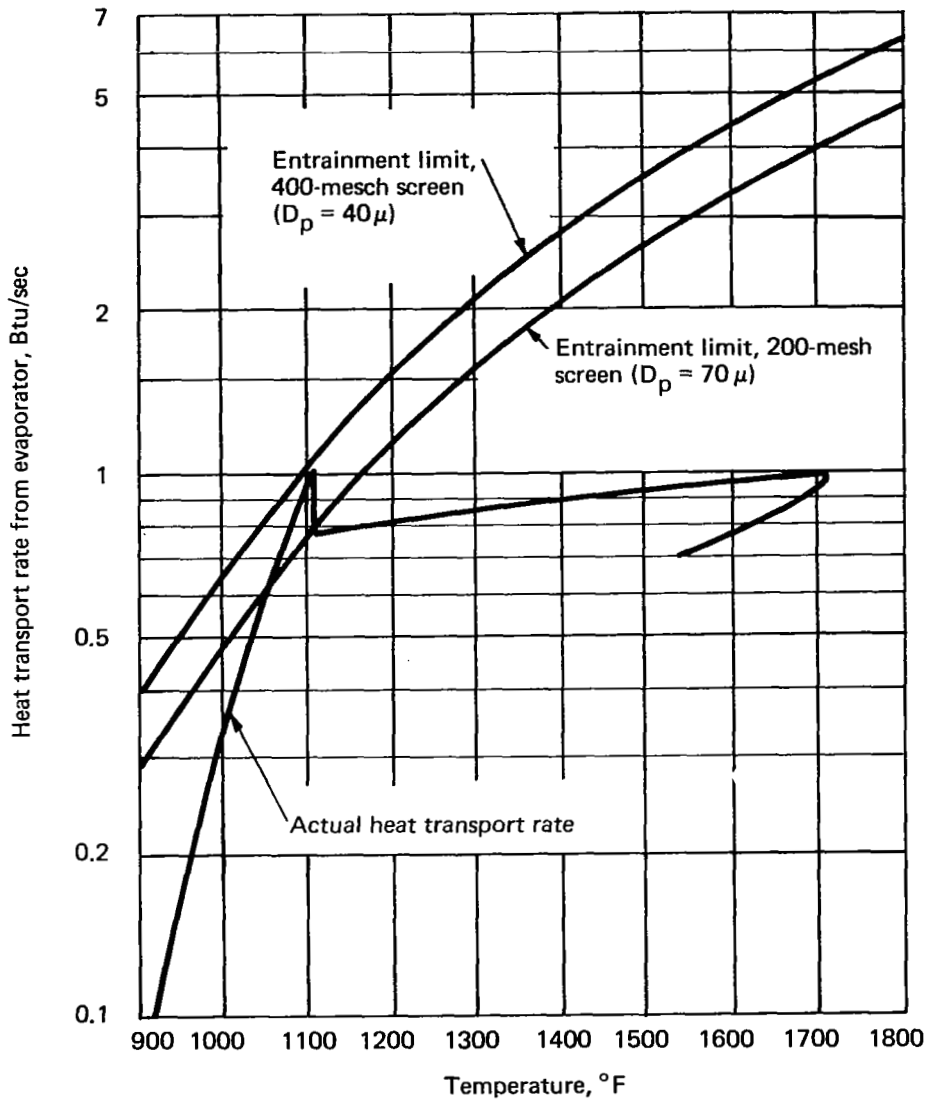


Figure 38. Heat transport rate and entrainment limit during climb transient.

However, the entrainment limit is not known precisely, and is based on an experiment with a single-layer screen (ref. 7). With multilayer screens, such as have been employed for the inner wick layer, the entrainment limit could be considerably larger than the values which have been calculated. If it should prove necessary, the entrainment limit can be increased by reducing the pore size of the inner wick layer. For example, if a 400-mesh screen (with a pore space of 40 microns) were used instead of the 200-mesh screen (with a pore space of 70 microns), the entrainment limit would be raised sufficiently so that Q was smaller than Q_e for the entire transient period. (See figure 38.)

Boiling and capillary pumping limits. - The diameter of curvature D_b below which boiling occurs and the minimum diameter of curvature D_c required for capillary pumping (i. e., the curvature needed for surface tension to balance the maximum difference between the vapor and liquid pressures) were calculated as a function of time during the climb transient. An upper limit of 7 microns was assumed for the nucleation site radius in the boiling calculation.

The capillary pumping equations of Appendix B, which were used for the calculation of D_c , were derived on the assumption of isothermal heat pipe operation. During phases of the climb transient when heat is transported through the heat pipe structure at the sonic heat transport rate, appreciable temperature gradients will exist along the heat pipe length. The analysis is therefore approximate, but consistent with the assumption of uniform temperature in the continuum region which was made in the transient temperature analysis. The heat pipe heat loads were obtained from equation (46).

To simplify the analysis, both legs of the heat pipe cooling structure were assumed to be parallel to the horizontal component of acceleration. The effective heat pipe length and the static liquid pressure drop due to the horizontal acceleration of 0.5 g were dependent on the transient phase involved as well as the elapsed time. In the calculation of vapor and liquid frictional pressure drops, the heat pipe length was augmented by 4.9 in. to allow for the increased frictional losses associated with flow around the 180° bend at the leading edge of the heat pipe cooling structure.

The boiling and capillary pumping limit calculations were initiated at the start of phase 2. In phase 2, when continuum fronts are advancing into both the upper and lower legs, the heat pipe cooling structure acts like two heat pipes in parallel, each of which extends from the leading edge to one of the continuum fronts.

In phase 3, when the lower leg has been completely filled with the continuum, the entire structure behind the continuum front in the upper leg

constitutes a single heat pipe. In phase 4, the hot continuum fills the entire structure, and geometric conditions are identical to those existing during steady state operation.

Results of the calculations are shown in figure 39, where the minimum diameter of curvature D_c and the diameter of curvature D_b below which boiling will occur are shown as a function of time. The minimum D_c occurs at the start of the evaporator section except in the vicinity of 275 sec.^c At that time, the minimum D_c occurs at the evaporator-condenser interface. Since D_c is always larger than D_b , it can be concluded that disruptive boiling will not occur during the climb transient. However, D_c is smaller than the pore opening of 70 microns in the inner wick layer between 340 and 360 sec, dropping to a minimum of 57 microns at 350 sec.

In order to prevent possible disruption of heat pipe operation in this time interval, the pore opening should be reduced below 57 microns. This is conveniently accomplished by the use of 400-mesh screen, for which the pore opening is about 40 microns, in place of the 200-mesh screen. This design modification was also suggested to prevent possible disruption of heat pipe operation by entrainment.

Vapor and liquid pressures. - The maximum vapor pressure, the minimum liquid pressure, the vapor pressure drop (frictional plus momentum), the liquid frictional pressure drop, and the liquid static pressure drop due to acceleration are shown as a function of time in figure 40 during the interval from 150 to 350 sec. The most unusual feature of these curves is the fact that the minimum liquid pressure is negative (i. e., the liquid sodium is in tension instead of under pressure) over almost the entire interval, reaching a maximum of -1.0 psi at 350 sec. (the minimum liquid pressure becomes positive very shortly after the start of phase 4 at 350 sec.)

On the basis of experimental observations, Kemme (ref. 18) concluded that a liquid sodium heat pipe had operated stably under a negative liquid pressure within the range of 0.8 to 2.3 psi. Thus, a negative liquid sodium pressure of 1.0 psi appears feasible. However, more experimental study is needed in this area, particularly when negative liquid pressures are encountered during a startup transient in the presence of vibration.

If necessary, the negative liquid pressure can be reduced or eliminated by increasing the vapor and liquid flow passage dimensions (to reduce the frictional pressure drops), by orienting the flow direction of the heat pipe fluid along the normal to the leading edge (to reduce the liquid static pressure drop), by modifying the climb trajectory to reduce aerodynamic heating (by a reduction in the dynamic pressure), or by raising the continuum temperature, and hence pressure, before high aerodynamic heating rates are encountered (by a reduction in the forward acceleration).

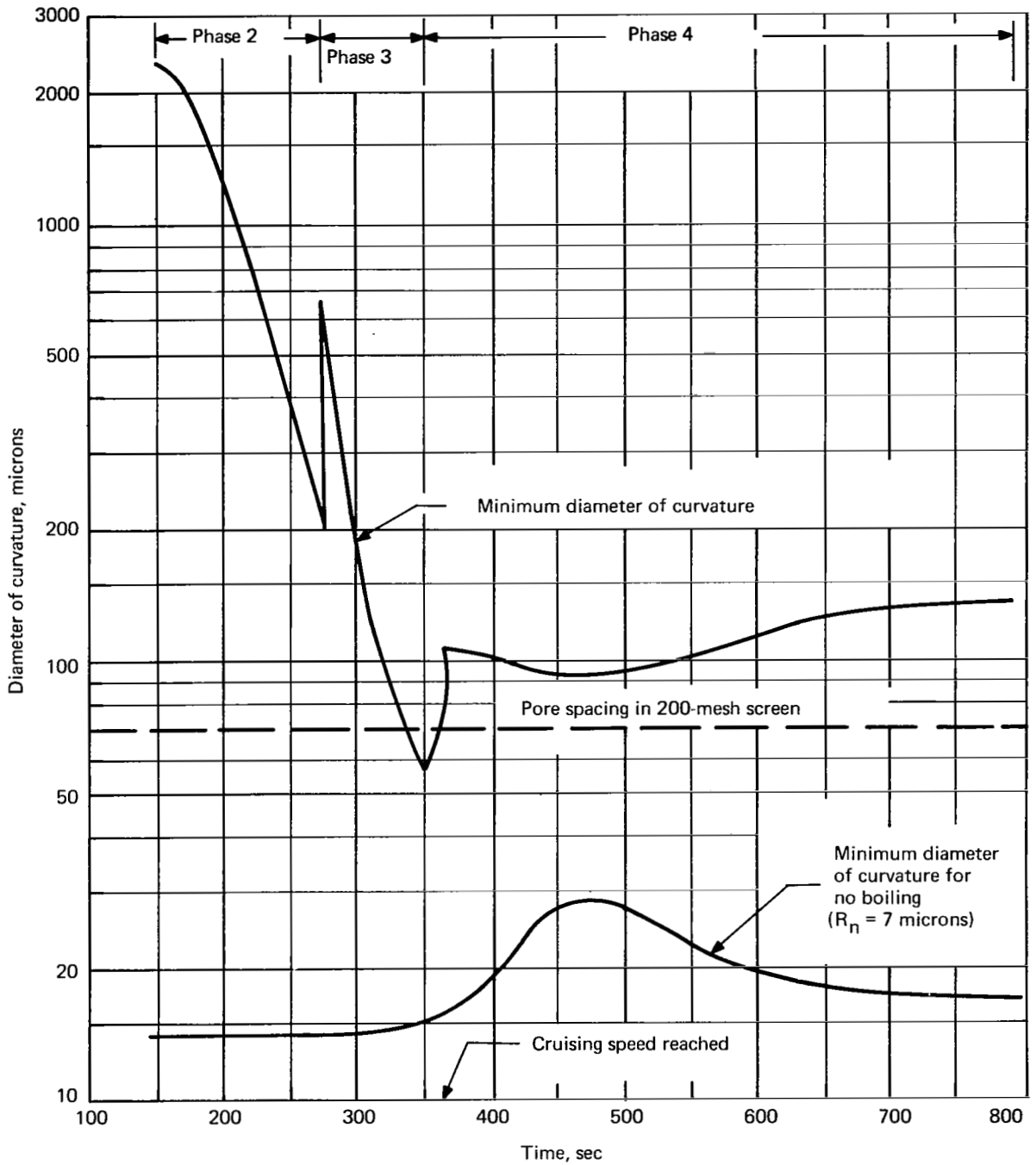


Figure 39. Diameter of curvature for capillary pumping and for no boiling during climb transient.

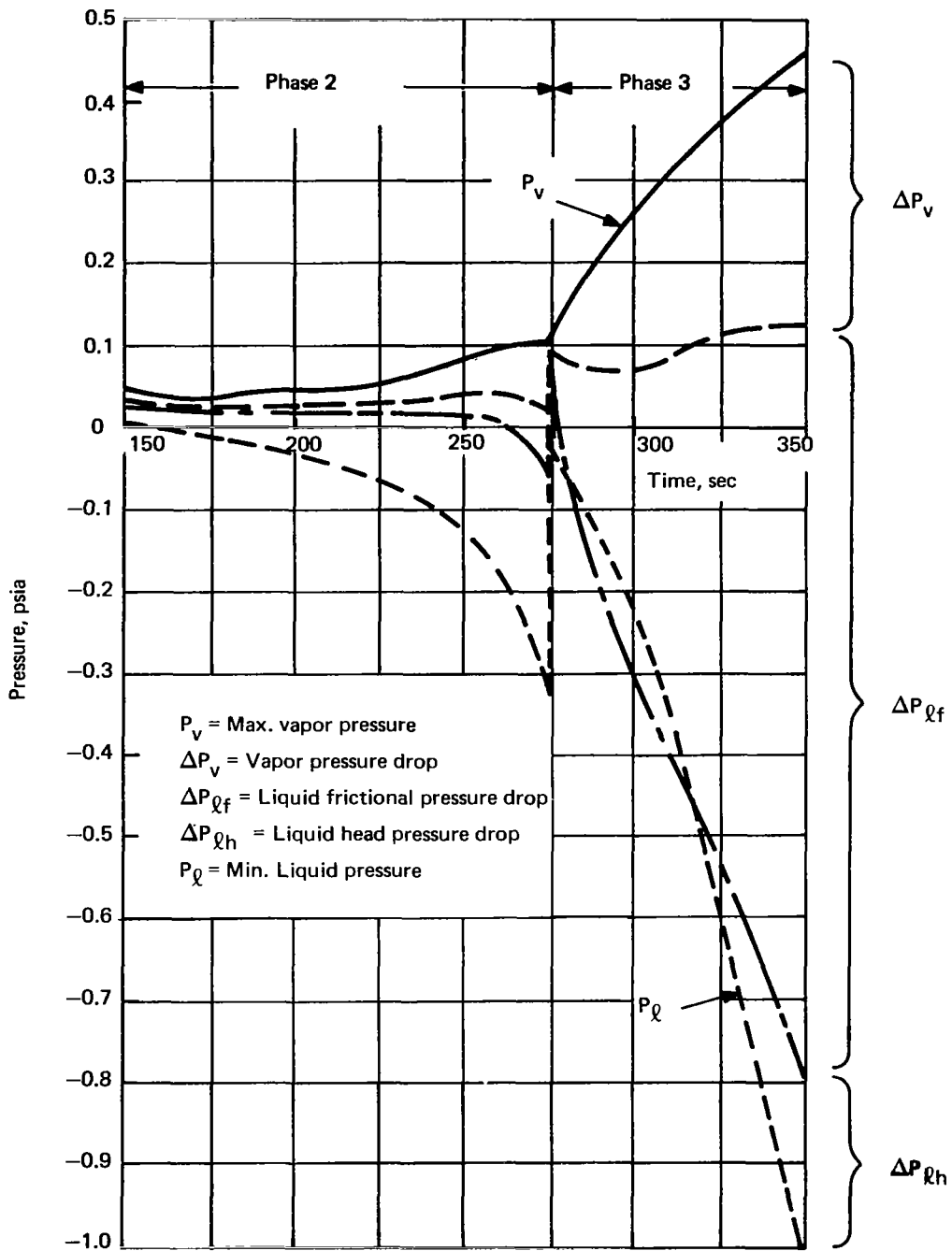


Figure 40. Internal heat pipe fluid pressures during climb transient.

Expansion of Liquid Sodium During Startup

Since the sodium heat pipe liquid expands appreciably when heated from room temperature to operating temperature, this fact must be taken into account in the heat pipe design. For example, the specific volume of liquid sodium at 1540° F is 24 percent larger than at 212° F.

Generally, a heat pipe is loaded with a slight excess of liquid to insure complete wetting of the entire wick. The excess liquid then accumulates at one end of the heat pipe, inactivating the section of heat pipe whose vapor space is occupied by the liquid. An excess of liquid sodium in the heat pipe cooling structure will not present any problem if the excess liquid is located at the condensing end of the structure, as will be the case when the aircraft is subjected to forward acceleration. All that would be required is a slight increase in length to compensate for the inactivated length which is filled with liquid.

However, if excess liquid were to accumulate at the leading edge, as might well be the case when the aircraft is undergoing horizontal deceleration, severe overheating and disruption of normal heat pipe operation could result. For this reason, overfilling of the heat pipe cooling structure with liquid is not advised. Only enough liquid should be added to just fill the wick pores at the normal operating temperature.

In the wick design of figure 30, 19.6 per cent of the wick void volume is contained within the inner wick layer. If all the wick pores were just filled with liquid at 1540° F, 42 percent of the pores of the inner wick layer would still be occupied by liquid sodium at 800° F, and the vapor-liquid interface would still be located within the inner wick layer. Maximum capillary pumping capability would then be maintained over a wide temperature range, while at the same time all of the liquid sodium would be confined within the wick structure.

On the other hand, if enough sodium were added to just fill the wick pores at 800° F, the resulting excess volume of liquid sodium at 1540° F would be sufficient to flood the vapor space over a length of 1.12 in. If this liquid were to be concentrated at the leading edge, overheating and disruption of heat pipe operation would be likely.

Conclusions

The heat pipe cooling structure may encounter more severe operating conditions during the climb to cruise altitude and speed than are experienced during steady state cruise, if the transient dynamic pressure and acceleration

are as high as 2000 psf and 0.5 g, respectively. Modifications to accommodate the more severe conditions encountered during the climb transient could include smaller pores for the inner wick layer, larger flow passages for the heat pipe vapor and liquid, smaller spacing between ribs, and re-orientation of the flow passage direction normal to the leading edge. These changes can be incorporated into the heat pipe cooling structure without difficulty. The extent to which they would be required would depend on the precise nature of the climb trajectory. Excess sodium in the heat pipe cooling structure could adversely affect operation during decelerative maneuvers, and should be avoided.

DISCUSSION OF RESULTS

Summary of Major Findings

The principal objective of the study reported herein was to investigate the feasibility of using heat-pipe-like structures for cooling the leading edges of hypersonic cruise aircraft. In order to achieve this end, parametric studies were first performed to determine heat pipe lengths and heat loads for a wide range of Mach numbers, sweep angles, leading edge radii, and temperatures. Then preliminary design studies of heat pipe cooling structures were carried out for a Mach 8 cruise condition, a 65° sweep angle, a leading edge radius of 0.5 in., and a heat pipe vapor temperature of 1540° F. The resulting design characteristics were compared with the characteristics of experimental heat pipes of comparable dimensions which had been operated at comparable temperatures. The influence of Mach number, leading edge radius, and angle of attack on design characteristics was investigated. Finally, the transient behavior of heat pipe cooling structures during the climb to cruising altitude and speed was studied.

The results of the study all point to the conclusion that the use of heat pipe structures for cooling leading edges offers a promising solution to one of the critical design problems of hypersonic cruise aircraft.

For Mach numbers up to 10, leading edge radii in the range of 0.25 to 2 in., and sweep angles greater than about 50°, cooling structure designs can be developed which are based on the current heat pipe state-of-the-art. Sodium appears to be the preferred heat pipe fluid. Operating temperatures will be in the range of 1600 to 1800° F, and the use of cobalt- or nickel-base superalloys appears feasible. Chordwise lengths will be on the order of several feet, lateral dimensions will be in the range of 0.25 to 0.50 in., and weights will be on the order of 2.5 to 3.5 lb per ft² of surface area. Designs may still be

feasible at higher Mach numbers, larger leading edge radii, and smaller sweep angles, but then they will tend to approach more closely the boundaries of the current heat pipe state-of-the-art.

At Mach 8, the temperature of the leading edge of a 65° sweep wing with a 0.5-inch-radius leading edge can be maintained below 1600° F with a heat pipe cooling structure whose length in the chordwise direction is 33 in. Heat loads and surface heat fluxes are comparable to or less than those which have been encountered in experimental sodium heat pipes with comparable dimensions and operating temperatures. The liquid static head due to acceleration is generally comparable to or less than static heads at which sodium heat pipes have successfully operated.

Heat pipe cooling structures should function effectively during the climb to cruising altitude and speed, but some design characteristics based on steady state operation may require alteration to meet more severe design criteria which can be encountered during the climb transient.

Design Uncertainties

A number of design questions have arisen in the course of this study which are best resolved through an experimental program. Such a program is also desirable to verify the predicted characteristics of heat pipe cooling structures during both steady state and transient operational modes and to determine performance degradation characteristics with time. Suggestions for an experimental program are given in Appendix D.

The principal design uncertainties which require experimental evaluation are summarized below.

1. The high heat flux at the nose section combined with the low heat flux along the lower leg of the heat pipe structure results in condensation of heat pipe vapor in the lower leg during the startup (i.e., climb) transient until the hot continuum region has completely filled the lower leg. This temporary reversal of the normal evaporation process over a portion of the heat input zone is believed to be a unique, although feasible, mode of operation which requires experimental verification.
2. The stability of heat pipe operation under possible disturbing influences during both transient and steady state operation should be established experimentally. The disturbing influences of primary interest are vibration, shock, and diffusion of gases into the interior

of the heat pipe cooling structure from the atmosphere. The ability of the heat pipe structure to recover its cooling function following disruption of normal operation is also of interest.

3. In the design studies, a porous liquid flow channel was selected over a thinner, lighter open flow channel because the porous channel was believed to be more stable under external disturbing influences. The relative stability of porous and open liquid flow channels should be determined experimentally.
4. The heat pipe cooling structure will be lighter and easier to fabricate if only the wall exposed to the air stream is lined with wicking material, and the designs which were developed employ this feature. Tests of this simplified design concept are necessary to determine whether temporary condensation on the unwicked walls during the startup transient will interfere with normal heat pipe operation.
5. In the process of loading the heat pipe cooling structure with liquid, a small amount of excess sodium may be added to insure that the capillary wick is fully saturated. The possible disruptive effect of excess liquid sodium, if it should be forced to the leading edge during a decelerative maneuver, should be determined experimentally. Information will then be available from which permissible tolerances on the liquid sodium content can be established.
6. The simplified transient analysis has indicated that the heat loads and temperatures encountered during the climb transient may, in some circumstances, have an adverse effect on the cooling capability of the heat pipe structure. Experimental information is needed on the transient response of the heat pipe cooling structure in order to identify trajectories for which startup difficulties can be expected.
7. If the cells of the heat pipe cooling structure are oriented normal to the wing leading edge instead of in the chordwise direction, flow lengths for the heat pipe fluid are reduced, as is the liquid static head due to longitudinal acceleration. However, this orientation prevents full use of heat pipe cooling for the wing leading edge in the vicinity of the fuselage. It would be desirable to experimentally compare the relative merits of the two orientations.

CONCLUDING REMARKS

On the basis of preliminary design studies, comparison of required heat pipe performance with the current state-of-the-art, and a transient analysis, heat pipe cooling appears to be an attractive, feasible technique for preventing excessive leading edge temperatures during hypersonic flight. Major design uncertainties include: operating lifetime in the atmosphere, limiting climb trajectories for assured startup capability, and recovery of cooling capability following disruption of the heat pipe liquid by external disturbances.

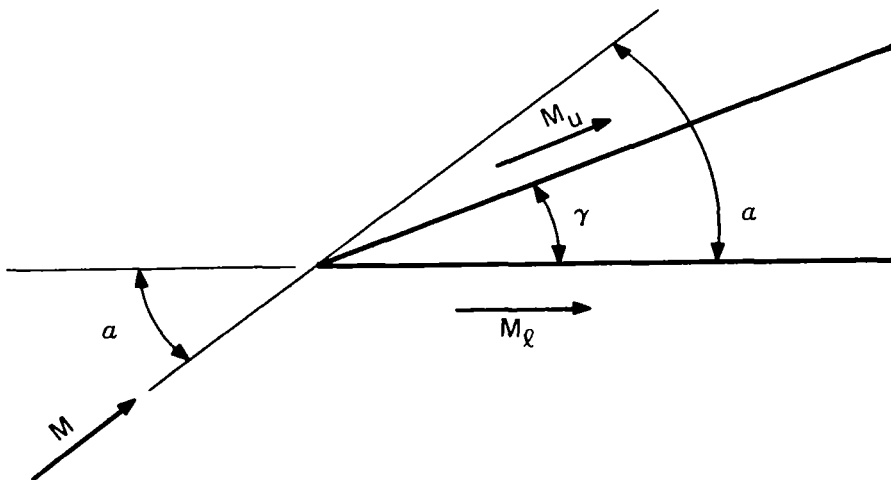
APPENDIX A

HEAT TRANSFER COEFFICIENT FOR AERODYNAMIC HEATING OF FLAT WING SURFACES

The heat transfer coefficient h for aerodynamic heating of flat surfaces of the wing was calculated by the method of Van Driest. Turbulent boundary flow was assumed. The needed local air flow properties at the flat surfaces were obtained from undisturbed free stream properties by assuming that the undisturbed free stream undergoes a Prandtl-Meyer expansion or a reversed Prandtl-Meyer expansion.

Local Free Stream Flow Properties at Flat Surfaces

Consider a wing with wedge angle γ which moves at an angle of attack α to the undisturbed free stream at Mach number M . In the sketch below, the undisturbed free stream is shown flowing at Mach M with respect to the fixed wing. The Prandtl-Meyer angle ν is associated with the Mach M flow. (The Prandtl-Meyer angle ν is the angle through which a flow stream initially at Mach 1 must expand isentropically to reach Mach M .)



On the upper surface the flow is assumed to expand isentropically through the angle $\Delta\nu = \alpha - \gamma$ to Mach M_u , whose Prandtl-Meyer angle is $\nu + (\alpha - \gamma)$. Expansions in excess of 8° were treated as if they were 8° expansions (ref. 10).

On the lower surface the flow is assumed to be isentropically compressed through the angle $\Delta\nu = \alpha$ to Mach M_l , whose Prandtl-Meyer angle is $\nu - \alpha$.

The flow properties for the undisturbed free stream at Mach M are listed in table 23.

TABLE 23. - PROPERTIES OF UNDISTURBED AIR FREE STREAM
(refs. 6, 21)
(Dynamic pressure = 800 psf)

M	T, °R	w, lb/ft ³	w/w _t	T/T _t	w _t , lb/ft ³	T _t , °R	ν , deg
6	405	1.470×10^{-3}	5.19×10^{-3}	0.1220	0.283	3 320	84.955
8	412	0.813	1.414	0.0725	0.575	5 690	95.625
10	427	0.502	0.495	0.0476	1.012	8 980	102.32
12	440	0.337	0.206	0.0336	1.635	13 110	106.88

In the above table, T is the temperature, T_t is the total temperature, w is the air density, w_t is the total density, and ν is the Prandtl-Meyer angle. From table II of reference 21, flow properties corresponding to the Prandtl-Meyer angles $\nu + (\alpha - \gamma)$ after expansion and $\nu - \alpha$ after compression may be found. The total properties w_t and T_t are assumed to be constant. The post-expansion or compression free stream properties are then, using the table II data,

$$\left. \begin{aligned} \text{Mach number} &= M' \\ w' &= \left(\frac{w'}{w_t} \right) w_t \\ T' &= \left(\frac{T'}{T_t} \right) T_t \end{aligned} \right\} \quad (47)$$

The primes denote local free stream conditions at the flat wing surfaces.

The sonic velocity C' in ft/sec is given by

$$C' = \sqrt{k g R_a T'} \quad (48)$$

where k is the ratio of constant pressure and constant volume specific heats for air ($= 1.4$), g is the acceleration of gravity (32.2 ft/sec), and R_a is the gas constant for air (53.3 lb-ft/lb-°R). The flow velocity V' is

$$V' = M' C' \quad (49)$$

According to reference 22, the skin friction coefficient C_f is a function of M' , T_w/T' , and Re' , where T_w is the wall temperature in °R and Re' is the Reynolds number. The skin friction coefficient is given in figure 3(b) of reference 22, assuming a constant value of $2000^\circ R$ for T_w and 10^6 for Re' .

The heat transfer coefficient is then calculated from the expression

$$h = c_p \rho' V' (0.6 C_f) \quad (50)$$

where c_p is the constant pressure specific heat of air (0.24 Btu/lb-°F) and h is the heat transfer coefficient in Btu/ft²-sec-°F.

The distance x from the start of the flat surface at which $Re' = 10^6$, and hence the distance at which the h of equation (50) occurs, is found from the equation

$$x = \frac{10^6 \mu'}{\rho' V'} \quad (51)$$

where μ' is the absolute viscosity of air in lb/sec-ft at T' . Since the heat transfer coefficient is a slowly varying function of the distance along the flat surface, and since the distance x corresponding to $Re' = 10^6$ is on the

order of 1 to 3 ft (as shown in table 5), h as calculated from equation (50) was assumed to be equal to the average heat transfer coefficient over the length of flat wing surface which is covered by the heat pipe cooling structure.

APPENDIX B

HEAT PIPE HEAT TRANSPORT LIMITS

The heat transport limits which determine the heat transport capacity of heat pipes are: the sonic limit, the entrainment limit, the isothermal limit, the capillary pumping limit, and the boiling limit. These limits are described in detail in reference 2. Methods for their calculation are summarized here.

Sonic Limit

The sonic heat transport limit Q_s in Btu/sec is given by

$$Q_s = 12 w_v C_v A_v \kappa \quad (52)$$

where w_v is the heat pipe vapor density in lb/in³, C_v is the sonic velocity of the heat pipe vapor in ft/sec, A_v is the vapor space cross-sectional area in in², and κ is the heat of vaporization in Btu/lb. All heat pipe vapor properties are evaluated at the evaporator-condenser interface of the heat pipe.

It is also convenient to express the sonic heat transport limit as the sonic axial heat flux ξ_s , where

$$\xi_s = \frac{Q_s}{A_v} = 12 w_v C_v \kappa \quad (53)$$

Sonic axial heat flux data for sodium are given in table 22. These data assume that, in the evaporator section of the heat pipe, the vapor pressure drop due to friction is negligible compared to the vapor pressure drop due to momentum generation. When the vapor pressure drop is not negligible, the sonic limit will be smaller than the data of table 22.

Entrainment Limit

The entrainment limit is given by

$$\xi_e = \frac{Q_e}{A_v} = 905 \left(\frac{\sigma \rho_v \kappa^2}{C_d D_p} \right)^{1/2} \quad (54)$$

where σ is the surface tension in lb/ft, D_p is the pore diameter at the liquid-vapor interface in microns, Q_e is the entrainment heat transport limit in Btu/sec, ξ_e is the entrainment axial heat flux in Btu/in²-sec, and C_d is a dimensionless drag coefficient. Entrainment limit data (ref. 2) suggests that $C_d = 3.33$ to 5.00 . If the largest (more conservative) value is used for C_d in equation (54),

$$\xi_e = 405 \left(\frac{\sigma \rho_v \kappa^2}{D_p} \right)^{1/2} \quad (55)$$

Table 24 gives entrainment limit data for sodium, potassium, cesium, and lithium heat pipes as a function of temperature, for a pore diameter D_p of 40 microns.

TABLE 24. - ENTRAINMENT AXIAL HEAT FLUX^a

Temperature, °F	Entrainment axial heat flux, Btu/in ² -sec			
	Sodium	Potassium	Cesium	Lithium
1300	13.8	13.3	6.80	7.70
1400	17.2	15.5	7.70	10.0
1500	21.3	18.2	8.65	13.0
1600	26.5	21.0	9.65	16.7
1700	32.5	24.0	10.6	21.6
1800	39.0	27.8	11.3	27.2
1900	45.8	31.8	11.7	35.0
2000	52.5	36.3	12.0	45.0

^a Wick pore diameter $D_p = 40$ microns.

The entrainment axial heat flux for any pore diameter D_p can be obtained from the above data and the expression

$$\xi_e (D_p) = \left(\frac{40}{D_p} \right)^{1/2} \xi_e (40) \quad (56)$$

where $\xi_e (40)$ is the axial heat flux when $D_p = 40$ microns and $\xi_e (D_p)$ is the axial heat flux for any D_p .

Isothermal Limit

The isothermal limit refers to the heat transport rate at which the temperature drop along the heat pipe length exceeds some specified limit. It is determined by finding the heat transport rate at which the vapor pressure drop in the heat pipe corresponds to a specified allowable drop in the saturation (i.e., vapor) temperature. Generally, for the liquid metals the saturation or vapor temperature drops about 1.5 to 2.0° F for each per cent drop in the vapor pressure. If the vapor pressure drop does not exceed 1 per cent, the heat pipe may be considered as isothermal for practical purposes.

Calculations of the isothermal limit, as well as of the capillary pumping limit, were performed for the three cross-sections of figure 26. To facilitate the calculations, pressure drop expressions were presented in a form which would be applicable to any of the cross-sectional geometries.

The axial heat flux ξ , which is utilized in the calculations, can be expressed in the general form

$$\xi = \frac{Q}{A_v} = \frac{(Q/B)}{H_v} \eta \quad (57)$$

where ξ is the axial heat flux in Btu/in²-sec, Q/B is the heat pipe heat transport rate per unit span length in Btu/in-sec, H_v is the vapor space thickness in inches, and η is a dimensionless geometric parameter which is defined below.

<u>Cross-section</u>	η
Circular, figure 26A	$\frac{4}{\pi} \left[1 + \frac{2(t_p + t_a + t_w)}{W_v} \right]$
Rectangular, figure 26B	$1 + \frac{2t_w}{W_v}$
Rectangular, figure 26C	$1 + \frac{2(t_p + t_a + t_w)}{W_v}$

In the above definitions of η , W_v is the vapor space width, t_w is the wall thickness, t_a is the thickness of the liquid flow channel, and t_p is the thickness of the inner wick layer.

The vapor pressure drop can be expressed in the form

$$\Delta P_v = bL \frac{(Q/B)}{H_v^3} \left(1 + \frac{H_v}{W_v} \right)^2 \eta + c \left[\frac{(Q/B)}{H_v} \eta \right]^2 \quad (58)$$

where L is the heat pipe length in inches, ΔP_v is the vapor pressure drop in psi, and b and c are dimensional parameters which are functions of the physical properties of the heat pipe fluid. The parameters b and c are defined as follows:

$$b = \frac{1.498 \mu_v}{\kappa W_v} \quad (59)$$

$$c = \frac{3.28}{\kappa^2 W_v} \quad (60)$$

In the above equations, μ_v is the vapor viscosity in lb/ft-sec, w_v is the vapor density in lb/ft³, and κ is the heat vaporization in Btu/lb. The constant in b includes the factor $1/g$, where $g = 32.2 \text{ ft/sec}^2$, for dimensional

consistency. Table 25 (on page 130) gives b and c , along with other fluid-property-dependent functions, as a function of temperature for sodium.

In equation (58), the first term on the right hand side is the frictional pressure drop, and the second term is the pressure drop due to momentum generation. The frictional pressure drop term is based on the assumption of laminar vapor flow. This assumption is valid for most of the heat pipe cooling structure designs which were considered.

In calculating the pressure drop, the actual heat pipe length was augmented to account for the increased pressure loss around the $\approx 180^\circ$ bend at the leading edge. Data for the equivalent length of straight pipe with the same pressure drop as a particular bend are given in reference 23 as a function of pipe diameter and the ratio of the bend radius to the pipe diameter. For the preliminary design studies described in this report, the equivalent length to account for bend friction was estimated to be 4.9 in. This length was added to the actual heat pipe length for all pressure drop calculations.

In equation (58), the assumption is also made that the surface heat flux is uniformly distributed over the heat input section and the heat rejection section. While the assumption is quite good for the heat rejection section, the heat flux over the rounded leading edge is quite nonuniform, as is evident from equation (1). It may be shown that, for laminar fluid flow in the heat pipe, the heat flux distribution of equation (1) results in a pressure drop along the curved leading edge which is 33 per cent larger than would be the case if the heat flux distribution were uniform. However, because the peripheral length of the leading edge is small compared to the total heat pipe length, the overall increase in the frictional pressure drop due to the nonuniform heat flux distribution over the leading edge is small, and was neglected in the calculations.

From equation (58), the heat transport rate corresponding to a given axial temperature drop (and hence, a specified ΔP_v), can be found. Conversely, the ΔP_v (and hence the axial temperature drop) corresponding to a given heat load can be determined.

Capillary Pumping Limit

The capillary pumping limit is the maximum heat transport rate for which the pressure difference across the common interface between the heat pipe vapor and liquid can be sustained by surface tension. The capillary pumping limit can be determined from one of the following equations.

$$P_v - P_\ell = \frac{a}{D_c} = b L \frac{(Q/B)}{H_v^3} \left(1 + \frac{H_v}{W_v}\right)^2 \eta + c \left[\frac{(Q/B)}{H_v} \eta\right]^2 + d L \frac{(Q/B)\eta\delta\epsilon}{t_a^3} + \frac{w_\ell L_a}{1728} \sum_j n_j \cos \Omega_j \quad (61)$$

$$P_v - P_\ell = \frac{a}{D_c} = b L_c \frac{(Q/B)}{H_v^3} \left(1 + \frac{H_v}{W_v}\right)^2 \eta - c' \left[\frac{(Q/B)}{H_v} \eta\right]^2 + d L_c \frac{(Q/B)\eta\delta\epsilon}{t_a^3} + \frac{w_\ell L_c}{1728} \sum_j n_j \cos \Omega_j \quad (62)$$

In the above equations, laminar flow is assumed for both vapor and liquid flow, the heat pipe length L includes an added 4.9 in. to account for the increased pressure drop around the nose bend, and the effect of the nonuniform heat flux distribution over the nose section is neglected. The liquid flow channel thickness t_a is in inches.

Equation (61) gives the vapor-liquid pressure difference $P_v - P_\ell$ in psi at the beginning of the evaporator section, while equation (62) gives $P_v - P_\ell$ at the evaporator-condenser interface. Generally, equation (61) results in a larger $P_v - P_\ell$, and is used for the capillary pumping limit calculation. However, because the heat pipe cooling structure includes a 180° bend, the liquid static pressure drop due to acceleration (the last term in the above equations) is greater at the evaporator-condenser interface than at the beginning of the evaporator. Hence, it is possible for the $P_v - P_\ell$ to be largest at the evaporator-condenser interface, even though the frictional pressure drops are smaller at that location than at the beginning of the evaporator section.

In the above equations, w is the liquid density in lb/ft³, L_c is the condensing (heat rejection) length in inches, L_a is the straight-line distance between the two ends of the heat pipe cooling structure in inches, n_j is the j th component of acceleration in number of g's, D_c is the diameter of curvature at the liquid-vapor interface in microns, and Ω_j is the angle between

the j th component of acceleration and L_a [in equation (61)] or L_c [in equation (62)]. The parameter δ accounts for differences in the liquid flow channel geometry of the cross-sections of figure 26, and the parameter ϵ is the ratio of the liquid pressure drop in a porous flow channel to the pressure drop in an open flow channel with the same geometry and dimensions. When an open flow channel is under consideration, $\epsilon = 1$. Expressions for δ and ϵ are given below.

Cross-section	δ	ϵ
Circular, Figure 26A	$\frac{H_v}{H_v + 2t_p + t_a}$	$\frac{K}{8} t_a^2$
Rectangular, Figure 26B	$4 \left(1 + \frac{t_a}{W_v} \right)^2$	$\frac{K}{8} \frac{t_a^2}{\left(1 + \frac{t_a}{W_v} \right)^2}$
Rectangular, Figure 26C	$\frac{2W_v}{W_v + H_v + 2(2t_p + t_a)}$	$\frac{K}{8} t_a^2$

In the above expressions, K is the porous flow channel friction factor in in.^{-2} .

The fluid property parameters b and c have already been defined by equations (59) and (60). The additional fluid property parameters a , c' , and d are defined as follows:

$$a = 8480 \sigma \quad (63)$$

$$c' = \frac{2.24}{\kappa W_v} = 0.682 c \quad (64)$$

$$d = \frac{0.374 \mu_\ell}{\kappa W_\ell} \quad (65)$$

In the above equations, σ is the surface tension in lb/ft, w_l is the liquid density in lb/ft³, and μ_l is the liquid viscosity in lb/sec-ft. Again, the gravitational factor 1/32.2 ft/sec² is included in the numerical constant of equation (65).

The fluid property parameters for sodium are given in table 25 as a function of temperature. The liquid density w_l is given in Appendix C.

TABLE 25. - FLUID PROPERTY PARAMETERS FOR SODIUM

Temperature, °F	a, psi-micron	b, $\frac{\text{psi-sec-in}^3}{\text{Btu}}$	c, $\frac{\text{psi-sec}^2\text{-in}^4}{\text{Btu}^2}$	c', $\frac{\text{psi-sec}^2\text{-in}^4}{\text{Btu}^2}$	d, $\frac{\text{psi-sec-in}^3}{\text{Btu}}$
1200	80.0	8.55x10 ⁻⁶	7.90x10 ⁻⁴	5.60x10 ⁻⁴	5.69x10 ⁻¹⁰
1300	76.7	4.42	4.00	2.73	5.46
1400	73.6	2.60	2.18	1.50	5.25
1500	70.4	1.487	1.300	0.888	5.09
1600	67.0	0.975	0.840	0.570	4.97
1700	63.6	0.645	0.550	0.376	4.90
1800	60.5	0.435	0.365	0.250	4.83
1900	57.2	0.306	0.254	0.1732	4.74
2000	54.1	0.226	0.184	0.1220	4.69
2100	50.9	0.1718	0.1392	0.0952	4.60

To find the capillary pumping heat transport limit, Q is solved from equations (61) and (62) for $D_c = D_p$, where D_p is the effective pore diameter (i.e., minimum possible diameter of curvature) of the inner wick layer. The smaller value of Q is the capillary pumping limit. Alternatively, the D_c for a given Q can be calculated from equations (61) and (62). Then the pore diameter D_p must be less than the smaller of the two calculated D_c 's if the given Q is to be transported through the heat pipe without breakdown of the capillary pumping mechanism.

Boiling Limit

The boiling limit is the heat transport rate at which boiling of the heat pipe liquid in the capillary wick is initiated. In heat pipe design, it is simpler and more convenient to establish whether the actual heat transport rate is less

than or larger than the boiling limit, instead of calculating the boiling limit itself. This approach was used in the heat pipe analyses which were performed for this report.

It can be shown* that boiling will be initiated at the inner wall surface of a heat pipe when

$$T_{wo} - T_v = \frac{2}{\Delta} \left(1 + \frac{k_c}{t_c h_i} \right) \left(\frac{\sigma T}{w_v \kappa} \right) \quad (66)$$

where T_{wo} is the wick temperature at the wick-wall interface in °R, T_v is the heat pipe vapor temperature in °R, k_c is the mean thermal conductivity of the heat pipe wick, t_c is the wick thickness, h_i is the interface heat transfer coefficient with the same units as $(k/t)_c$, $\left(\frac{\sigma T}{w_v \kappa}\right)$ is a fluid parameter in °R-micron which is evaluated at $\bar{T} = 1/2 (T_{wo} + T_i)$, T_i is the wick temperature at the liquid-vapor interface in °R, \bar{T} is the mean wick temperature in °R, and Δ is a geometric parameter defined by

$$\Delta = \frac{R_n D_b}{D_b - 2 R_n} \quad (67)$$

In equation (67), R_n is the radius of nucleation sites at the inner wall surface from which vapor bubbles originate, and D_b is the diameter of curvature at the liquid-vapor interface. All dimensions in equation (67) are in microns.

For vapor pressures below about 0.1 psia, the interface heat transfer coefficient h_i can be evaluated from gas kinetics considerations (ref. 24). At higher vapor pressures, h_i is not known accurately, but generally is large compared to $(k/t)_c$. It is assumed here that $h_i \gg (k/t)_c$. Then $T_i = T_v$, $\bar{T} = 1/2 (T_{wo} + T_v)$, and equation (66) reduces to

$$T_{wo} - T_v = \frac{2}{\Delta} \left(\frac{\sigma T}{w_v \kappa} \right) = \left(\frac{t}{k} \right)_c q_b \quad (68)$$

* Unpublished analysis of author.

where q_b is the surface heat flux at which boiling is initiated.

Now if q_b is taken to be the actual surface heat flux of the heat pipe, $T_{wo} - T_v$ is just the temperature drop across the wick, and \bar{T} is the mean wick temperature. The value of Δ required for the initiation of boiling is then, from equation (68).

$$\Delta = \left(\frac{2}{T_{wo} - T_v} \right) \left(\frac{\overline{\sigma T}}{w_v \kappa} \right) \quad (69)$$

The required diameter of curvature D_b below which boiling will proceed is obtained by substituting Δ from equation (69) into equation (67) and solving for D_b . Thus,

$$D_b = \frac{2R_n \Delta}{\Delta - R_n} = \frac{4 R_n \left(\frac{\overline{\sigma T}}{w_v \kappa} \right)}{2 \left(\frac{\overline{\sigma T}}{w_v \kappa} \right) - R_n (T_{wo} - T_v)} \quad (70)$$

If $D_b < D_c$, the boiling limit will be larger than the actual heat transport rate, and boiling will not occur. If $D_b \geq D_c$, the boiling limit will be equal to or less than the actual heat transport rate, and boiling can be expected.

The solution of equation (70) requires a knowledge of the nucleation site radius R_n . While there are little definitive data on R_n for liquid metal heat pipes, an upper limit of 3 to 7 microns has been estimated for sodium heat pipes from the experimental data of reference 7.* Recent measurements of the liquid superheat necessary to initiate boiling of liquid sodium (ref. 25) correlate with an effective R_n of 0.81 microns. Therefore, R_n for liquid metal heat pipes can reasonably be expected to lie within the range of 1 to 7 microns, most probably closer to the lower limit. The larger the value of R_n which is selected, the more conservative will be the calculation for D_b (i.e., the larger will be D_b).

To facilitate the calculation of D_b , the boiling parameter $\overline{(\sigma T/w_v \kappa)}$ is given in table 26 as a function of the mean wick temperature for several liquid metals.

* Unpublished calculation of author.

TABLE 26. - BOILING PARAMETER FOR LIQUID METALS

Mean wick temperature, ° F	$\left(\frac{\sigma T}{w_v \kappa}\right)$, microns - ° R			
	Sodium	Potassium	Cesium	Lithium
900			295	
1000		1325	202	
1100		650	135	
1200	2650	390	86.5	
1300	1325	215	57.5	
1400	725	132.5	38.5	
1500	425	81.0	26.0	
1600	265	56.0	18.0	
1700	175	38.5	12.6	
1800	112.5	27.0		
1900	77.5	19.5		
2000	55.0			3450
2200				1475
2400				660
2600				335
2800				185
3000				106

APPENDIX C

LIQUID METAL PROPERTY DATA

Liquid metal property data needed for heat pipe calculations are listed below. The data was obtained from references 26 through 29.

The symbols used are defined as follows:

P_v	vapor pressure
w_v	vapor density
w_l	liquid density
μ_v	vapor viscosity
μ_l	liquid viscosity
k_l	liquid thermal conductivity
c_l	liquid specific heat
κ	heat of vaporization
σ	surface tension

Temperature, °F	P_v , psi	w_v , lb/ft ³	w_g , lb/ft ³	μ_v , lb/hr-ft	μ_g , lb/hr-ft	k_g , Btu/hr-ft- °F	c_g , Btu/lb-°F	κ , Btu/lb	σ , lb/ft
Sodium									
1300	2.1	2.7×10^{-3}	48.6	0.0500	0.444	34.6	0.301	1742	9.05×10^{-3}
1500	7.2	8.8	47.2	0.0532	0.392	33.0	0.304	1695	8.30
1700	20.8	22.0	45.8	0.0562	0.356	31.6	0.310	1648	7.50
1900	48.	50.0	44.5	0.0591	0.326	30.5	0.318	1606	6.75
2100	100.	96.0	43.3	0.0620	0.300	29.5	0.330	1564	6.00
Potassium									
1100	2.4	5.6×10^{-3}	44.0	0.0622	0.375	20.3	0.185	881	5.27×10^{-3}
1300	8.8	18.0	42.3	0.0660	0.332	18.6	0.189	846	4.77
1500	24.5	50.0	40.5	0.0697	0.302	16.9	0.195	813	4.28
1700	56.	107.	38.7	0.0730	0.280	15.3	0.205	782	3.80
1900	110.	205.	37.0	0.0763	0.260	13.8	0.215	752	3.28
Cesium									
900	1.6	$28. \times 10^{-3}$	99.5	0.0576	0.470	10.8	0.057 ^a	228	3.56×10^{-3}
1100	6.6	65.	95.2	0.0617	0.420	9.97		218	3.15
1300	20.0	152.	91.0	0.0657	0.377	9.18		209	2.74
1500	48.0	360.	86.5	0.0692	0.345	8.38		199	2.32
1700	97.	680.	82.0	0.0726	0.320	7.60		189	1.92
Lithium									
2000	2.1	0.6×10^{-3}	27.2	0.0424	0.500	29.1	0.986	8700	19.0×10^{-3}
2200	5.5	1.47	26.7	0.0445	0.460	29.4	0.983	8530	17.8
2400	13.0	3.35	26.3	0.0470		29.7	0.980	8370	16.6
2600	27.2	6.7	25.8	0.0491		30.0	0.976	8210	15.4 ^b
2800	54.	12.2	25.4	0.0510		30.3	0.973	8070	14.2 ^b
3000	97.	21.0	25.0	0.0530		30.6	0.970	7930	13.0 ^b

^a For temperatures greater than 570° F.

^b Estimated values.

APPENDIX D

EXPERIMENTAL PROGRAM

An experimental program to resolve questions relating to design and operation of the heat pipe cooling structure should include both short and long term tests. These tests can best be carried out under static conditions in the laboratory, using electrical heaters to simulate aerodynamic heating and controlled atmospheres to simulate desired environmental conditions.

The short term tests would include steady state and transient tests designed to measure the heat pipe temperature distribution as a function of heating rate and various conditions of vibration and acceleration. Since the effect of acceleration is to develop a static pressure head in the liquid sodium, its effect can be simulated by inclination of the test heat pipe at an appropriate angle to the horizontal. The long term tests would measure possible changes in heat pipe temperature from gaseous diffusion, oxidation, and internal corrosion. The heat pipes undergoing long term test could operate continuously under steady state heating conditions, or could be cycled to conform to anticipated flight patterns.

It is suggested that the Mach 8 design with a leading edge radius of 0.5 in. and a sweep angle of 65° be considered as the basis for test models. The overall dimensions would then be as shown in figure 30, and would be compatible with requirements for a laboratory-scale test program.

Test models would consist of single sodium heat pipes of rectangular cross-section equivalent to that of a single cell between ribs of the heat pipe cooling structure. To facilitate fabrication and reduce dimensional tolerance requirements, it may be desirable to use thicker flow channels for the vapor and liquid flow passages in the initial test models than are called for in the Mach 8 design. It may also be necessary to stiffen the lateral walls, since the internal and external pressures on the lateral walls of a single cell are no longer balanced as they are in the multicelled designs. Also, thermal insulation should be used for all external surfaces of the test models except the surface which simulates the external surface of the wing. During testing, heat transfer to and from the heat pipe should be confined to the uninsulated surface, which should be preoxidized prior to testing.

It is suggested that the five models shown in figure 41 be considered for a static test program. Model 1 is a straight heat pipe which is fully wicked, with a porous liquid sodium flow channel; it is intended as a reference model to establish basic heat pipe performance. Models 3 and 5 have the same

Notes — 1. Not to scale.

2. Bent models are configured to simulate maximum longitudinal acceleration of 0.5 g.

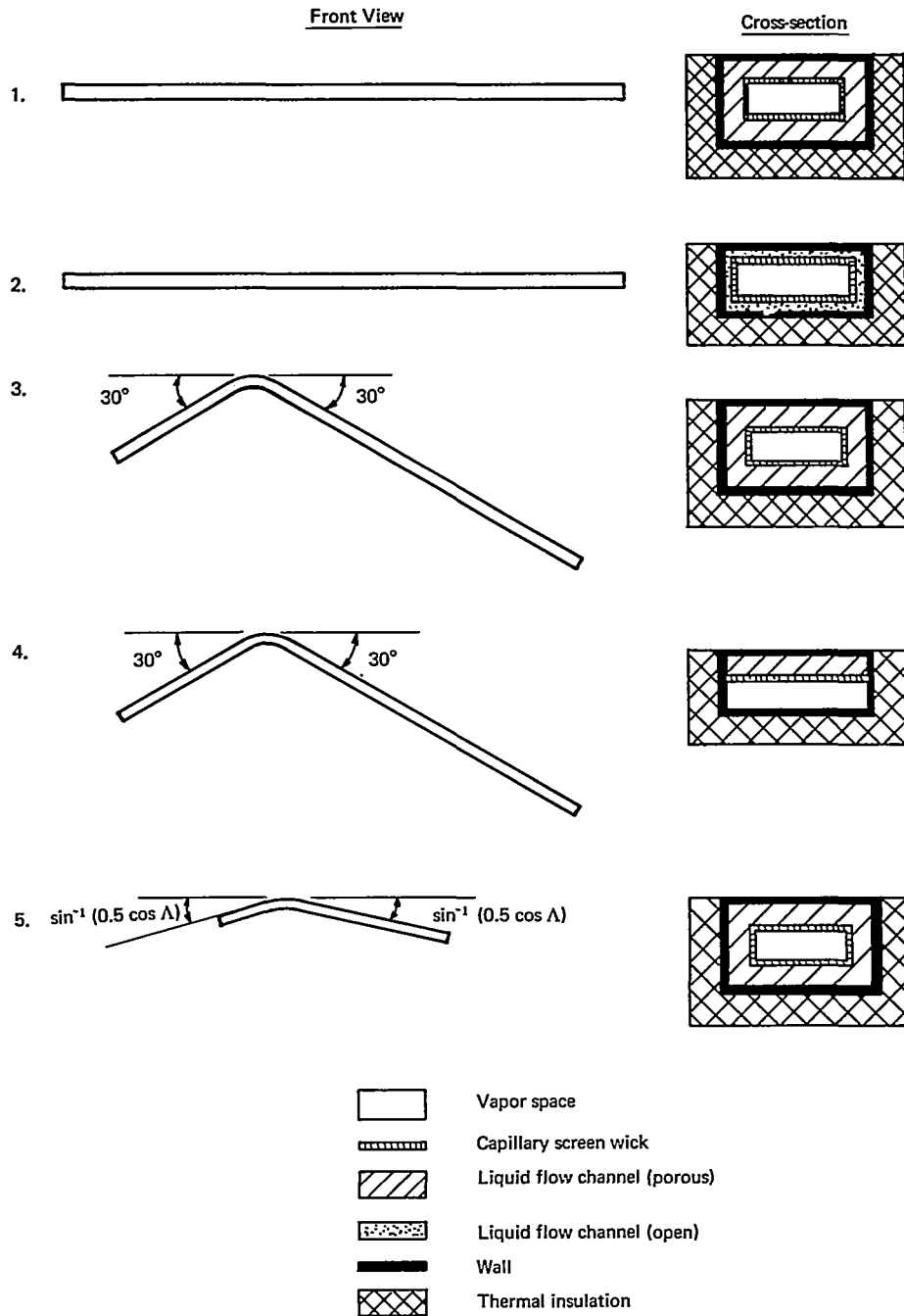


Figure 41. Heat pipe static test model configurations.

cross-section as Model 1, but are bent to simulate the liquid static head due to longitudinal acceleration. Model 3 simulates the application of 0.5 g to a heat pipe which is oriented in the chordwise direction. Model 5 simulates the application of 0.5 g to a heat pipe which is oriented along the normal to the leading edge. In model 5 the heat pipe length has been reduced by $\cos \Lambda$, where Λ is the sweep angle, and the component of acceleration along the heat pipe axis has also been reduced by $\cos \Lambda$.

Models 3 and 5 can be tested under lower simulated accelerations simply by inclining the plane defined by the heat pipe legs at an appropriate angle to the horizontal. Decelerations can be simulated by orienting the heat pipes with the bend below the ends of the legs.

Models 2 and 4 are intended to test the adequacy of design modifications which can result in lower weight, simplified fabrication, and reduced costs. Model 2 uses an open liquid flow channel which is thinner and lighter than a porous channel, but has lower refilling capability if the liquid sodium column should be disrupted by external disturbances. It is shown as a straight heat pipe to avoid possible distortion of the flow channel during bending. Model 4 is wicked only on the uninsulated surface, and is lighter, cheaper, and easier to fabricate than a fully-wicked heat pipe. However, condensation of liquid sodium on the inner, unwicked walls during startup could possibly interfere with normal heat pipe operation.

It would be highly desirable to analytically predict temperatures and heat transport limits for the models under test heating and environmental conditions, so that the adequacy of calculational methods can be evaluated. In support of the calculational effort, a supplementary test program to measure the flow resistance of the liquid flow channels and the effective pore size of the inner wick layer may be warranted.

Following successful conclusion of the static test program, dynamic testing in a hypersonic wind tunnel may then be undertaken with a model which is accurately configured to the wing shape. A multicelled model which is similar to a section of the actual heat pipe cooling structure would probably be preferable for dynamic testing. (See figure 30.)

REFERENCES

1. Heldenfels, R. R.: Structural Prospects for Hypersonic Air Vehicles. Presented at the 5th Congress of the International Council of the Aeronautical Sciences (London, England), Sept. 12-16, 1966.
2. Silverstein, Calvin C.: A Study of Heat Pipe Applications in Nuclear Aircraft Propulsion Systems. NASA CR-72610, 1969.
3. Deverall, J.E.: Effect of Vibration on Heat Pipe Performance. LA-3798-MS, Los Alamos Scientific Laboratory, 1967.
4. Walker, C. L.: Final Report - Investigation of Bimetallic Liquid Metal Systems. Rep. GMAD 3654-8, Allison Div., General Motors, Sept. 1966.
5. Aerodynamic Heat Transfer Handbook - Vol. 1, Document No. D2-9514, Boeing Aircraft Company, Seattle, Wash., May, 1961.
6. U. S. Standard Atmosphere Tables, U. S. Government Printing Office, Washington 25, D. C., 1959.
7. Kemme, J. E.: High Performance Heat Pipes. Presented at 1967 Thermionic Conversion Specialist Conference (Palo Alto, Calif.), Oct. 30 - Nov. 1, 1967.
8. Peters, J. T.; and Hannah, R. G.: Development of an Advanced Space Radiation System. Proceedings of Fourth Intersociety Energy Conversion Engineering Conference (Washington, D. C.), Sept. 22-26, 1969, pp. 1010-1015.
9. Plank, P. P.; Sakata, I. F.; Davis, G. W.; and Richie, C. C.: Hypersonic Cruise Vehicle Wing Structure Evaluation. NASA CR-1568, 1970.
10. Plank, P. P.; Sakata, I. F.; Davis, G. W.; and Richie, C. C.: Substantiation Data for Hypersonic Cruise Vehicle Wing Structure Evaluation. NASA CR-66897-1, 1970.
11. DeVan, J. H.: Corrosion of Iron-and Nickel-Base Alloys in High-Temperature Sodium and NaK. Alkali Metal Coolants, International Atomic Energy Agency, 1967, pp. 643-661.
12. Klueh, R. L.; and Jansen, D. H.: Effects of Liquid and Vapor Cesium on Structural Materials. ORNL-TM-1813, Oak Ridge National Laboratory, 1967.

13. Harms, W. O.; and Litman, A. P.: Compatibility of Materials for Advanced Space Nuclear Power Systems. Preprint 67-WA/AV-1, ASME, Nov. 1967.
14. Eastman, G. Y.: The Heat Pipe -- A Progress Report. Proceedings of Fourth Intersociety Energy Conversion Engineering Conference (Washington, D.C.) Sept. 22-26, 1969, pp. 873-878.
15. Roark, R. J.: Formulas for Stress and Strain. Second ed., McGraw-Hill Book Co., Inc., 1964.
16. Eshback, O. V.: Handbook of Engineering Fundamentals. John Wiley & Sons, Inc., 1936.
17. Kunz, H. R.; Langston, L. S.; Hilton, B. H.; Wyde, S. S.; and Nashick, G. H.: Vapor Chamber Fin Studies - Transport Properties and Boiling Characteristics of Wicks. NASA CR-812, 1967.
18. Kemme, J. E.: Ultimate Heat Pipe Performance. Presented at 1968 Thermionic Conversion Specialist Conference (Framingham, Mass.), Oct. 1968.
19. Cotter, T. P.: Heat Pipe Startup Dynamics. Presented at 1967 Thermionic Conversion Specialist Conference (Palo Alto, Calif.), Oct. 30-Nov. 1, 1967.
20. Eckert, E. R. G.; and Drake, Jr., Robert M.: Heat and Mass Transfer. Second ed., McGraw-Hill Book Company, Inc., 1959, p. 274.
21. Ames Research Staff: Equations, Tables, and Charts for Compressible Flow. NACA Rept. 1135, 1950.
22. Lee, Dorothy B.; and Faget, Maxime A.: Charts Adapted From Van Driest's Turbulent Flat-Plate Theory for Determining Values of Turbulent Aerodynamic Friction and Heat-Transfer Coefficients. NACA TN 3811, 1956.
23. Salisbury, J. K., ed.: Kent's Mechanical Engineer's Handbook. Power Volume. John Wiley & Sons, Inc., 1950, p. 6-40.
24. Barry, R. E.; and Springer, G. S.: Vapor Phase Resistance in Filmwise Condensation. Preprint 69-WA/HT-26, ASME, Nov. 1969.

25. Lewis, James P.; Groesbeck, Donald E.; and Christensen, Tests of Sodium Boiling in a Single Tube-in-Shell Heat Exchanger Over the Range 1720° to 1980° F. NASA TN D-5323, 1965.
26. Weatherford, Jr., W. D.; Tyler, J. C.; and Ku, P. M.: Performance of Inorganic Energy Conversion and Heat Transfer Fluids in Various Applications. WADD TR 61-96, 1961.
27. Hoffman, H. W.; and Robin, Jr., T. T.: A Preliminary Collation of Thermodynamic and Transport Properties of Cesium. ORNL-1755, Oak Ridge National Laboratory, 1967.
28. Hoffman, H. W.; and Cox, B.: A Preliminary Collation of Thermodynamic and Transport Properties of Potassium. ORNL-1756, Oak Ridge National Laboratory, 1968.
29. Burdi, G. F.: Snap Technology Handbook, Volume I, Liquid Fuel Systems. NAA-SR-8617, 1964.